Title
The rates and processes affecting the deposition of NOx to vegetation at leaf-level and canopy-level scales: impacts on NOx lifetimes and budgets in the troposphere

Author
Delaria, Erin Rose

Publication Date
2020

Peer reviewed|Thesis/dissertation

The rates and processes affecting the deposition of NO_x to vegetation at leaf-level and canopy-level scales: impacts on NO_x lifetimes and budgets in the troposphere

by

Erin R Delaria

A dissertation submitted in partial satisfaction of the

requirements for the degree of

Doctor of Philosophy

in

Chemistry

in the

Graduate Division

of the

University of California, Berkeley

Committee in charge:

Professor Ronald C. Cohen, Chair
Professor Daniel Neumark
Professor Inez Fung

Spring 2020

The rates and processes affecting the deposition of NO_x to vegetation at leaf-level and canopy-level scales: impacts on NO_x lifetimes and budgets in the troposphere

Abstract

The rates and processes affecting the deposition of NO_x to vegetation at leaf-level and canopy-level scales: impacts on NO_x lifetimes and budgets in the troposphere

by

Erin R Delaria

Doctor of Philosophy in Chemistry

University of California, Berkeley

Professor Ronald C. Cohen, Chair

Both canopy-level field measurements and laboratory studies suggest that absorption of NO_2 through the leaf stomata of vegetation is a significant sink of atmospheric NO_x ($NO_x \equiv NO_2 + NO$), removing a large fraction of the global soil-emitted NO_x. Understanding the mechanisms of NO_x foliar loss is important for constraining surface ozone, constraining NO_x mixing ratios, and assessing nitrogen inputs to ecosystems. However, the mechanisms of this foliar NO_2 uptake and their impact on NO_x lifetimes remains incompletely understood.

To understand the leaf-level processes affecting ecosystem scale atmosphere-biosphere NO_x exchange, I have conducted laboratory experiments of branch-level NO_2 deposition fluxes to six coniferous and four broadleaf native California trees using a branch enclosure system with direct Laser Induced Fluorescence (LIF) detection of NO_2, which excludes biases from other reactive nitrogen compounds and has a low detection limit of 5—50 ppt. I report NO_2 foliar deposition that demonstrates a large degree of inter-species variability, with maximum observed deposition velocities ranging from 0.15—0.51 cm/s during the daytime, as well as significant stomatal opening during the night. I also find that the contribution of mesophyllic processing to the overall deposition rate of NO_2 varies by tree species, but has an ultimately inconsequential impact on NO_x budgets and lifetimes. Additionally, I report no evidence of any emission of NO_2 from leaves, suggesting an effective uni-directional exchange of NO_x between the atmosphere and vegetation.

In parallel with these laboratory experiments, I have constructed a detailed 1-D atmospheric model to assess the contribution of leaf-level NO_x deposition to the total NO_x loss and canopy flux. My model is able to closely replicate canopy fluxes and above-canopy NO_x daytime mixing ratios observed during two field campaigns, one in a western Sierra Nevada pine forest (BEARPEX-2009) and the other in a northern Michigan mixed hardwood forest (UMBS-2012). I present a conceptual argument for the importance of NO_2 dry deposition and demonstrate that NO_2 deposition can provide a mechanistic explanation for the canopy

reduction of NO_x. Using the leaf uptake rates measured in the laboratory, these modeling studies suggest that loss of NO_x to deposition in forests competes with the pathways of HNO_3 and alkyl nitrate ($RONO_2$) formation, with deposition making up to ∼40% of the total NO_x loss. Additionally, foliar uptake of NO_x at these rates could account for as much as ∼60% canopy reduction of soil NO_x emissions, reconciling inferences of canopy NO_x reduction with leaf-level deposition processes. Finally, I show NO_2 foliar deposition has a significant impact on ozone and nitrogen budgets under both high- and low-NO_x conditions.

For my mom

Contents

List of Figures

List of Tables

Acknowledgments

Thank you to my advisor, Ron Cohen, for his support and guidance throughout my PhD and for inspiring me to have confidence in my work. Thank you to Paul Wooldrige for his experience and tremendous electronics help when things inevitably stopped working in lab. Thanks to the entire current and former Cohen group for their support and scientific advice. Thank you especially to Josh for introducing me to coding and providing seemingly endless support, encouragement, and patience during my first three years on the Cohen Research Team.

Thank you to my committee members, Daniel Neumark and Inez Fung, for their helpful comments on this dissertation and their insights throughout graduate school.

Thank you to my undergraduate advisor, Dr. Fred Grieman, for being a phenomenal teacher that taught me to love chemistry and gave me my incredible first research opportunity. Thank you to Linhan, my first research mentor, who taught me how to be a scientist. It is due to how engaging and fun it was to work with her that I decided to continue research in chemistry.

Thank you to my mom–my best friend, my constant companion, my adventure buddy, and my kayaking partner–for more than I know how to express in words. So I will just say thank you for absolutely everything. Thank you to my mom and Jean, who are two of the most incredibly strong and independent women. Because of their influence I never doubted that women could be successful businesswomen, scientists, or have the capacity to be extraordinarily tough. Thank you also to my grandma, Rose, for being equally strong and independent and raising the two most amazing women. Cheers to the three chicks on the loose!

Thanks to Dave for his positive outlook, endless creativity, inspirational spirit, and always making me feel like everything is going to be okay.

Thank you to my dad for sparking my interest in environmental science through the trips we took together whale watching, hiking, and bird watching, and the many discussions we had along the way. Thank you also to Jerry S., for telling me I had reason to be confident and encouraging me to believe in myself. I wish they both could see me complete this journey.

Thank you so much to to my ride-or-die friends who are forever part of my family. Thank you to Clare and Ella for their wonderful friendship. They are both such extraordinary people that constantly inspire me with their strength, bravery, intelligence, and adventuring spirits. Thank you to Juliana for being my longest friend, for always knowing how to make me laugh even when I feel heartbroken, and for so many many other things that it would make this acknowledgement section longer than my dissertation itself if I listed them all. A special thank you to those friends I have made at Berkeley that have made this graduate school process rather wonderful. I am so thankful to Erin S. and Bryan for the time we having spent running and beer drinking together, and for the interesting and entertaining conversations we have had as a result of these activities. Thank you to Bryan for being, in addition to an amazing friend, a phenomenal lab mate that made every day working with him such a blast.

I could not have hoped for a more fun, thoughtful, kind, or brilliant human to have worked with.

Thank you to Alonso, with whom every day is a gift. There is no one I would rather be stuck in an indefinite lockdown with.

Chapter 1

Introduction

1.1 Interactions between the atmosphere and biosphere

The exchange of gases between the atmosphere and the biosphere plays a fundamental role in determining the composition of the atmosphere. At the same time, changes in atmospheric composition and climate provide important feedbacks that affect biological communities.

This dynamic interaction between the atmosphere and biosphere is best exemplified by photosynthesis–the process by which plants take up carbon dioxide (CO_2) and water to synthesize glucose and oxygen. By this process, vegetation provides one of the largest sinks of CO_2 (IPCC, 2013), and is the source of the oxygen in our atmosphere. Not only does photosynthesis drive much of the carbon cycle, through the simultaneous release of water vapor (a process called transpiration) vegetation also influences the water cycle and climate. Transpiration may return approximately 40% of incident precipitation back to the atmosphere, which in turn encourages later precipitation events (Schlesinger and Jasechko, 2014).

Exchange of gases between vegetation and the atmosphere drives important atmospheric chemical processes. Emission of biogenic volatile organic compounds (BVOCs) from vegetation (e.g. terpenoids, isoprene, pinene, and 2-methyl-3-buten-2-ol), drives the formation of secondary organic aerosols through reactions with the atmospheric oxidants ozone (O_3), hydroxyl radicals (OH), and nitrate radicals (NO_3) (Seinfeld and Pandis, 2006; Atkinson, 2013). These reactions produce a variety of lower volatility products that readily condense to form particles. Aerosols affect the climate by reflecting incoming solar radiation, and by serving as cloud condesation nuclei (CCN), which also influence precipitation. The emission of these BVOCs has been shown to have a strong positive temperature dependence, creating a complex climate feedback (Monson et al., 1992). Vegetation and fungi also directly emit primary organic aersols in the form of pollen and spores (Heald and Spracklen, 2009; Despres et al., 2012).

Activity of the biosphere is also instrumental in the global nitrogen cycle. Archae and bacteria in the roots of some plants fix atmospheric N_2 to ammonium (NH_4^+) (Franche et al.,

2009). Autotrophic nitrifying bacteria oxidize this ammonium to nitrate, both of which are usable forms of nitrogen for plants. Denitrification by anaerobic bacteria reduces nitrate and nitrite back to N_2. Nitrous oxide (N_2O) and nitric oxide (NO) are major bi-products of denitrification (Aulakh et al., 1992). Consequently, these nitrogen-containing gases are released to the atmosphere (Bouwman, 1996; Davidson and Kingerlee, 1997). Nitrous oxide is an inert and potent greenhouse gas, and nitric oxide is a highly reactive form of nitrogen that, as will be discussed in the following section, drives radical chain reactions in the atmosphere.

1.2 The role of NO_x in chemical oxidation in the troposphere

Although trace gases constitute only a tiny fraction of air, they are responsible for driving vast majority of the chemistry in the atmosphere. Trace gas chemistry has important consequences for human and ecosystem health, agricultural productivity, climate, weather, and equity. Globally, exposure to poor air quality leads to approximately 2 million excess deaths per year (Forouzanfar et al., 2015). The passage of the Clean Air Act in 1970 has led to a substantial improvement of the air quality in the United States over the past fifty years (Samet, 2011). However, hundreds of millions of people in the US are still exposed to concentrations of air pollutants, particularly ozone (O_3) and fine particulate matter ($PM_{2.5}$) that exceed national ambient air quality standards (Environmental Protection Agency Air Data, 2020).

Although ozone is essential to the absorption of ultraviolet radiation in the stratosphere, in the troposphere (the region of the atmosphere extending from the surface to ∼10—18 km above sea level), particularly in urban areas, O_3 is a major pollutant that has adverse respiratory health effects and and causes damage to plants (Seinfeld and Pandis, 2006; Jacob, 1999). The concentration of O_3 in the troposphere can be particularly difficult to control, as it is non-linearly dependent on the emissions of nitrogen oxides ($NO_x \equiv NO_2 + NO$) and volatile organic compounds (VOCs), as well as on temperature (Thornton et al., 2002; Pusede and Cohen, 2012; Pusede et al., 2014; Romer et al., 2018, e.g.). Pre-industrial backgrounds of ozone, resulting from slow transport from the stratosphere (where it is produced in large amounts by photochemical reactions of oxygen) and reactions of biogenic NO and VOCs, were typically 5—20 ppb (10^{-9} mol mol^{-1}). Due to anthropogenic (caused by human activity) emissions of NO_x, methane, carbon monoxide, and other VOCs, the present ozone background in clean surface air is 20—50 ppb (Jacob, 1999; Seinfeld and Pandis, 2006; Cooper et al., 2012). The US Environmental Protection Agency has recommended that the 8-hour average of O_3 not exceed 70 ppb. The highest concentrations of O_3, in the US occurs in the Los Angeles basin, the San Joaquin Valley, eastern Texas, industrial Midwestern regions, and mid-Alantic eastern states, where concentrations frequently exceed this 70 ppb limit.

Trospheric ozone is produced through the reaction of VOCs, NO_x, reactive hydrogen

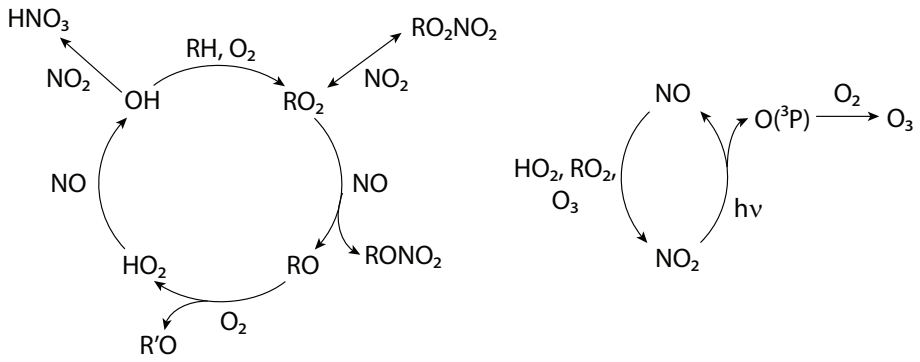

Figure 1.1: Radical propagation and termination reactions leading to the production of ozone and loss of NO_x in the troposphere.

species ($HO_x \equiv OH + HO_2$), and organic peroxy radicals (RO_2) (Fig. 1.1) (Jacob, 1999; Seinfeld and Pandis, 2006; Stockwell et al., 2011). The chain reaction of ozone formation is initiated by sunlight ≈80% by R1.1 and R1.2 and with more minor, but important, radical production from R1.3 and R1.4:

$$O_3 + h\nu \longrightarrow O_2 + O(^1D) \quad (R\,1.1)$$

$$O(^1D) + H_2O \longrightarrow 2\,OH \quad (R\,1.2)$$

$$H_2CO + h\nu \xrightarrow{O_2} 2\,HO_2 \quad (R\,1.3)$$

$$HONO + h\nu \longrightarrow NO + OH \quad (R\,1.4)$$

The rate of OH production is determined by the photolysis frequency, which is dependent on the flux of solar radiation. The OH radicals react with VOCs by either hydrogen abstraction or addition to a double bond (in the case of alkenes) (Jacob, 1999; Seinfeld and Pandis, 2006; Stockwell et al., 2011). Both pathways result in the formation of RO_2.

$$OH + RH \xrightarrow{O_2} RO_2 + H_2O \quad (R\,1.5)$$

$$RO_2 + NO \longrightarrow RO + NO_2 \quad (R\,1.6)$$

The RO radical subsequently reacts with molecular oxygen to form an aldehyde or ketone. RO can also decompose or isomerize to form a range of carbonyl products.

$$RO + O_2 \longrightarrow R'CHO + HO_2 \quad (R\,1.7)$$

$$HO_2 + NO \longrightarrow OH + NO_2 \quad (R\,1.8)$$

Each molecule of NO_2 produced in this reaction mechanism is photolyzed by sunlight, serving as the primary tropospheric source of $O(^3P)$. $O(^3P)$ is a highly reactive radical that rapidly recombines with molecular oxygen to produce ozone (Crutzen, 1979):

$$NO_2 + h\nu \longrightarrow O(^3P) + NO \quad (R\,1.9)$$

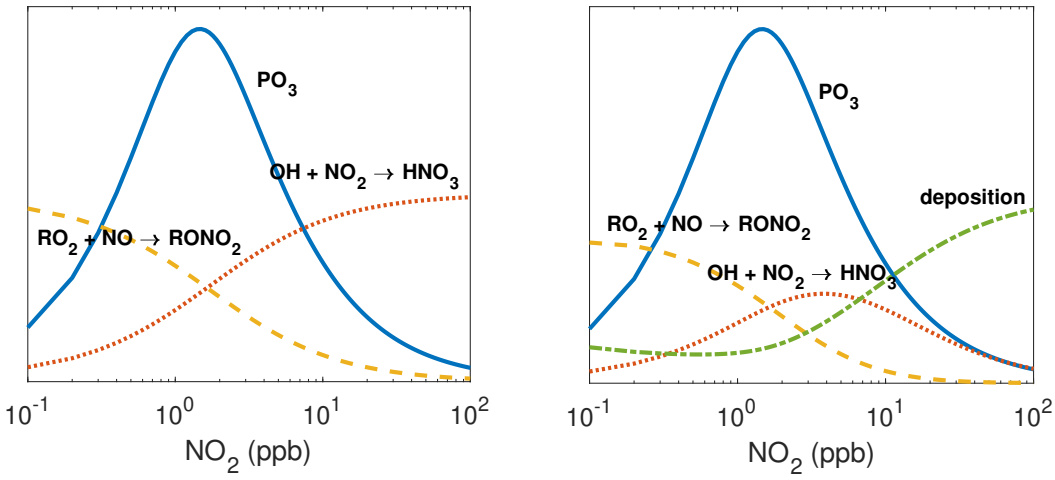

Figure 1.2: The production of ozone, alkyl nitrates, and nitric acid from NO_x (left) without, and (right) with deposition to vegetation considered. To generate this figure the fraction of the RO_2 + NO reaction that forms $RONO_2$ was set to 7.5%, the VOC reactivity with OH (VOCR) was set to 4 s^{-1}, and the production rate of HO_x was set to 1×10^6 molecules cm^{-3} s^{-1}.

$$O(^3P) + O_2 \longrightarrow O_3 \qquad \text{(R 1.10)}$$

The resulting net reaction for the catalysis of ozone formation in the troposphere is thus (Jacob, 1999; Seinfeld and Pandis, 2006; Stockwell et al., 2011):

$$\text{Net:}\quad RH + 4\,O_2 \longrightarrow R'CHO + 2\,O_3 + H_2O$$

NO_x is emitted to the atmosphere through fossil fuel burning, forest fires, and lightning–high temperature processes leading to the dissociation of N_2 (Seinfeld and Pandis, 2006). NO_x is also emitted through the soil microbial processes of nitrification and de-nitrification (Caranto and Lancaster, 2017). Ozone production can be reduced either through decreasing emissions of NO_x or VOCs. However, the emission of VOCs from vegetation creates a large biogenic background (e.g König et al., 1995; Sindelarova et al., 2014; Karl et al., 2003) that limits the effectiveness of reducing VOC emissions. Typically, constraining the production of surface ozone requires controlling emissions of NO_x (Pusede and Cohen, 2012; Pusede et al., 2014). Fig. 1.2 shows the production of ozone as a function of NO_x mixing ratio. At low concentrations of NO_x, increases in NO_x mixing ratios causes more efficient radical cycling, greater OH concentrations and more ozone production. In very high NO_x conditions, further increases in NO_x augments the efficiency of the chain terminating reactions:

$$RO_2 + NO \longrightarrow (1-\alpha)RO + (1-\alpha)NO_2 + \alpha RONO_2 \qquad \text{(R 1.11)}$$

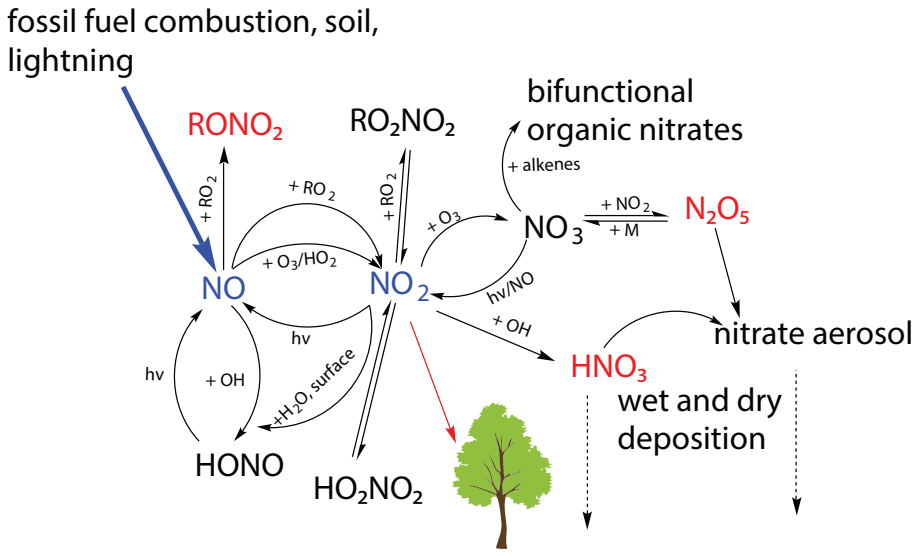

Figure 1.3: Sources, sinks, and reactions of NO_x in the troposphere.

$$OH + NO_2 \longrightarrow HNO_3 \qquad \text{(R 1.12)}$$

where α is the fraction of the $NO + RO_2$ reaction that is chain-terminating, producing an alkyl nitrate (Jacob, 1999; Romer et al., 2018). The reactions R1.11 and R1.12–forming alkyl nitrates and nitric acid–serve as the primary chemical sinks of NO_x. Although it is relatively less well-understood, NO_x has also been shown in a number of direct laboratory measurements (e.g. Sparks et al., 2001; Teklemmariam and Sparks, 2006; Chaparro-Suarez et al., 2011; Breuninger et al., 2013; Delaria et al., 2018, 2020), and indirect field observations (e.g. Jacob and Wofsy, 1990; Geddes and Murphy, 2014) to deposit directly to vegetation.

Understanding the budgets and lifetimes of NO_x requires understanding both its production and loss processes, including this deposition to vegetation. Figure 1.3 shows the complex physical and chemical processes controlling the budgets of NO_x and its higher oxidized forms.

1.3 Canopy-processes: The exchange of NO_x between the atmosphere and biosphere

In a remote forested environment, the primary source of NO_x to the atmosphere is emission from soil microbial activities, mostly in the form of NO. This NO reacts with O_3 to form NO_2, and the two are rapidly inter-converted on the order of a few minutes (Crutzen, 1979). Only a fraction of the soil-emitted NO_x is ventilated above the canopy (Yienger and Levy, 1995; Jacob and Wofsy, 1990). Deposition of NO_x to trees and understory vegetation has long been thought to be an important cause of this canopy NO_x reduction (Lerdau et al., 2000). Indeed, many laboratory leaf-level chamber experiments have directly measured the

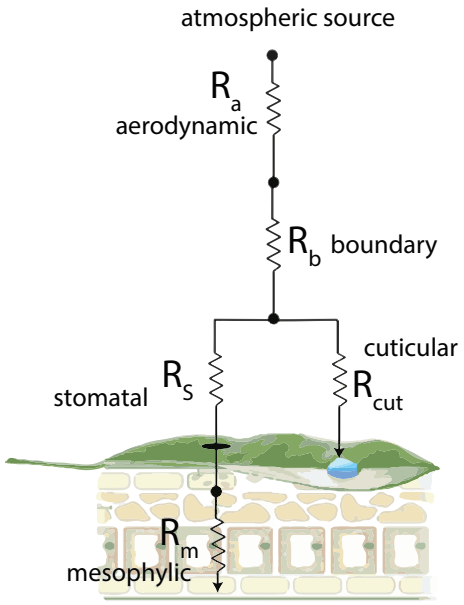

Figure 1.4: Resistance model for the deposition of an atmospheric trace gas to a leaf.

foliar uptake of NO_x, primarily in the form of NO_2. Many atmospheric models have employed a "canopy reduction factor" to account for the loss of NO_x within the canopy (e.g. Yienger and Levy, 1995). However, this parameter is non-physical and acts only on NO_x emitted below the canopy (i.e. not NO_x advected from near-by anthropogenic sources that also has the potential to deposit). A more physical way to think of of the loss of NO_x within the canopy is as a flux process:

$$Flux = -V_d \cdot LAI \cdot [NO_x] \tag{1.1}$$

where LAI is the leaf area index–the ratio of the total leaf area in a region to the ground area–and V_d is the deposition velocity. Many direct leaf-level laboratory measurements have also observed emission, rather than deposition, of NO_2 and NO at the low NO_x mixing ratios relevant to remote forested environments. This would imply that vegetation acts as an additional 10^{10} molecules cm^{-2} s^{-1} emission source of NO_x, contrary to field observations suggesting an equivalent sink of NO_x (Lerdau et al., 2000). The ambient NO_x concentration at which vegetation instead acts as a source of NO_x is known as the compensation point. Compensation points in laboratory experiments have been sometimes observed (Gessler et al., 2000; Sparks et al., 2001; Hereid and Monson, 2001; Teklemmariam and Sparks, 2006) and sometimes not (Breuninger et al., 2013; Chaparro-Suarez et al., 2011; Delaria et al., 2018, 2020).

The deposition of trace gases, like NO_x, to vegetation is often thought of using the resistance model framework of Baldocchi et al. (1987) (Fig. 1.4). An atmospheric source of NO_x must pass through a series of "barriers", analogous to resistors in an electrical circuit. Transfer of a trace gas over each of these "barriers" is a steady-state process. The first

resistor is the aerodynamic resistance (R_a), which describes the resistance associated with a trace gas diffusing through a turbulently flowing parcel of air and reaching the surface of a leaf. This parameter is dependent upon the diffusivity of the gas in question and the wind speed. The second resistor is the boundary layer resistance (R_b) and represents the diffusion of a trace gas through a region of laminarly flowing air layer directly above a leaf surface. This parameter is dependent upon microscopic surface properties of the leaf and trace gas diffusivity. Once a trace gas reaches the leaf surface, it can either deposit directly to the cuticles (i.e. leaf surface), or diffuse through the stomata–pores in the leaf through which CO_2, O_2, and H_2O are exchanged through the processes of photosynthesis, respiration, and transpiration. The stomatal aperture is controlled through a variety of plant signaling processes dependent on air humidity, temperature, soil water availability, availability of sunlight, and the CO_2 mixing ratio, among other factors (Jarvis, 1976; Emberson et al., 2000; Medlyn et al., 2011; Bonan et al., 2014). Once the trace gas enters into the stomata, it can undergo hydrolysis, enzymatic reactions, etc. within the leaf tissue. This later step determines the resistance of the mesophyll (R_m). Many different gases can deposit to leaves in this manner, most notably VOCs, O_3, H_2O_2, HNO_3, peroxyacyl nitrate, and alkyl nitrates. In the case of NO_2, the currently understood mechanism of uptake is dissolution into the aqueous phase of the apoloplasts to form nitrate and nitrite, and subsequent reaction with nitrate reductase to form ammonium (Ammann et al., 1995; Tischner, 2000). Isotope labelling experiments with ^{15}N have demonstrated atmospheric NO_2 is assimilated into amino acids of plant leaves (Rogers et al., 1979; Okano and Totsuka, 1986; Nussbaum et al., 1993). It has also been suggested that a significant fraction of a plant's nitrogen can be obtained through atmospheric nitrogen (Templer et al., 2015). Deposition of NO_x can thus have important consequences on the regional oxidative capacity of the troposphere, ecosystem nitrogen inputs, ozone production, the atmospheric lifetime of NO_x, and air quality.

Although there are a number of studies on leaf-level deposition of NO_x the understanding of the processes governing foliar uptake remains incomplete. In addition to discrepancies over the existence of a compensation point, previous investigations have also resulted in a wide range of deposition velocities for tree species in the same land category (i.e. evergreen needleleaf, evergreen broadleaf, deciduous broadleaf, etc.). These land classifications are used in global chemical transport models for representing foliar deposition (Zhang et al., 2003). Studies have also disagreed on the degree of mesophyllic influence on the total uptake rate–with some (e.g Chaparro-Suarez et al., 2011) finding the deposition rates essentially equivalent to the stomatal conductance, and others (e.g Breuninger et al., 2012) finding substantially lower rates. There is thus a need for further studies on the deposition of NO_x to a wider range of plant species, under a broad spectrum of conditions.

In this dissertation I present new understandings of the deposition of NO_x to trees and the impacts of this deposition pathway on the atmospheric NO_x budget and ozone production.

In Chapter 2 I present laboratory measurements for the first time of NO_2 and NO deposition to the leaves a North American tree species, in this case *Quercus agrifolia*. The method used for detecting NO_2 is laser-induced fluorescence–a highly sensitive and specific detection method previously used in a number of field experiments (e.g. Thornton et al., 2000; Min

et al., 2014; Nault et al., 2015; Romer et al., 2016). I show that the rates of deposition measured can account for canopy reduction factors and serve as an significant loss process for NO_x, competitive with its chemical sinks. I argue that the the bi-directional exchange of NO is atmospherically negligible compared with the large uni-directional deposition flux of NO_2. I also find no evidence of any emission from leaves at a concentration of zero ppb NO_x, further calling in question the existence of a compensation point.

In Chapter 3 I describe a multi-box 1D model I have constructed to examine the impacts of leaf-level NO_x deposition on the canopy scale. I investigate the effects of different model parameterizations of stomatal conductance on the deposition of NO_2, and subsequently on ozone production, NO_x lifetimes, and NO_x canopy fluxes. Although relative humidity, temperature, solar light intensity, season, CO_2 mixing ratios, ozone levels, and soil moisture are all known to affect the degree of stomatal opening, only temperature and light intensity are currently included in global chemical transport models. I find that the effects of humidity and soil moisture will be crucial additions to these models and can greatly influence predictions of NO_x deposition, particularly in areas, like California, with frequent droughts. I argue that relatively small changes in stomatal conductance can have substantial effects on ozone production, NO_x lifetimes, and NO_x canopy fluxes.

In Chapter 4 I investigate the deposition of NO_2 to ten native California tree species–six conifers and four broadleaf species–and consider evidence for contribution of the mesophyllic resistance to the total deposition rate. I also examine the effects of drought stress and excess soil nitrogen on the mesophyllic resistance. I again find no evidence of any compensation point, and, although I observe significant indications of the existence of a mesophyllic resistance, argue that this mesophyllic resistance is atmospherically irrelevant. I also report substantial nighttime stomatal opening during these laboratory measurements–a phenomenon not currently considered in atmospheric models, which I show may have a substantial impact on the fate and lifetime of NO_x at night. I conclude there is a considerable degree of interspecies variability in stomatal opening, and consequently on NO_2 deposition, which would have meaningful regional ramifications for the NO_x cycle.

In Chapter 5 I conclude with a discussion of the implications of the results presented in these works on regional and global budgets of NO_x and recommend areas for future investigation.

1.4 References

IPCC: Climate Change 2013: The Physical Science Basis. Contribution of Working Group I to the Fifth Assessment Report of the Intergovernmental Panel on Climate Change, Tech. rep., IPCC, 2013.

Environmental Protection Agency Air Data: Ozone Exceedances, online database, URL https://www.epa.gov/outdoor-air-quality-data, 2020.

Ammann, M., von Ballmoos, P., Stalder, M., Suter, M., and Brunold, C.: Uptake and assimilation of atmospheric NO2 — N by spruce needles (Picea abies): A field study, Water Air and Soil Pollution, 85, 1497–1502, https://doi.org/10.1007/BF00477193, 1995.

Atkinson, R.: Atmospheric chemistry of VOCs and NOx. Atmos Environ 34:2063-2101, Atmospheric Environment, 34, 2063–2101, https://doi.org/10.1016/S1352-2310(99)00460-4, 2013.

Aulakh, M., Doran, J., and Mosier, A.: Soil Denitrification—Significance, Measurement, and Effects of Management, vol. 18, pp. 1–57, https://doi.org/10.1007/978-1-4612-2844-8_1, 1992.

Baldocchi, D. D., Hicks, B. B., and Camara, P.: A canopy stomatal resistance model for gaseous deposition to vegetated surfaces, Atmospheric Environment (1967), 21, 91 – 101, https://doi.org/10.1016/0004-6981(87)90274-5, 1987.

Bonan, G., Williams, M., Fisher, R., and Oleson, K.: Modeling stomatal conductance in the Earth system: Linking leaf water-use efficiency and water transport along the soil-plant-atmosphere continuum, Geoscientific Model Development, 7, 2193–2222, https://doi.org/10.5194/gmd-7-2193-2014, 2014.

Bouwman, A.: Direct emission of nitrous oxide from agricultural soils, Nutrient Cycling in Agroecosystems, 46, 53–70, https://doi.org/10.1007/BF00210224, 1996.

Breuninger, C., Oswald, R., Kesselmeier, J., and Meixner, F. X.: The dynamic chamber method: trace gas exchange fluxes (NO, NO_2, O_3) between plants and the atmosphere in the laboratory and in the field, Atmospheric Measurement Techniques, 5, 955–989, https://doi.org/10.5194/amt-5-955-2012, 2012.

Breuninger, C., Meixner, F. X., and Kesselmeier, J.: Field investigations of nitrogen dioxide (NO_2) exchange between plants and the atmosphere, Atmospheric Chemistry and Physics, 13, 773–790, https://doi.org/10.5194/acp-13-773-2013, 2013.

Caranto, J. and Lancaster, K.: Nitric oxide is an obligate bacterial nitrification intermediate produced by hydroxylamine oxidoreductase, Proceedings of the National Academy of Sciences, 114, 201704 504, https://doi.org/10.1073/pnas.1704504114, 2017.

Chaparro-Suarez, I., Meixner, F., and Kesselmeier, J.: Nitrogen dioxide (NO2) uptake by vegetation controlled by atmospheric concentrations and plant stomatal aperture, Atmospheric Environment, 45, 5742 – 5750, https://doi.org/10.1016/j.atmosenv.2011.07.021, 2011.

Cooper, O., Gao, R.-S., Tarasick, D., Leblanc, T., and Sweeney, C.: Long-term ozone trends at rural ozone monitoring sites across the United States, 1990-2010, Journal of Geophysical Research (Atmospheres), 117, 22 307–, https://doi.org/10.1029/2012JD018261, 2012.

Crutzen, P. J.: The Role of NO and NO2 in the Chemistry of the Troposphere and Stratosphere, Annual Review of Earth and Planetary Sciences, 7, 443–472, https://doi.org/10.1146/annurev.ea.07.050179.002303, 1979.

Davidson, E. and Kingerlee, W.: A global inventory of nitric oxide emissions from soils, Nutrient Cycling in Agroecosystems, 48, 37–50, https://doi.org/10.1023/A:1009738715891, 1997.

Delaria, E., Vieira, M., Cremieux, J., and Cohen, R.: Measurements of NO and NO2 exchange between the atmosphere and Quercus agrifolia, Atmospheric Chemistry and Physics, 18, 14 161–14 173, https://doi.org/10.5194/acp-18-14161-2018, 2018.

Delaria, E. R., Place, B. K., Liu, A. X., and Cohen, R. C.: Laboratory measurements of stomatal NO2 deposition to native California trees and the role of forests in the NOx cycle, Atmospheric Chemistry and Physics Discussions, 2020, 1–32, https://doi.org/10.5194/acp-2020-240, 2020.

Despres, V., Huffman, J., Burrows, S., Hoose, C., Safatov, A., Buryak, G., Fröhlich-Nowoisky, J., Elbert, W., Andreae, M., Pöschl, U., and Jaenicke, R.: Primary biological aerosols in the atmosphere: a review, Tellus B, 64, 1–58, 2012.

Emberson, L., Ashmore, M., Cambridge, H., Simpson, D., and Tuovinen, J.: Modelling stomatal flux across Europe, Environmental pollution (Barking, Essex : 1987), 109, 403–13, https://doi.org/10.1016/S0269-7491(00)00043-9, 2000.

Forouzanfar, M., Alexander, L., Anderson, H., Tellez Rojo Solis, M. M., Bachman, V., Biryukov, S., Brauer, M., Burnett, R., Casey, D., Coates, M., Cohen, A., Delwiche, K., Estep, K., Frostad, J., Kc, A., Kyu, H., Moradi-Lakeh, M., Ng, M., Slepak, E., and Murray, C.: Global, regional, and national comparative risk assessment of 79 behavioural, environmental and occupational, and metabolic risks or clusters of risks in 188 countries, 1990–2013: A systematic analysis for the Global Burden of Disease Study 2013, The Lancet, 386, 2287–2323, https://doi.org/10.1016/S0140-6736(15)00128-2, 2015.

Franche, C., Lindström, K., and Elmerich, C.: Nitrogen-fixing bacteria associated with leguminous and non-leguminous plants, Plant and Soil, 321, 35–59, https://doi.org/10.1007/s11104-008-9833-8, 2009.

Geddes, J. A. and Murphy, J. G.: Observations of reactive nitrogen oxide fluxes by eddy covariance above two midlatitude North American mixed hardwood forests, Atmospheric Chemistry and Physics, 14, 2939–2957, https://doi.org/10.5194/acp-14-2939-2014, 2014.

Gessler, A., Rienks, M., and Rennenberg, H.: NH3 and NO2 fluxes between beech trees and the atmosphere – correlation with climatic and physiological parameters, New Phytologist, 147, 539–560, https://doi.org/10.1046/j.1469-8137.2000.00712.x, 2000.

Heald, C. and Spracklen, D.: Heald CL, Spracklen DV.. Atmospheric budget of primary biological aerosol particles from fungal spores. Geophys Res Lett 36: L09806, Geophysical Research Letters, 36, https://doi.org/10.1029/2009GL037493, 2009.

Hereid, D. and Monson, R.: Nitrogen Oxide Fluxes between Corn (Zea mays L.) Leaves and the Atmosphere, Atmospheric Environment, 35, 975–983, https://doi.org/10.1016/S1352-2310(00)00342-3, 2001.

Jacob, D.: Introduction to Atmospheric Chemistry, Princeton University Press, Princeton, N.J., 1999.

Jacob, D. J. and Wofsy, S. C.: Budgets of reactive nitrogen, hydrocarbons, and ozone over the Amazon forest during the wet season, Journal of Geophysical Research: Atmospheres, 95, 16 737–16 754, https://doi.org/10.1029/JD095iD10p16737, 1990.

Jarvis, P.: The Interpretation of the Variations in Leaf Water Potential and Stomatal Conductance Found in Canopies in the Field, Philosophical Transactions of the Royal Society of London. Series B, Biological Sciences, 273, 593–, https://doi.org/10.1098/rstb.1976.0035, 1976.

Karl, T., Guenther, A., Spirig, C., Hansel, A., and Fall, R.: Seasonal variation of biogenic VOC emissions above a mixed hardwood forest in northern Michigan, Geophysical Research Letters, 30, https://doi.org/10.1029/2003GL018432, 2003.

König, G., Brunda, M., Puxbaum, H., Hewitt, C. N., Duckham, C., and Rudolph, J.: Relative contribution of oxygenated hydrocarbons to the total biogenic VOC emissions of selected mid-European agricultural and natural plant species, Atmospheric Environment, 29, 861–874, https://doi.org/10.1016/1352-2310(95)00026-U, 1995.

Lerdau, M. T., Munger, J. W., and Jacob, D. J.: The NO2 Flux Conundrum, Science, 289, 2291–2293, https://doi.org/10.1126/science.289.5488.2291, 2000.

Medlyn, B., Duursma, R., Eamus, D., and Ellsworth, D.: Reconciling the optimal and empirical approaches to modelling stomatal conductance, Global Change Biology, 2011.

Min, K.-E., Pusede, S. E., Browne, E. C., LaFranchi, B. W., and Cohen, R. C.: Eddy covariance fluxes and vertical concentration gradient measurements of NO and NO_2 over a ponderosa pine ecosystem: observational evidence for within-canopy chemical removal of NO_x, Atmospheric Chemistry and Physics, 14, 5495–5512, https://doi.org/10.5194/acp-14-5495-2014, 2014.

Monson, R. K., Jaeger, C. H., Adams, W. W., Driggers, E. M., Silver, G. M., and Fall, R.: Relationships among Isoprene Emission Rate, Photosynthesis, and Isoprene Synthase Activity as Influenced by Temperature, Plant Physiology, 98, 1175–1180, https://doi.org/10.1104/pp.98.3.1175, 1992.

Nault, B., Garland, C., Wooldridge, P., Brune, W., Campuzano-Jost, P., Crounse, J., Day, D., Dibb, J., Hall, S., Huey, L., Jimenez, J. L., Liu, X., Mao, J., Mikoviny, T., Peischl, J., Pollack, I., Ren, X., Ryerson, T., Scheuer, E., and Cohen, R.: Observational Constraints on the Oxidation of NOx in the Upper Troposphere, The Journal of Physical Chemistry A, 120, https://doi.org/10.1021/acs.jpca.5b07824, 2015.

Nussbaum, S., von Ballmoos, P., Gfeller, H., Schlunegger, U., Fuhrer, J., Rhodes, D., and Brunold, C.: Incorporation of atmospheric 15NO2 -nitrogen into free amino acids by Norway spruce Picea abies (L.) Karst, Oecologia, 94, 408–414, https://doi.org/10.1007/BF00317117, 1993.

Okano, K. and Totsuka, T.: Absorption of nitrogen dioxide by sunflower plants grown at various levels of nitrate, New Phytologist, 102, 551–562, https://doi.org/10.1111/j.1469-8137.1986.tb00831.x, 1986.

Pusede, S. E. and Cohen, R. C.: On the observed response of ozone to NOx and VOC reactivity reductions in San Joaquin Valley California 1995-present, Atmospheric Chemistry and Physics, 12, 8323–8339, https://doi.org/10.5194/acp-12-8323-2012, 2012.

Pusede, S. E., Gentner, D. R., Wooldridge, P. J., Browne, E. C., Rollins, A. W., Min, K.-E., Russell, A. R., Thomas, J., Zhang, L., Brune, W. H., Henry, S. B., DiGangi, J. P., Keutsch, F. N., Harrold, S. A., Thornton, J. A., Beaver, M. R., St. Clair, J. M., Wennberg, P. O., Sanders, J., Ren, X., VandenBoer, T. C., Markovic, M. Z., Guha, A., Weber, R., Goldstein, A. H., and Cohen, R. C.: On the temperature dependence of organic reactivity, nitrogen oxides, ozone production, and the impact of emission controls in San Joaquin Valley, California, Atmospheric Chemistry and Physics, 14, 3373–3395, https://doi.org/10.5194/acp-14-3373-2014, 2014.

Rogers, H. H., Jeffries, H. E., and Witherspoon, A. M.: Measuring Air Pollutant Uptake by Plants: Nitrogen Dioxide, Journal of Environmental Quality, 8, 551–557, https://doi.org/10.2134/jeq1979.00472425000800040022x, 1979.

Romer, P. S., Duffey, K. C., Wooldridge, P. J., Allen, H. M., Ayres, B. R., Brown, S. S., Brune, W. H., Crounse, J. D., de Gouw, J., Draper, D. C., Feiner, P. A., Fry, J. L., Goldstein, A. H., Koss, A., Misztal, P. K., Nguyen, T. B., Olson, K., Teng, A. P., Wennberg, P. O., Wild, R. J., Zhang, L., and Cohen, R. C.: The lifetime of nitrogen oxides in an isoprene-dominated forest, Atmospheric Chemistry and Physics, 16, 7623–7637, https://doi.org/10.5194/acp-16-7623-2016, 2016.

Romer, P. S., Duffey, K. C., Wooldridge, P. J., Edgerton, E., Baumann, K., Feiner, P. A., Miller, D. O., Brune, W. H., Koss, A. R., de Gouw, J. A., Misztal, P. K., Goldstein, A. H., and Cohen, R. C.: Effects of temperature-dependent NO_x emissions on continental ozone production, Atmospheric Chemistry and Physics, 18, 2601–2614, https://doi.org/10.5194/acp-18-2601-2018, 2018.

Samet, J.: The Clean Air Act and Health — A Clearer View from 2011, The New England journal of medicine, 365, 198–201, https://doi.org/10.1056/NEJMp1103332, 2011.

Schlesinger, W. and Jasechko, S.: Transpiration in the global water cycle, Agricultural and Forest Meteorology, s 189–190, 115–117, https://doi.org/10.1016/j.agrformet.2014.01.011, 2014.

Seinfeld, J. and Pandis, S.: Atmospheric Chemistry and Physics: From Air Pollution to Climate Change, A Wiley-Interscience publication, Wiley, 2006.

Sindelarova, K., Granier, C., Bouarar, I., Guenther, A., Tilmes, S., Stavrakou, T., Müller, J.-F., Kuhn, U., Stefani, P., and Knorr, W.: Global dataset of biogenic VOC emissions calculated by the MEGAN model over the last 30 years, Atmospheric Chemistry and Physics, 14, 10 725–10 788, https://doi.org/10.5194/acp-14-9317-2014, 2014.

Sparks, J., Monson, R., Sparks, K., and Lerdau, M.: Leaf uptake of nitrogen dioxide (NO2) in a tropical wet forest: Implications for tropospheric chemistry, Oecologia, 127, 214–221, https://doi.org/10.1007/s004420000594, 2001.

Stockwell, W., Lawson, C., Saunders, E., and Goliff, W.: A Review of Tropospheric Atmospheric Chemistry and Gas-Phase Chemical Mechanisms for Air Quality Modeling, Atmosphere, 3, 1–32, https://doi.org/10.3390/atmos3010001, 2011.

Teklemmariam, T. and Sparks, J.: Leaf fluxes of NO and NO2 in four herbaceous plant species: The role of ascorbic acid, Atmospheric Environment, 40, 2235–2244, https://doi.org/10.1016/j.atmosenv.2005.12.010, 2006.

Templer, P., Weathers, K., Ewing, H., Dawson, T., Mambelli, S., Lindsey, A., Webb, J., Boukili, V., and Firestone, M.: Fog as a source of nitrogen for redwood trees: Evidence from fluxes and stable isotopes, Journal of Ecology, 103, 1397–1407, https://doi.org/10.1111/1365-2745.12462, 2015.

Thornton, J. A., Wooldridge, P. J., and Cohen, R. C.: Atmospheric NO2: In Situ Laser-Induced Fluorescence Detection at Parts per Trillion Mixing Ratios, Analytical Chemistry, 72, 528–539, https://doi.org/10.1021/ac9908905, pMID: 10695138, 2000.

Thornton, J. A., Wooldridge, P. J., Cohen, R. C., Martinez, M., Harder, H., Brune, W. H., Williams, E. J., Roberts, J. M., Fehsenfeld, F. C., Hall, S. R., Shetter, R. E., Wert, B. P., and Fried, A.: Ozone production rates as a function of NOx abundances and HOx production rates in the Nashville urban plume, Journal of Geophysical Research: Atmospheres, 107, ACH 7–1–ACH 7–17, https://doi.org/10.1029/2001JD000932, 2002.

Tischner, R.: Nitrate uptake and reduction in higher and lower plants, Plant, Cell & Environment, 23, 1005–1024, https://doi.org/10.1046/j.1365-3040.2000.00595.x, 2000.

Yienger, J. J. and Levy, H.: Empirical model of global soil-biogenic NO emissions, Journal of Geophysical Research: Atmospheres, 100, 11 447–11 464, https://doi.org/10.1029/95JD00370, 1995.

Zhang, L., Brook, J., and R, V.: A revised parameterization for gaseous dry deposition in air-quality models, Atmospheric Chemistry and Physics, 3, https://doi.org/10.5194/acpd-3-1777-2003, 2003.

Chapter 2

Measurements of NO and NO_2 exchange between the atmosphere and *Quercus agrifolia*

Adapted from E. R. Delaria et al., Measurements of NO and NO_2 exchange between the atmosphere and Quercus agrifolia, *Atmos. Chem. Phys.*, 18, 14161—14173, https://doi.org/10.5194/acp-18-14161-2018, 2018.

2.1 Introduction

Nitrogen oxides ($NO_x \equiv NO+NO_2$) are a group of highly reactive trace gases that control the oxidative capacity of the atmosphere by regulating the amounts of ozone, hydroxyl radicals, volatile organic compounds, and other key atmospheric species (Crutzen, 1979). NO_x is also directly toxic in high concentrations, plays a major role in tropospheric ozone production, and serves as a source of NO_3^-, a key nutrient for ecosystems and a component of acid rain. NO_x is primarily emitted as nitric oxide (NO) through fossil fuel combustion, biomass burning, lightning, and microbial activity in soils (Seinfeld and Pandis, 2006). NO is rapidly oxidized to nitrogen dioxide (NO_2) through reactions with ozone and peroxy radicals, and in the daytime NO_2 subsequently photolyzes to re-form NO. The interconversion of NO and NO_2 reaches steady state within a few minutes during the daytime (Crutzen, 1979). The effects of NO_x on urban chemistry, where anthropogenic emissions dominate the NO_x source, have been extensively studied. However, the processes affecting NO_x in forested and agricultural regions are less well understood.

In forests and agricultural lands, the major source of NO_x is NO emitted as a by-product of microbial denitrification and nitrification (McKenney et al., 1982; Caranto and Lancaster, 2017). Deposition of NO_2 to plant canopies is thought to be an important sink of NO_x in forests, substantially reducing the contribution of soil-emitted NO_x to the atmospheric NO_x budget. Jacob and Wofsy (1990) observed low NO_x above the canopy over the Amazon forest

during the wet season. Using a 1-D chemical and transport model constrained by observed NO_x and ozone, they concluded that a substantial fraction of soil NO_x must be absorbed by the canopy. Extrapolation of these ideas to forests with different leaf area indices suggest that 20%—50% of the global fraction of soil-emitted NO_x is lost to vegetation (Yienger and Levy, 1995; Lerdau et al., 2000). Using the framework of Jacob and Wofsy (1990) and Yienger and Levy (1995), global atmospheric models have been tuned to describe observed atmospheric NO_x concentrations and tropospheric ozone production using a canopy reduction factor (CRF). The CRF is an adjustable parameter that accounts for the difference between soil NO emissions and the amount of NO_x ventilated through the canopy (Yienger and Levy, 1995; Vinken et al., 2014). However, CRFs are implemented in an unphysical manner where they act only on soil NO_x emissions and not on other NO_x present in the plant canopy. An improved understanding is needed of the physical and biochemical processes governing the foliar uptake of NO_x at the ecosystem and leaf scales.

Many studies have also directly observed the leaf-level uptake of NO_2 (Neubert et al., 1993; Rondón and Granat, 1994; Hereid and Monson, 2001; Sparks et al., 2001; Teklemmariam and Sparks, 2006; Pape et al., 2009; Chaparro-Suarez et al., 2011; Breuninger et al., 2013). Isotope labeling experiments investigating the mechanism of NO_2 uptake have demonstrated that atmospheric NO_2 can be absorbed through the stomata of plant leaves, converted to nitrate (NO_3^-) and nitrite (NO_2^-), and eventually assimilated into amino acids (Rogers et al., 1979; Okano and Totsuka, 1986; Nussbaum et al., 1993; Weber et al., 2006; Yoneyama et al., 2003). The mechanism of NO_2 assimilation is diffusion into the stomata followed by dissolution into the aqueous phase and disproportionation to NO_3^- and NO_2^- in the apoplasm (Lee and Schwartz, 1981). NO_2 can also be transformed to nitrate and nitrite through scavenging by antioxidants, most notably ascorbate (Ramge et al., 1993). The influence of ascorbate on foliar uptake was theoretically calculated by Ramge et al. (1993) and experimentally demonstrated by Teklemmariam and Sparks (2006). The enzyme nitrate reductase converts NO_3^- to NO_2^- in the cytosol, and NO_2^- is then transported into the plastids where it is further reduced by the enzyme nitrite reductase to ammonium (NH_4^+), the product required for amino acid synthesis (Ammann et al., 1995; Tischner, 2000; Teklemmariam and Sparks, 2006). Alternatively, NO_2 can deposit directly onto the leaf cuticles or a leaf-surface water film (Burkhardt and Eiden, 1994). However, foliar uptake of NO_2 has been demonstrated to be controlled primarily by the stomata, with deposition to the leaf surface representing only a small fraction of the total NO_2 flux (Thoene et al., 1991; Gessler et al., 2000; Chaparro-Suarez et al., 2011). Strong correlations have been observed among NO_2 concentrations, stomatal conductances, and the NO_2 deposition flux, suggesting foliar uptake is mainly controlled by stomatal aperture and internal leaf resistances (Johansson, 1987; Thoene et al., 1991; Rondón et al., 1993; Otter et al., 1999; Chaparro-Suarez et al., 2011; Breuninger et al., 2013).

Despite the large existing body of research on the leaf-level deposition of NO_2 to vegetation, there are still discrepancies present in NO_2 exchange rates and the role of mesophilic processes. Many laboratory experiments have failed to measure uptake rates necessary to describe the observed 20%—50% reduction of soil-emitted NO_x (Hanson and Lindberg, 1991;

Breuninger et al., 2013), despite the many modeling studies that have suggested dry deposition makes up most of this reduction (Jacob and Wofsy, 1990; Yienger and Levy, 1995; Ganzeveld et al., 2002b; Geddes and Murphy, 2014). Photolysis gradients and reaction of NO_x to form higher nitrogen oxides could account for a large fraction of this reduction in soil NO_x, as has been suggested by Min et al. (2012, 2014), but the relative importance of dry deposition processes versus in-canopy chemical transformations is still a matter of considerable uncertainty (Lerdau et al., 2000; Ganzeveld et al., 2002a). Another controversy is the existence of a compensation point – a concentration below which leaves would instead act as a source of NO_x. Compensation points of 0.1—3.2 ppb NO_2 have been observed in a number of laboratory chamber studies, suggesting trees instead may serve as a large source of NO_x in forests (Johansson, 1987; Rondón et al., 1993; Hereid and Monson, 2001; Sparks et al., 2001; Teklemmariam and Sparks, 2006). Emission of NO at these low NO_x mixing ratios has also been detected in laboratory chamber studies (Wildt et al., 1997; Hereid and Monson, 2001). More recent laboratory studies of leaf level deposition have, however, questioned the existence of a compensation point (Chaparro-Suarez et al., 2011; Breuninger et al., 2013). Most observations of NO_x canopy fluxes and atmospheric models predict or assume substantial NO_x deposition at concentrations as low as 0.1 ppb, typical of NO_x mixing ratios in remote areas (Jacob and Wofsy, 1990; Wang and Leuning, 1998; Lerdau et al., 2000; Sparks et al., 2001; Wolfe et al., 2011; Min et al., 2012; Geddes and Murphy, 2014). However, some modeling studies have suggested that an NO_2 compensation point is necessary to describe (Seok et al., 2013) or has only a small effect on canopy fluxes in most regions (Ganzeveld et al., 2002a). More research is thus needed on leaf and canopy-level processes to understand the full complexity of the soil–canopy–atmosphere system.

2.2 Materials and methods

Quercus agrifolia samples

NO_x uptake by *Quercus agrifolia* (coastal live oak) was investigated in the laboratory. Three *Quercus agrifolia* individuals were purchased from a local native California plant nursery (Native Here Nursery), where the plants were grown from seeds and cuttings collected in Contra Costa County. The tree specimens were grown in a nutrient-rich commercial soil mixture (a mixture of orchard potting soil and EB stone cactus mix) at the Jane Grey Research Greenhouse at the University of California, Berkeley. The trees were 2—3 years old when measurements were taken.

Laser-induced fluorescence detection

NO_2 was measured using LIF. A blue diode laser (Z-Laser ZM18H3) centered at a wavelength of 405 nm was focused into each detection cell and made 20 passes in White multipass optical configuration (Fig. 2.2b) (Thornton et al., 2000; Fuchs et al., 2009). Upon absorption of a

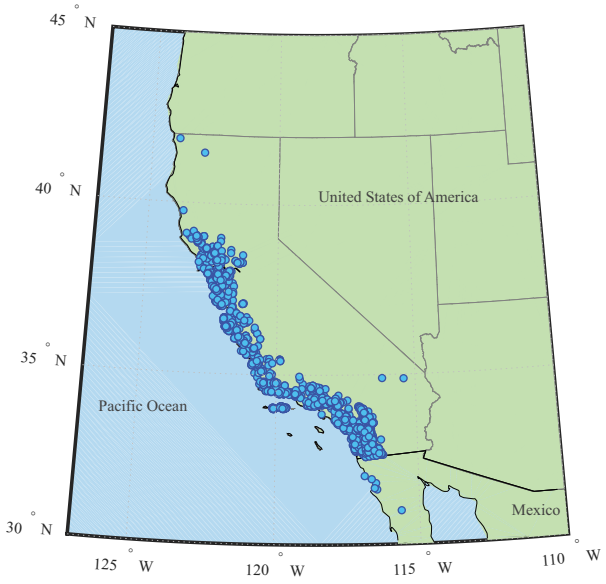

Figure 2.1: Species distribution map of *Quercus agrifolia*. Each dot represents an observation of *Q. agrifolia* occurrence. Data provided by the participants of the Consortium of California Herbaria.

visible photon, NO_2 undergoes a transition from the $^2A_1$ ground to the $^2B_2$ excited electronic state. The excited NO_2 molecule is either quenched by collision or emits a red-shifted photon as it relaxes back to ground state (e.g. Thornton et al., 2000). These emitted photons were detected using a red-sensitive photomultiplier tube (PMT) (Hamamatsu H7421-50). To minimize collisional quenching, each detection cell was maintained at a pressure of around 0.4 kPa. Excitation at 405 nm was chosen because it is near the region of maximum absorption in the NO_2 spectrum and is not subject to interferences from absorption by water vapor or O_3 (Matsumoto and Kajii, 2003).

Calibrations were performed every hour by diluting NO (4.97 ppm ± 5%, Praxair) and NO_2 standard gases (5.08 ppm ± 5%, Praxair) to 1—10ppb in humidified (RH ∼ 60%) zero air. The limit of detection (LOD) for the detection cells is described as follows:

$$LOD = \frac{S/N}{m}\sqrt{\frac{2b}{t}} \tag{2.1}$$

where m is the slope of the calibration curve constructed from standard dilutions, b is the PMT signal at 0 ppb NO or NO_2, S/N is the desired signal-to-noise ratio, and t is the time of signal averaging. At a S/N of 2 and signal averaging over 5 min, the LOD for detection cells

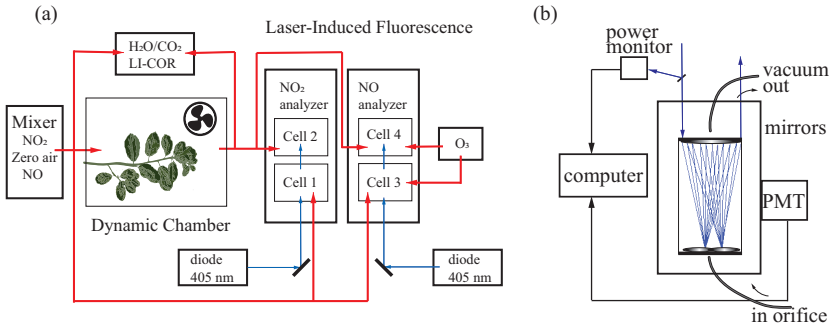

Figure 2.2: Schematic of the experimental dynamic chamber (a) and laser-induced fluorescence detection (b) setups.

1—4 was 15, 4, 10, and 30 ppt, respectively. NO_2 in the incoming and outgoing airstreams was measured simultaneously in the first two detection cells. In the second two detection cells, NO was quantitatively converted to NO_2 in the presence of excess ozone, allowing for detection of total NO_x (Fig. 2.2a). Ozone was produced using an ozone generator (Jelight 600), and flow rates of ozone delivered were adjusted to achieve unity conversion of NO to NO_2.

Dynamic chamber system

The NO_x flux measurements were performed with a dynamic branch enclosure system, consisting of a thin transparent double-walled Teflon film (FEP) bag (American Durafilm), which transmits 90% of photosynthetically active radiation. The chamber was illuminated by an LED diode array of 430—-475 and 620—-670 nm lights (Apollo Horticulture). This light source was selected because it does not emit wavelengths below 420 nm, where NO_2 dissociates, preventing loss of NO_2 to photodissociation and resultant photochemistry. In order to ensure turbulent mixing and minimal aerodynamic and boundary layer resistances, a Teflon-coated fan was installed inside the inner chamber (Otter et al., 1999; Pape et al., 2009; Breuninger et al., 2013).

Before experiments with Quercus agrifolia individuals, the deposition to an empty chamber was measured and background subtracted from subsequent branch measurements. The measured loss of NO_2 to chamber walls was 5% of the NO_2 mixing ratio flowing into the chamber. This corresponded to a maximum loss of 0.4 ppb at 8 ppb NO_2 and minimum loss of 0.05 ppb at 1 ppb NO_2. Emission of less than 0.05 ppb NO_2 from the Teflon walls was also observed when chamber lights were turned on with 0 ppb NO_2 flowing through the system. It is likely that the chamber walls buffer uptake of NO_2, but this is a minor effect,

as the wall emission observed was a tiny fraction of the measured fluxes.

During measurements, the enclosed branch was exposed to known amounts of either NO_2 or NO mixed with zero air. The inner chamber had an inner diameter of 20 cm, a length of 40 cm, and a total volume of 13 L (American Durafilm 200A Teflon FEP). Flow rates into the inner chamber (Q) during experiments were typically 5 L min^{-1}, creating a residence time in the chamber of 3 min. The outer chamber had an inner diameter of 30 cm and a length of 55 cm (American Durafilm 500C20 Teflon FEP). Zero air at a flow rate of 3 L min^{-1} constantly fumigated the outer bag, serving as a buffer region to ensure the laboratory air, with high mixing ratios of NO_x, did not diffuse into the bag enclosing the branch.

The photosynthetic photon flux density (PPFD) was monitored outside the chamber with a LiCor quantum sensor (LiCor LI-190SA). The flux density measured above the chamber was 1190 μmol m^{-2} s^{-1}, approximately the PPFD for Berkeley, California, at noon during the month of October. This is well above the photon flux required to achieve maximal stomatal aperture for broadleaf evergreen trees (von Caemmerer and Farquhar, 1981; Chaparro-Suarez et al., 2011; Breuninger et al., 2013). We confirmed this assumption by covering the lights with a filter to reduce the intensity by 40% and monitoring CO_2 and H_2O exchange. No reduction in the exchange rates of these gases were observed. The relative humidity of air entering the chamber was maintained at 50%—65% in all experiments by flowing zero air through a bubbler before mixing with NO_x. Measurements of NO_x exchange fluxes occurred under a light/dark cycle with a photoperiod of 12 h and a temperature of 26/22 $\pm$ 2 °C. No change in NO_x uptake was observed when heating the chamber with the lights off or cooling the chamber with the lights on. We therefore expect no significant temperature effects caused by the 4 °C difference in temperature between light and dark periods. We also observed a relative humidity increase in the delivered air of about 2% with the lights off, but do not expect this increase to produce any significant changes in NO_x deposition or plant physiology (von Caemmerer and Farquhar, 1981; Chaparro-Suarez et al., 2011).

Exchange of CO_2 and H_2O with the leaves were monitored with a LiCor-6262 H_2O/CO_2 analyzer operating in differential mode. Flows of 0.1 L min^{-1} of air entering and exiting the chamber were diverted to the LiCor analyzer to measure the CO_2 assimilation and transpiration rates. To measure the CO_2 content and relative humidity of air delivered to the chamber, 0.5 L min^{-1} of the humidified zero air/NO_x mixture was diverted to a second external 1.5 L cuvette. The temperature and relative humidity of air entering the chamber were measured with a temperature and relative humidity module in the external cuvette (TE Connectivity HTM2500LF). The CO_2 mixing ratios in the external chamber were monitored with a Vaisala CarboCap GMP343 sensor.

NO_x flux densities

The leaf-level exchange flux of NO or NO_2 (F_{NO_x}) was calculated according to Eq. (2.2):

$$F_{NO_x} = \frac{Q \cdot (C_0 - C_i)}{A} \tag{2.2}$$

where Q is the flow rate ($m^3\ s^{-1}$), A is the enclosed leaf area (m^2), C_0 is the concentration leaving the chamber, and C_i is the concentration entering the chamber (nmol m^{-3}). The calculated flux is related to a deposition velocity (Vd_{NO_x}) by Eq. (2.3):

$$F_{NO_x} = -Vd_{NO_x} \cdot (C_0 + C_{comp}) \tag{2.3}$$

where C_{comp} is the compensation point, the concentration of NO_2 below which the tree would instead act as a source of NO_x. The deposition velocities were calculated through weighted least-square regression of calculated fluxes and outlet NO_x concentrations (C_0). The absolute value of the slope of the regression line was equal to the deposition velocity, with the x-intercept representing the compensation point concentration. The precision error in the NO_x exchange flux (σ_F) was calculated through propagation of the uncertainties in the inlet (σ_{C_i}) and outlet (σ_{C_0}) concentrations (Eq. 2.4).

$$\sigma_F = \frac{Q}{A}\sqrt{\sigma_{C_i}^2 + \sigma_{C_0}^2} \tag{2.4}$$

σ_{C_i} and σ_{C_0} were estimated as the larger of the errors in the calibration slopes and the standard deviation of the 5 min signal average. From observations in daily deviations of the flow rate and uncertainty in measured leaf area using the ImageJ software (Schneider et al., 2012), we estimate the uncertainty in Q/A to be a maximum of 0.005 cm s^{-1}. This usually was only a minor contribution to the total error in the NO_x exchange flux.

The calculated deposition velocity was used to find the total resistance to deposition, R, via Eq. (2.5).

$$Vd_{NO_2} = \frac{1}{R} \tag{2.5}$$

The total resistance is described by the canopy stomatal resistance model (Baldocchi et al., 1987) and defined in Eqs. (2.6—2.7).

$$R = R_a + R_b + R_{leaf} \tag{2.6}$$

$$R_{leaf} + \left(\frac{1}{R_{cut}} + \frac{1}{R_{st} + R_m}\right)^{-1} \tag{2.7}$$

where R_{leaf} is the total leaf resistance and R_a, R_b, R_{cut}, R_{st}, and R_m are the aerodynamic, boundary layer, cuticular, stomatal, and mesophilic resistances, respectively. The aerodynamic resistance is characterized by the micrometeorology above a surface and is dependent upon the wind speed and turbulence of air flow. The boundary layer resistance describes the diffusion of a molecule through a shallow boundary of air above a surface and is dependent on microscopic surface properties, diffusivity of the gas species, wind speed, and turbulence of air flow (Baldocchi et al., 1987). R_{cut}, R_{st}, and R_m are the resistances associated with deposition to the leaf cuticles or through the stomata, and are dependent upon plant physiology.

The chamber fan, installed to create turbulent mixing, allowed for the assumption that R_a was negligible (Pape et al., 2009; Breuninger et al., 2012). R_b is chamber-specific, and

has typically not been measured in previous chamber experiments of NO_2 leaf-level deposition (Chaparro-Suarez et al., 2011; Breuninger et al., 2012, 2013). R_b was experimentally measured in this study by placing a tray of activated carbon into the chamber (assumed to have zero surface resistance to deposition of NO_2) and calculating the deposition flux of NO_2. The leaf components to the total deposition resistance were determined through dark and light experiments. During dark experiments, the stomata were closed (confirmed with measurements of CO_2 and H_2O exchange), and the deposition observed was assumed to be entirely driven by deposition to the cuticles.

2.3 Results

Determination of the boundary resistance R_b

To estimate the chamber boundary layer resistance and test the assumption that $R_b \ll R_{leaf}$, a dish of activated carbon, which theoretically has zero chemical resistance to deposition of NO_2, was placed inside the chamber. The boundary layer resistance was considered to be the only component of the total resistance to deposition. The deposition velocity of NO_2 to activated carbon was measured as 0.52 ± 0.06 cm s^{-1}, corresponding to a boundary layer resistance to NO_2 deposition of 1.94 ± 0.02 s cm^{-1} (Fig. 2.3). This boundary resistance is approximately double what was measured by Pape et al. (2009)–a reasonable difference given differences in chamber design (Fig. 2.2). The R_b for NO_2 was scaled with the ratio of diffusivities of NO_2 and NO in air to obtain the resistance to deposition of NO of 2.59 ± 0.03 s cm^{-1}. However, with a branch enclosed inside the chamber, the effective boundary resistance to deposition will likely be reduced, as the surface roughness and surface area for deposition is increased (Galbally and Roy, 1980; Pape et al., 2009). The boundary resistances presented above thus serve as an upper limit for R_b with vegetation inside the chamber.

The boundary resistance was also estimated in an additional experiment (not shown) in which a de-ionized water-soaked Whatman no. 1 filter paper was placed inside the chamber and the evaporation of water vapor into the chamber filled with dry zero air was measured. The emission flux of water vapor from the filter paper was calculated in a similar manner to that of NO_x deposition flux (Eq. 2.2). The conductance to water vapor was then calculated via

$$\frac{Q \cdot (P_{H_2O})}{A} = g_w(P_{sat} - P_{H_2O}) \tag{2.8}$$

where P_{H_2O} is the partial pressure of water vapor inside the chamber, P_{sat} is the saturation vapor pressure at the temperature in the chamber, and g_w is the conductance to water vapor. The measured conductance to water vapor was scaled with the ratio of diffusivities of NO_2 to water vapor (D_{NO_2}/D_{H_2O}) and inverted to find the NO_2 boundary layer resistance:

$$R_b = \frac{D_{NO_2}}{D_{H_2O}} \frac{1}{g_w} \tag{2.9}$$

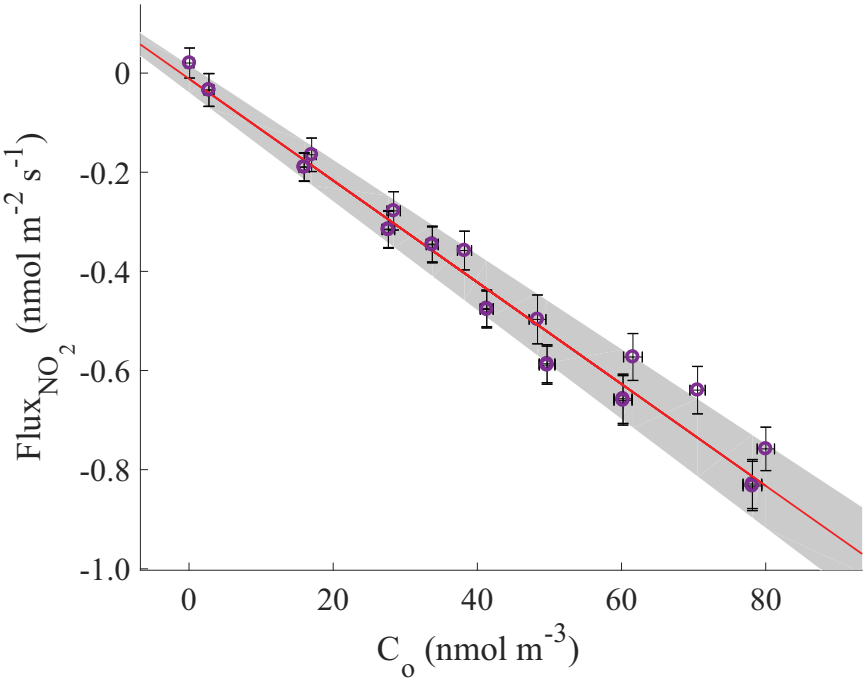

Figure 2.3: Flux to a 5.1 cm diameter dish filled with activated charcoal. The chemical surface resistance to deposition is approximately zero, so the deposition velocity for deposition of NO_2 to the surface of the charcoal dish is the reciprocal of the boundary layer resistance. The line of best fit is $(0.51\pm0.032)C_0$, where C_0 is the concentration of NO_2 in the outgoing airstream.

The boundary resistance to NO_2 deposition by this method was found to be 2 s cm^{-1}, essentially identical to the measurement on the activated-carbon.

NO_x deposition velocity and compensation point concentration

The deposition velocities and compensation points were respectively calculated as the slope and x-axis intercept of the regression line between NO_x exchange flux and chamber NO_x concentrations (Fig. 2.4). The detection limit was the dominant source of error in the estimation of the NO exchange flux and compensation point. The large relative uncertainties in NO flux measurements were caused by the much slower deposition of NO compared with that of NO_2, inhibiting our ability to observe the very small changes between the NO concentration in the chamber and the incoming airstream (Fig. 2.4). Additional uncertainty in NO_2 flux measurements because of enhanced water vapor quenching of excited-state NO_2 should be minimal, as calibrations and measurements were performed at equivalent relative humidities. However, transpiration of the enclosed leaves caused the absolute humidity within chamber

to be enhanced by 0.3%–0.5% relative to the incoming airstream. We expect this to result in a maximum error in calculated NO_2 mixing ratios of 1%—1.75% (Thornton et al., 2000), resulting in maximum errors in the calculated fluxes and deposition velocities of 2% and 4%, respectively. This 4% error in the calculated deposition velocity during lights-on experiments is less that the uncertainty of the linear fit (Fig. 2.4). Correlation coefficients, deposition velocities, compensation points, and statistical testing of the compensation point for NO_2 and NO deposition are shown in Table 2.1 and Table 2.2, respectively, and were calculated according to Breuninger et al. (2013). For NO_2 experiments, only one dark and one light experiment with *Quercus agrifolia* 1 were found to have statistically significant ($\alpha = 0.05$) nonzero intersections with the x-axis (Table 2.1). The range of C_{comp} measured was -0.02 to 0.300 ppb NO_2, with probabilities of $C_comp = 0$ ranging from 10.3% to 91.6% (excluding the two *Quercus agrifolia* 1 experiments) (Table 2.1). Conversely, all three *Quercus agrifolia* individuals during all dark and light NO deposition experiments demonstrated compensation points significantly above zero, ranging from 0.74 to 3.8 ppb NO. The average compensation point was calculated as 0.84 ± 0.32 ppb NO during light experiments and 2.4 ± 1.1 ppb NO during dark experiments (Table 2.2).

Correlation coefficients, deposition velocities, compensation points, and statistical testing of the compensation point for NO_2 and NO deposition are shown in Table 2.1 and Table 2.2, respectively, and were calculated according to Breuninger et al. (2013). For NO_2 experiments, only one dark and one light experiment with Quercus agrifolia 1 were found to have statistically significant ($\alpha = 0.05$) nonzero intersections with the x axis (Table 2.1). The range of Ccomp measured was -0.02 to 0.300 ppb NO_2, with probabilities of C_{comp}=0 ranging from 10.3% to 91.6% (excluding the two *Quercus agrifolia* 1 experiments) (Table 2.1). Conversely, all three *Quercus agrifolia* individuals during all dark and light NO deposition experiments demonstrated compensation points significantly above zero, ranging from 0.74 to 3.8 ppb NO. The average compensation point was calculated as 0.84 ± 0.32 ppb NO during light experiments and 2.4 ± 1.1 ppb NO during dark experiments (Table 2.2).

Student's t tests (not shown) demonstrated that deposition velocities and compensation points measured during NO and NO_2 lights-on and lights-off experiments were not significantly different (to the α=0.05 confidence level) between different *Quercus agrifolia* individuals. Deposition velocities for NO_2 light experiments were between 0.08 and 0.18 cm s^{-1}, with a deposition of 0.123 ± 0.009 cm s^{-1} calculated from the regression of all light experiments. Dark experiments resulted in deposition velocities between 0.013 and 0.022 cm s^{-1}, with a deposition velocity of 0.015 ± 0.001 cm s^{-1} calculated from the regression of all dark experiments (Table 2.1). NO demonstrated much slower deposition, with deposition velocities from all light and dark experiments calculated as 0.012 ± 0.002 and 0.005 ± 0.002 cm s^{-1}, respectively (Table 2.2). Despite the large compensation point measured for NO, the leaf emission fluxes of NO were a maximum of only 8 pmol m^{-2} s^{-1} at 0.1 ppb NO, approximately half of the deposition flux measured for NO_2 at 0.1 ppb (Fig. 2.4). At typical NO_2/NO ratios and gradients measured in forest canopies, the leaf-level NO_2 and NO exchange fluxes measured make dry stomatal deposition to *Quercus agrifolia* a net sink of NO_x within the canopy.

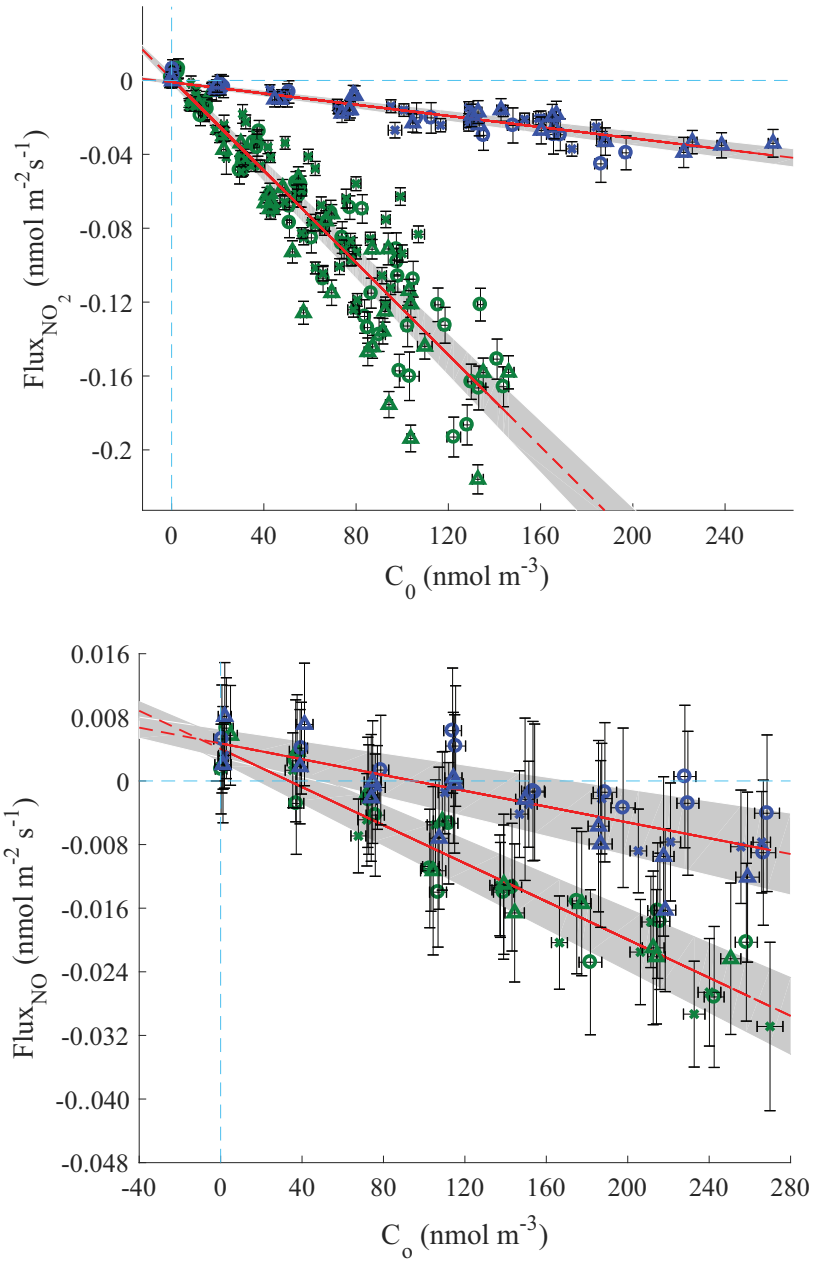

Figure 2.4: NO_2 (a) and NO (b) fluxes versus the outlet concentrations for all *Quercus agrifolia* individuals with the chamber lights on (green) and off (blue). The line of best fit is shown in red and was calculated to minimize the weighted residuals in both the x- and y-axes. The blue dotted lines show where flux and C_0 are zero. A significantly positive ($\alpha = 0.5$) x-intercept occurs for NO, but not NO_2 experiments.

Table 2.1: Parameters of NO_2 bivariate linear least-square fitting regression analysis.

Run	N	R^2	$[NO_2]_{comp}$ (ppb)	P($[NO_2]_{comp}$=0) (%)	V_{dep} (cm s^{-1})
Q. agrifolia 1, light					
1	13	0.979	0.056 ± 0.013	42.7	0.10 ± 0.013
2	13	0.95	0.046 ± 0.19	63.7	0.12 ± 0.023
3	16	0.978	0.099 ± 0.086	3.87	0.15 ± 0.016
4	16	0.958	0.077 ± 0.14	28.7	0.12 ± 0.021
All	58	0.927	0.080 ± 0.10	11.6	0.12 ± 0.012
Q. agrifolia 2, light					
1	16	0.963	0.10 ± 0.12	10.3	0.08 ± 0.011
2	5	0.969	-0.01 ± 0.96	83.8	0.12 ± 0.014
3	9	0.997	0.023 ± 0.032	20.3	0.16 ± 0.011
4	16	0.974	-0.019 ± 0.074	61.9	0.14 ± 0.017
5	15	0.979	0.015 ± 0.082	72.7	0.12 ± 0.014
All	61	0.845	-0.0077 ± 0.091	91.6	0.11 ± 0.014
Q. agrifolia 3, light					
1	11	0.969	0.016 ± 0.18	87.4	0.12 ± 0.024
2	15	0.961	0.074 ± 0.16	39.1	0.18 ± 0.029
3	5	0.99	0.30 ± 0.20	5.9	0.12 ± 0.038
All	31	0.83	0.019 ± 0.064	77.6	0.14 ± 0.029
All *Q. agrifolia*, light	150	0.885	0.030 ± 0.072	41.3	0.123 ± 0.0092
Q. agrifolia 1, dark					
1	16	0.964	0.056 ± 0.14	0.9*	0.022 ± 0.0034
Q. agrifolia 2, dark					
1	16	0.858	-0.16 ± 0.47	50.8	0.016 ± 0.0050
2	12	0.932	-0.34 ± 0.40	11.8	0.013 ± 0.0038
All	28	0.853	-0.24 ± 0.32	15.6	0.015 ± 0.0030
Q. agrifolia 3, dark					
1	14	0.9	-0.30 ± 0.48	24.1	0.015 ± 0.0042
2	11	0.909	-0.001 ± 0.69	36.7	0.015 ± 0.0057
All	25	0.898	-0.22 ± 0.38	25.3	0.014 ± 0.0029
All *Q. agrifolia*, dark	69	0.881	-0.16 ± 0.24	12.2	0.015 ± 0.0018

*Significant nonzero compensation point.

Table 2.2: Parameters of NO bivariate linear least-square fitting regression analysis.

Run	N	R^2	$[NO_2]$comp (ppb)	P($[NO_2]_{comp}$=0)	V_{dep}
Q. agrifolia 1					
Light	17	0.874	0.74 ± 0.65	3.5*	0.011 ± 0.0032
Dark	13	0.699	3.8 ± 2.2	0.52*	0.0040 ± 0.0025
Q. agrifolia 2					
Light	14	0.954	0.76 ± 0.49	0.92*	0.013 ± 0.0027
Dark	10	0.866	1.7 ± 1.0	1.1*	0.0046 ± 0.0018
Q. agrifolia 3					
Light	12	0.936	1.3 ± 0.60	0.17*	0.0123 ± 0.0029
Dark	15	0.803	2.0 ± 1.0	2.5*	0.0074 ± 0.0033
All Q. agrifolia					
Light	13	0.908	0.84 ± 0.32	<0.01*	0.012 ± 0.0015
Dark	13	0.602	2.4 ± 1.1	<0.01*	0.0050 ± 0.0016

*Significant nonzero compensation point.

Resistances to leaf-level NO_x deposition

The deposition velocity measured from linear regression of NO_x exchange fluxes and NO_x chamber concentrations is the inverse of the total resistance to deposition (Eq. 2.6), with R_a assumed to be zero. The total resistance in the chamber is thus

$$R = R_b + \left(\frac{1}{R_{cut}} + \frac{1}{R_s^*}\right)^{-1} \tag{2.10}$$

where R_s^* is the sum of R_m and R_{st}. The leaf resistance to deposition can then be found by subtracting the boundary layer resistance from the total resistance. Total leaf resistances, R_{leaf}, were calculated using the boundary layer resistances for NO_2 and NO of 1.94 ± 0.02 and 2.59 ± 0.03 s cm^{-1}, respectively. During the dark experiments, R_{leaf} is equal to R_{cut}, and the deposition velocity measured was estimated as the inverse of the sum of the boundary and cuticular resistances. After calculation of R_{cut} from dark experiments, the sum of the stomatal and mesophilic contributions (R_s^*) to the total leaf resistance was determined. R_b, R_{cut}, and R_s^* are shown in Table 2.3. It should be noted that since the reported R_b is the maximum possible boundary resistance, the reported R_{cut} and R_s^* are lower limits. If we were to assume the chamber boundary resistance with the branch enclosed is insignificant (∼0 s cm^{-1}), this would introduce maximum systematic 30% and 3% errors to the calculated NO_2, R_s^* and R_{cut}, respectively (giving an R_s^* of 9.2 ± 0.9 s cm^{-1} and an R_{cut} of 67 ± 8 s cm^{-1}). The errors in the calculated NO resistances would be negligible.

Table 2.3: Summary of deposition resistance parameters of *Quercus agrifolia*.

Gas	R_b (s cm^{-1})	R_{cut} (s cm^{-1})	R_s^* (s cm^{-1})
NO_2	1.94 ± 0.02	65 ± 8	6.9 ± 0.9
NO	2.59 ± 0.03	200 ± 60	140 ± 40

It is possible that the stomata were not entirely closed during dark experiments. Evidence exists that nocturnal stomatal conductance can be large enough to allow for transpiration (Dawson et al., 2007), and low (within the range of uncertainty observed for the LICOR-6262) emission of water vapor during dark experiments was measured. However, even if all the deposition during dark experiments was stomatal, this would cause only a 0.5 s cm^{-1} reduction in the calculated R_s^* for NO_2–less than the uncertainty from the error in the measured deposition velocity (∼10% error). The cuticular resistances reported here during dark experiments are nonetheless atmospherically relevant to nighttime NO_x deposition.

2.4 Discussion

NO_x deposition velocities and compensation points

The strong linear dependence between NO_2 fluxes and NO_2 chamber concentrations that we observe is consistent with previous observations that NO_2 exchange is largely driven by NO_2 concentration differences between the atmosphere and gaseous phase of the leaf (Rondón and Granat, 1994; Gessler et al., 2000; Hereid and Monson, 2001; Sparks et al., 2001; Teklemmariam and Sparks, 2006; Pape et al., 2009; Chaparro-Suarez et al., 2011; Breuninger et al., 2012). Our measurements of NO_2 stomatal resistance parameters for *Quercus agrifolia* represent a stomatal deposition velocity ($1/R_s^*$) of 0.14 ± 0.02 cm s^{-1}. This value is similar to the range of 0.1—0.15 cm s^{-1} that Chaparro-Suarez et al. (2011) found for two European oak tree species, *Quercus robur* and *Quercus ilex*. The deposition velocity measured here for *Quercus agrifolia* is also much larger than 0.007—0.042 cm s^{-1} range found for Norway spruce (*Picea abies*) by Breuninger et al. (2012), but surprisingly comparable, given the differences in plant species, to the 0.12 cm s^{-1} deposition velocity found for maize (*Zea mays*) by Hereid and Monson (2001). We also find here an NO_2 flux at 5 ppb of 0.2 nmol m^{-2} s^{-1}, similar in magnitude to the 0.1, 0.15—1.5, and 0.18 nmol m^{-2} s^{-1} fluxes measured for *Fagus sylvatica* (Gessler et al., 2000), tropical Panamanian native trees (Sparks et al., 2001), and periwinkle (*Catharanthus roseus*) (Teklemmariam and Sparks, 2006), respectively.

Resistance parameters reported above for NO deposition to *Quercus agrifolia* represent a stomatal deposition velocity of 0.007 ± 0.002 cm s^{-1} and cuticular deposition velocity of 0.005 ± 0.001 cm s^{-1}. This observation of very minor NO uptake–at least an order

of magnitude less than that of NO_2 uptake–is also consistent with previous observations (Hanson and Lindberg, 1991; Hereid and Monson, 2001; Teklemmariam and Sparks, 2006). We also detected a statistically significant NO compensation point, with low emissions up to 8 pmol m^{-2} s^{-1} observed below 1 ppb. These observations are similar to the 8—14 pmol m^{-2} s^{-1} emission fluxes of NO reported by Hereid and Monson (2001) and Teklemariam and Sparks (2006) at low NO_x concentrations.

No significant NO_2 compensation point was found for our measurements of *Quercus agrifolia* NO_x uptake. Many previous studies have reported NO_2 compensation points, ranging from 0.1 to 3.0 ppb, implicating trees as a constant source of NO_x in forest ecosystems (Gessler et al., 2000; Hereid and Monson, 2001; Sparks et al., 2001; Teklemmariam and Sparks, 2006). Our findings of a lack of NO_2 compensation point support field observations and modeling studies that have recognized NO_2 dry deposition to vegetation as an important NO_x loss process in forests (Jacob and Wofsy, 1990; Ganzeveld et al., 2002b; Geddes and Murphy, 2014). Our results also support the works of Chaparro-Suarez et al. (2011) and Breuninger et al. (2013), who did not find evidence of an NO_2 compensation point.

The primary difference in our experimental setup, compared to previous dynamic chamber studies that have found an NO_2 compensation point, is the use of a direct NO_2 measurement technique. Measurements of a significant NO_2 compensation point have mostly been obtained using techniques requiring conversion of NO_2, followed by chemiluminescence detection of NO (Gessler et al., 2000; Hereid and Monson, 2001; Sparks et al., 2001; Teklemmariam and Sparks, 2006). Such methods have utilized either nonspecific photolytic (Gessler et al., 2000; Hereid and Monson, 2001), luminol (Sparks et al., 2001), or catalytic conversion (Teklemmariam and Sparks, 2006) techniques, which may have also resulted in the conversion of PAN, HONO, HNO_3, and other organic nitrates, as well as interferences from alkene + ozone reactions (Carter et al., 2005; Reed et al., 2016). If any of these interfering compounds are not excluded from the chamber system, outgas from the chamber itself, or form from reactions of biogenic emissions, this would cause an enhancement in the observed NO_2 compensation point, and a suppression of observed deposition velocity. Our measurements of NO_2 mixing ratios also demonstrate a much higher degree of precision, due largely to a lower detection limit, than comparable experiments with specific photolytic conversion and chemiluminescence measurement of NO_2 (Chaparro-Suarez et al., 2011; Breuninger et al., 2012, 2013). Additionally, previous chamber measurements have sometimes employed chamber setups that would let in a substantial amount of UV light, yet did not exclude photochemical reactions between NO_2, NO, and O_3. Such corrections are excluded here because of our use of chamber lights with only wavelengths above 420 nm. To avoid this issue, other experiments have instead involved a setup including a simultaneously measured blank chamber, which would theoretically allow for correction for any reactions resulting from photolysis of NO_2, O_2, or O_3 (Gessler et al., 2000; Hereid and Monson, 2001). Such corrections might be complicated by secondary chemistry not present in our experiments.

Implication for canopy NO_x loss

Resistance parameters reported above (Table 2.3) were used in a 1-D seven-layer multibox model representing chemical reactions, vertical transport, and leaf-level processes scaled to the canopy level to assess the impacts of NO_x deposition velocities on the NO_x lifetime and fluxes. The model is constructed in a manner similar to Wolfe et al. (2011) with the following modifications: the model domain consists of seven well-mixed vertical layers extending to a planetary boundary layer height of 1000 m, with the forest canopy represented by the first three layers; NO_x cuticular and stomatal resistances are adjustable input parameters; and the chemistry implemented in the model is the simplified reaction mechanism presented in Browne and Cohen (2012). The 1-D model was run for meteorological conditions representing the native habitat of *Quercus agrifolia* and two different leaf area indices (LAIs), approximately representing the lower and upper limits of LAIs found in California oak woodlands. As shown in Fig. 2.5a and b, the model predicts NO_x deposition to *Q. agrifolia* accounts for 3%—7% of the total NO_x loss within the boundary layer if the only source of NO_x is emissions from the soil. This represents a total NO_x lifetime of 7—7.5 h in the boundary layer, and a lifetime to deposition of 4—11 days in the boundary layer and 0.5—1.2 h below the canopy. Under these scenarios approximately 15—30% of soil-emitted NO_x is removed in the canopy (Fig. 2.6)–on the lower end of the range of 25%—80% reduction observed in field studies (Jacob and Wofsy, 1990; Lerdau et al., 2000; Ganzeveld et al., 2002a; Min et al., 2014).

The coastal regions of California where *Q. agrifolia* is found frequently experience much higher NO_x mixing ratios of 10—50 ppb. This is particularly important for oak woodlands of the San Francisco Bay and Los Angeles areas, where anthropogenic emissions from nearby urban centers are the majority of the NO_x source. To account for this extra NO_x source, additional model runs were performed with an added term accounting for NO_x advection from a more concentrated upwind source (C_{NO_x}(adv)), with advection treated as a simple mixing process:

$$\frac{dC_{NO_x}}{dt} = -k_{mix}(C_{NO_x} - dC_{NO_x}(adv)) \tag{2.11}$$

where k_{mix}=0.3 h^{-1} and C_{NO_x}(adv) is 10 ppb.

In this case, deposition to *Q. agrifolia* could account for 10—22% of the total NO_x loss in the boundary layer (Fig. 2.5c, d), representing a lifetime to deposition of 5—14 days in the boundary layer and a total NO_x lifetime of 28—33 h. Deposition in this higher NO_x scenario decreased the total NO_x lifetime by 3—8 h, compared with a no-deposition case.

2.5 Conclusions

This work constitutes the first measurements of NO_2 and NO foliar deposition resistance parameters for a North American tree species. We report observations of leaf-level resistances to NO_2 and NO deposition, corresponding to total deposition velocities of NO_2 and NO

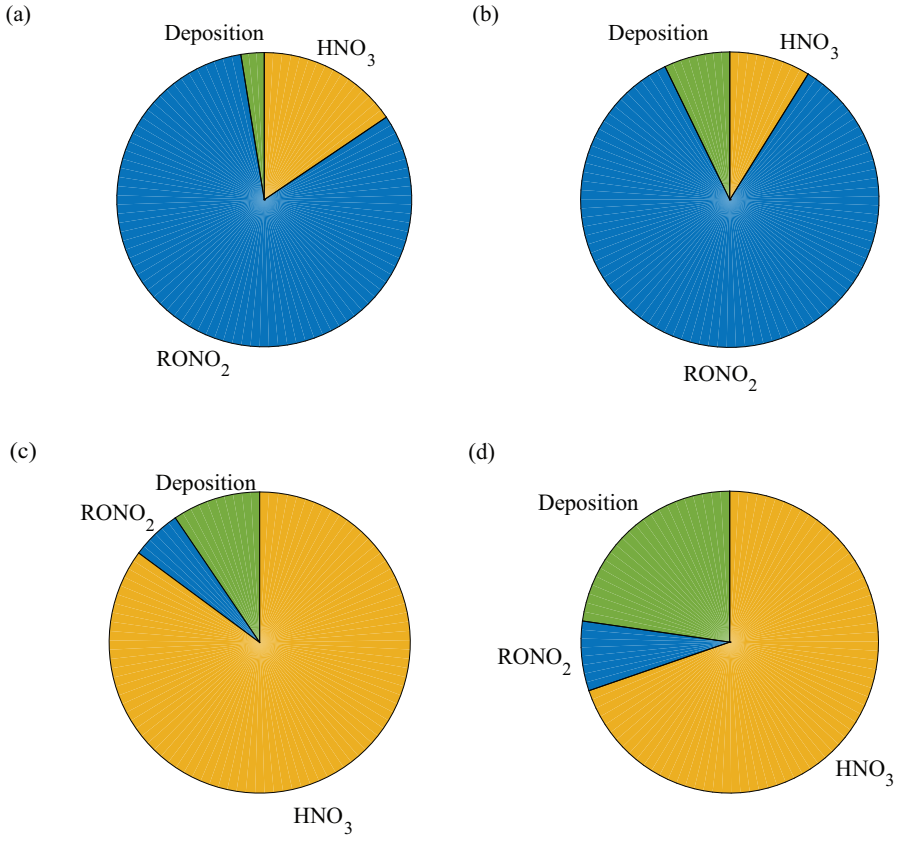

Figure 2.5: Model predictions of the fraction of NO_x loss to alkyl nitrate formation, nitric acid formation, and deposition in a *Q. agrifolia* woodland. The model was run using scenarios with only soil emissions and LAI of 1 m^2 m^{-2} (a), only soil emissions and LAI of 3 m^2 m^{-2} (b), CNO_x(adv)=10 ppb and LAI of 1 m^2 m^{-2} (c), and C_{NO_x}(adv) = 10 ppb and LAI of 3 m^2 m^{-2} (d).

of 0.123 ± 0.007 and 0.012 ± 0.002 cm s^{-1} in the light and 0.015 ± 0.001 and 0.005 ± 0.002 cm s^{-1} in the dark, respectively. No compensation point was observed for NO_2, but compensation points of 0.74—3.8 ppb were recorded for NO. The magnitude of NO emission below the compensation point was significantly less than the magnitude of NO_2 uptake in the same concentration range, making *Q. agrifolia* an overall large net sink of NO_x. The observed deposition is large enough to explain canopy reduction factors observed in canopy-level studies, but is at the lower end of estimated global CRFs. The results of the 1-D multibox model demonstrate that the deposition observed accounts for 5%—20% of NO_x removal with a NO_x lifetime to deposition of 0.5—1.2 h beneath the canopy of a California oak woodland. We show that foliar deposition of NO_x represents a significant removal mechanism of NO_x and can have a large impact on NO_x mixing ratios and fluxes in such

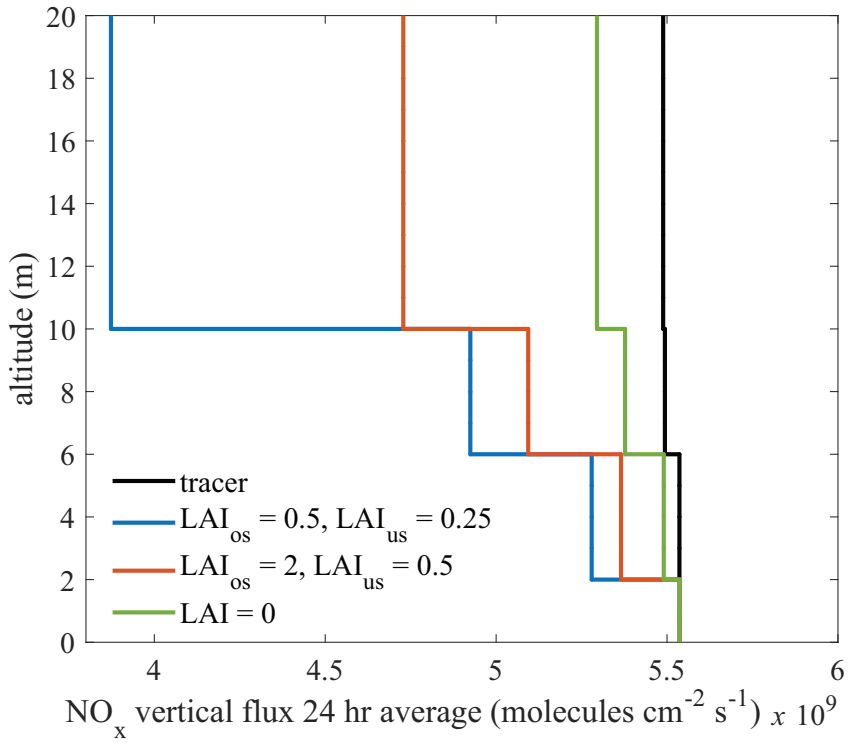

Figure 2.6: 24 h average vertical fluxes of NO_x predicted by the 1-D multibox model for a California oak woodland using the leaf resistances measured in this study. Model runs were conducted for low (red) and high (blue) LAI cases and for a no-deposition scenario (green).

ecosystems. Further investigations of NO_2 deposition to a larger variety of plant species under a range of environmental conditions are needed to accurately understand the global impacts of NO_2 deposition across diverse ecosystems.

2.6 References

Ammann, M., von Ballmoos, P., Stalder, M., Suter, M., and Brunold, C.: Uptake and assimilation of atmospheric NO2 — N by spruce needles (Picea abies): A field study, Water Air and Soil Pollution, 85, 1497–1502, https://doi.org/10.1007/BF00477193, 1995.

Baldocchi, D. D., Hicks, B. B., and Camara, P.: A canopy stomatal resistance model for gaseous deposition to vegetated surfaces, Atmospheric Environment (1967), 21, 91 – 101, https://doi.org/10.1016/0004-6981(87)90274-5, 1987.

Breuninger, C., Oswald, R., Kesselmeier, J., and Meixner, F. X.: The dynamic chamber

method: trace gas exchange fluxes (NO, NO_2, O_3) between plants and the atmosphere in the laboratory and in the field, Atmospheric Measurement Techniques, 5, 955–989, https://doi.org/10.5194/amt-5-955-2012, 2012.

Breuninger, C., Meixner, F. X., and Kesselmeier, J.: Field investigations of nitrogen dioxide (NO_2) exchange between plants and the atmosphere, Atmospheric Chemistry and Physics, 13, 773–790, https://doi.org/10.5194/acp-13-773-2013, 2013.

Browne, E. C. and Cohen, R. C.: Effects of biogenic nitrate chemistry on the NO_x lifetime in remote continental regions, Atmospheric Chemistry and Physics, 12, 11 917–11 932, https://doi.org/10.5194/acp-12-11917-2012, 2012.

Burkhardt, J. and Eiden, R.: Thin water films on coniferous needles: A new device for the study of water vapour condensation and gaseous deposition to plant surfaces and particle samples, Atmospheric Environment, 28, 2001 – 2011, https://doi.org/10.1016/1352-2310(94)90469-3, 1994.

Caranto, J. and Lancaster, K.: Nitric oxide is an obligate bacterial nitrification intermediate produced by hydroxylamine oxidoreductase, Proceedings of the National Academy of Sciences, 114, 201704 504, https://doi.org/10.1073/pnas.1704504114, 2017.

Carter, W. P., Cocker, D. R., Fitz, D. R., Malkina, I. L., Bumiller, K., Sauer, C. G., Pisano, J. T., Bufalino, C., and Song, C.: A new environmental chamber for evaluation of gas-phase chemical mechanisms and secondary aerosol formation, Atmospheric Environment, 39, 7768 – 7788, https://doi.org/10.1016/j.atmosenv.2005.08.040, 2005.

Chaparro-Suarez, I., Meixner, F., and Kesselmeier, J.: Nitrogen dioxide (NO2) uptake by vegetation controlled by atmospheric concentrations and plant stomatal aperture, Atmospheric Environment, 45, 5742 – 5750, https://doi.org/10.1016/j.atmosenv.2011.07.021, 2011.

Crutzen, P. J.: The Role of NO and NO2 in the Chemistry of the Troposphere and Stratosphere, Annual Review of Earth and Planetary Sciences, 7, 443–472, https://doi.org/10.1146/annurev.ea.07.050179.002303, 1979.

Dawson, T. E., Burgess, S. S. O., Tu, K. P., Oliveira, R. S., Santiago, L. S., Fisher, J. B., Simonin, K. A., and Ambrose, A. R.: Nighttime transpiration in woody plants from contrasting ecosystems, Tree Physiology, 27, 561–575, https://doi.org/10.1093/treephys/27.4.561, 2007.

Fuchs, H., Dubé, W. P., Lerner, B. M., Wagner, N. L., Williams, E. J., and Brown, S. S.: A Sensitive and Versatile Detector for Atmospheric NO2 and NOX Based on Blue Diode Laser Cavity Ring-Down Spectroscopy, Environmental Science & Technology, 43, 7831–7836, https://doi.org/10.1021/es902067h, pMID: 19921901, 2009.

Galbally, I. E. and Roy, C. R.: Destruction of ozone at the earth's surface, Quarterly Journal of the Royal Meteorological Society, 106, 599–620, https://doi.org/10.1002/qj.49710644915, 1980.

Ganzeveld, L. N., Lelieveld, J., Dentener, F. J., Krol, M. C., Bouwman, A. J., and Roelofs, G.-J.: Global soil-biogenic NOx emissions and the role of canopy processes, Journal of Geophysical Research: Atmospheres, 107, ACH 9–1–ACH 9–17, https://doi.org/10.1029/2001JD001289, 2002a.

Ganzeveld, L. N., Lelieveld, J., Dentener, F. J., Krol, M. C., and Roelofs, G.-J.: Atmosphere-biosphere trace gas exchanges simulated with a single-column model, Journal of Geophysical Research: Atmospheres, 107, ACH 8–1–ACH 8–21, https://doi.org/10.1029/2001JD000684, 2002b.

Geddes, J. A. and Murphy, J. G.: Observations of reactive nitrogen oxide fluxes by eddy covariance above two midlatitude North American mixed hardwood forests, Atmospheric Chemistry and Physics, 14, 2939–2957, https://doi.org/10.5194/acp-14-2939-2014, 2014.

Gessler, A., Rienks, M., and Rennenberg, H.: NH3 and NO2 fluxes between beech trees and the atmosphere – correlation with climatic and physiological parameters, New Phytologist, 147, 539–560, https://doi.org/10.1046/j.1469-8137.2000.00712.x, 2000.

Hanson, P. J. and Lindberg, S. E.: Dry deposition of reactive nitrogen compounds: A review of leaf, canopy and non-foliar measurements, Atmospheric Environment. Part A. General Topics, 25, 1615 – 1634, https://doi.org/10.1016/0960-1686(91)90020-8, 1991.

Hereid, D. and Monson, R.: Nitrogen Oxide Fluxes between Corn (Zea mays L.) Leaves and the Atmosphere, Atmospheric Environment, 35, 975–983, https://doi.org/10.1016/S1352-2310(00)00342-3, 2001.

Jacob, D. J. and Wofsy, S. C.: Budgets of reactive nitrogen, hydrocarbons, and ozone over the Amazon forest during the wet season, Journal of Geophysical Research: Atmospheres, 95, 16 737–16 754, https://doi.org/10.1029/JD095iD10p16737, 1990.

Johansson, C.: Pine forest: a negligible sink for atmospheric NOx in rural Sweden, Tellus B, 39B, 426–438, https://doi.org/10.1111/j.1600-0889.1987.tb00204.x, 1987.

Lee, Y. N. and Schwartz, S. E.: Reaction kinetics of nitrogen dioxide with liquid water at low partial pressure, The Journal of Physical Chemistry, 85, 840–848, https://doi.org/10.1021/j150607a022, 1981.

Lerdau, M. T., Munger, J. W., and Jacob, D. J.: The NO2 Flux Conundrum, Science, 289, 2291–2293, https://doi.org/10.1126/science.289.5488.2291, 2000.

Matsumoto, J. and Kajii, Y.: Improved analyzer for nitrogen dioxide by laser-induced fluorescence technique, Atmospheric Environment, 37, 4847 – 4851, https://doi.org/10.1016/j.atmosenv.2003.08.023, 2003.

McKenney, D. J., Shuttleworth, K. F., Vriesacker, J. R., and Findlay, W. I.: Production and Loss of Nitric Oxide from Denitrification in Anaerobic Brookston Clay, Applied and Environmental Microbiology, 43, 534–541, 1982.

Min, K.-E., Pusede, S. E., Browne, E. C., LaFranchi, B. W., Wooldridge, P. J., Wolfe, G. M., Harrold, S. A., Thornton, J. A., and Cohen, R. C.: Observations of atmosphere-biosphere exchange of total and speciated peroxynitrates: nitrogen fluxes and biogenic sources of peroxynitrates, Atmospheric Chemistry and Physics, 12, 9763–9773, https://doi.org/10.5194/acp-12-9763-2012, 2012.

Min, K.-E., Pusede, S. E., Browne, E. C., LaFranchi, B. W., and Cohen, R. C.: Eddy covariance fluxes and vertical concentration gradient measurements of NO and NO_2 over a ponderosa pine ecosystem: observational evidence for within-canopy chemical removal of NO_x, Atmospheric Chemistry and Physics, 14, 5495–5512, https://doi.org/10.5194/acp-14-5495-2014, 2014.

Neubert, A., Kley, D., Wildt, J., Segschneider, H., and Förstel, H.: Uptake of NO, NO2 and O3 by sunflower (Helianthus annuus L.) and tobacco plants (Nicotiana tabacum L.): dependence on stomatal conductivity, Atmospheric Environment. Part A. General Topics, 27, 2137 – 2145, https://doi.org/10.1016/0960-1686(93)90043-X, 1993.

Nussbaum, S., von Ballmoos, P., Gfeller, H., Schlunegger, U., Fuhrer, J., Rhodes, D., and Brunold, C.: Incorporation of atmospheric 15NO2 -nitrogen into free amino acids by Norway spruce Picea abies (L.) Karst, Oecologia, 94, 408–414, https://doi.org/10.1007/BF00317117, 1993.

Okano, K. and Totsuka, T.: Absorption of nitrogen dioxide by sunflower plants grown at various levels of nitrate, New Phytologist, 102, 551–562, https://doi.org/10.1111/j.1469-8137.1986.tb00831.x, 1986.

Otter, L. B., Yang, W. X., Scholes, M. C., and Meixner, F. X.: Nitric oxide emissions from a southern African savanna, Journal of Geophysical Research: Atmospheres, 104, 18 471–18 485, https://doi.org/10.1029/1999JD900148, 1999.

Pape, L., Ammann, C., Nyfeler-Brunner, A., Spirig, C., Hens, K., and Meixner, F. X.: An automated dynamic chamber system for surface exchange measurement of non-reactive and reactive trace gases of grassland ecosystems, Biogeosciences, 6, 405–429, https://doi.org/10.5194/bg-6-405-2009, 2009.

Ramge, P., Badeck, F.-W., Plochl, M., and Kohlmaier, G. H.: Apoplastic antioxidants as decisive elimination factors within the uptake process of nitrogen dioxide into leaf tissues, New Phytologist, 125, 771–785, https://doi.org/10.1111/j.1469-8137.1993.tb03927.x, 1993.

Reed, C., Evans, M. J., Di Carlo, P., Lee, J. D., and Carpenter, L. J.: Interferences in photolytic NO_2 measurements: explanation for an apparent missing oxidant?, Atmospheric Chemistry and Physics, 16, 4707–4724, https://doi.org/10.5194/acp-16-4707-2016, 2016.

Rogers, H. H., Jeffries, H. E., and Witherspoon, A. M.: Measuring Air Pollutant Uptake by Plants: Nitrogen Dioxide, Journal of Environmental Quality, 8, 551–557, https://doi.org/10.2134/jeq1979.00472425000800040022x, 1979.

Rondón, A. and Granat, L.: Studies on the dry deposition of NO2 to coniferous species at low NO2 concentrations, Tellus B: Chemical and Physical Meteorology, 46, 339–352, https://doi.org/10.3402/tellusb.v46i5.15809, 1994.

Rondón, A., Johansson, C., and Granat, L.: Dry deposition of nitrogen dioxide and ozone to coniferous forests, Journal of Geophysical Research: Atmospheres, 98, 5159–5172, https://doi.org/10.1029/92JD02335, 1993.

Seinfeld, J. and Pandis, S.: Atmospheric Chemistry and Physics: From Air Pollution to Climate Change, A Wiley-Interscience publication, Wiley, 2006.

Seok, B., Helmig, D., Ganzeveld, L., Williams, M. W., and Vogel, C. S.: Dynamics of nitrogen oxides and ozone above and within a mixed hardwood forest in northern Michigan, Atmospheric Chemistry and Physics, 13, 7301–7320, https://doi.org/10.5194/acp-13-7301-2013, 2013.

Sparks, J., Monson, R., Sparks, K., and Lerdau, M.: Leaf uptake of nitrogen dioxide (NO2) in a tropical wet forest: Implications for tropospheric chemistry, Oecologia, 127, 214–221, https://doi.org/10.1007/s004420000594, 2001.

Teklemmariam, T. and Sparks, J.: Leaf fluxes of NO and NO2 in four herbaceous plant species: The role of ascorbic acid, Atmospheric Environment, 40, 2235–2244, https://doi.org/10.1016/j.atmosenv.2005.12.010, 2006.

Thornton, J. A., Wooldridge, P. J., and Cohen, R. C.: Atmospheric NO2: In Situ Laser-Induced Fluorescence Detection at Parts per Trillion Mixing Ratios, Analytical Chemistry, 72, 528–539, https://doi.org/10.1021/ac9908905, pMID: 10695138, 2000.

Tischner, R.: Nitrate uptake and reduction in higher and lower plants, Plant, Cell & Environment, 23, 1005–1024, https://doi.org/10.1046/j.1365-3040.2000.00595.x, 2000.

Thoene, B., Schröder, P., Papen, H., Egger, A., and Rennenberg, H.: Absorption of atmospheric NO2 by spruce (Picea abies L. Karst.) trees, New Phytologist, 117, 575–585, https://doi.org/10.1111/j.1469-8137.1991.tb00962.x, 1991.

Vinken, G. C. M., Boersma, K. F., Maasakkers, J. D., Adon, M., and Martin, R. V.: Worldwide biogenic soil NO_x emissions inferred from OMI NO_2 observations, Atmospheric Chemistry and Physics, 14, 10 363–10 381, https://doi.org/10.5194/acp-14-10363-2014, 2014.

von Caemmerer, S. and Farquhar, G. D.: Some relationships between the biochemistry of photosynthesis and the gas exchange of leaves, Planta, 153, 376–387, https://doi.org/10.1007/BF00384257, 1981.

Wang, Y.-P. and Leuning, R.: A two-leaf model for canopy conductance, photosynthesis and partitioning of available energy I:: Model description and comparison with a multi-layered model, Agricultural and Forest Meteorology, 91, 89 – 111, https://doi.org/10.1016/S0168-1923(98)00061-6, 1998.

Weber, P., Nußbaum, S., Fuhrer, J., Gfeller, H., Schlunegger, U., Brunold, C., and Rennenberg, H.: Uptake of atmospheric 15NO2 and its incorporation into free amino acids in wheat (Triticum aestivum), Physiologia Plantarum, 94, 71 – 77, https://doi.org/10.1111/j.1399-3054.1995.tb00786.x, 2006.

Wildt, J., Kley, D., Rockel, A., Rockel, P., and Segschneider, H. J.: Emission of NO from several higher plant species, Journal of Geophysical Research: Atmospheres, 102, 5919–5927, https://doi.org/10.1029/96JD02968, 1997.

Wolfe, G., Thornton, J., Bouvier-Brown, N., Goldstein, A., Park, J., McKay, M., Matross, D., Mao, J., Brune, W., Lafranchi, B., Browne, E., Min, K.-E., Wooldridge, P., Cohen, R., Crounse, J., Faloona, I., Gilman, J., Kuster, W., de Gouw, J., and Keutsch, F.: The Chemistry of Atmosphere-Forest Exchange (CAFE) Model Part 2: Application to BEARPEX-2007 observations, Atmos. Chem. Phys., 11, 1269–1294, https://doi.org/10.5194/acpd-10-21791-2010, 2011.

Yienger, J. J. and Levy, H.: Empirical model of global soil-biogenic NO emissions, Journal of Geophysical Research: Atmospheres, 100, 11 447–11 464, https://doi.org/10.1029/95JD00370, 1995.

Yoneyama, T., Ito, O., and Engelaar, W.: Uptake, metabolism and distribution of nitrogen in crop plants traced by enriched and natural 15N: Progress over the last 30 years, Phytochemistry Reviews, 2, 121–132, https://doi.org/10.1023/B:PHYT.0000004198.95836.ad, 2003.

Chapter 3

A model-based analysis of foliar NO_x deposition

Adapted from Delaria, E. R. and Cohen, R. C.: A model-based analysis of foliar NO_x deposition, Atmos. Chem. Phys. Discuss., https://doi.org/10.5194/acp-2019-538, in review, 2019.

3.1 Introduction

The chemistry of nitrogen oxides ($NO_x \equiv NO + NO_2$) has a large impact on the oxidative capacity of the atmosphere and the budget of global surface ozone (Crutzen, 1979). NO_x is primarily removed from the atmosphere by chemical reactions to form nitric acid, alkyl nitrates, and peroxynitrates, and by dry deposition of NO_2 (Crutzen, 1979; Jacob and Wofsy, 1990; Romer et al., 2016). The chemical loss pathways of NO_x have been extensively studied, but the physical loss of NO_2 to dry deposition remains much more uncertain. Globally, foliar deposition of NO_2 removes 20—50% of soil-emitted NO (Jacob and Wofsy, 1990; Yienger and Levy, 1995), and constrains near-surface NO_x concentrations and input to ecosystems (Hardacre et al., 2015). Understanding the processes that control this removal of NO_x by the biosphere is important for predicting anthropogenic surface ozone and understanding flows in the nitrogen cycle.

Reactive nitrogen oxides also serve as an important nutrient in ecosystems. Exchange processes cycle nitrogen between the biosphere and atmosphere, influencing the availability of nitrogen to ecosystems (Townsend et al., 1996; Holland et al., 1997; Galloway et al., 2004; Holland et al., 2005). Deposition of atmospheric reactive nitrogen species can fertilize ecosystems with limited nitrogen availability (Ammann et al., 1995; Townsend et al., 1996; Williams et al., 1996; Holland et al., 1997; Galloway et al., 2004; Teklemmariam and Sparks, 2006). Although nitrogen is often the limiting nutrient for plant growth (Oren et al., 2001; Galloway et al., 2004), anthropogenic activities have in some cases caused an excess loading of nitrogen to ecosystems, leading to dehydration, chlorosis, soil acidification, and a decline

in productivity (Vitousek et al., 1997; Fenn et al., 1998; Galloway et al., 2004).

The current understanding of the exchange of nitrogen oxides between the atmosphere and biosphere remains incomplete. Despite the importance of dry deposition processes, they are among the most uncertain and poorly constrained aspects of atmosphere-biosphere nitrogen exchange and the tropospheric budgets of O_3 and NO_x (Wild, 2007; Min et al., 2014; Hardacre et al., 2015). This uncertainty arises from the complex dependence of dry deposition processes on surface cover, meteorology, seasonal changes in leaf area index (LAI), species of vegetation, and the chemical species carrying odd-N. Developing a mechanistic understanding of dry deposition of NO_2 has largely depended on inferences from scarce long-term field observation data and a limited number of laboratory studies on the effects of environmental factors on deposition at the leaf-level. This understanding is represented by a deposition velocity, V_d. Many global scale chemical transport models (Wesely, 1989; Jacob and Wofsy, 1990; Ganzeveld and Lelieveld, 1995; Wang and Leuning, 1998; Ganzeveld et al., 2002b) parameterize V_d using the resistance in-series approach similar to that developed by Baldocchi et al. (1987). These treatments are heavily parameterized, leading to a large degree of uncertainty, many of which (Jacob and Wofsy, 1990; Wesely, 1989) do not account for the effects of VPD, SWP, CO_2 mixing ratio, or other factors known to influence stomatal conductance (Hardacre et al., 2015). A common approach for modelling canopy uptake of trace gases is with a one- or two- layer "big-leaf" dry deposition model, in which the forest is treated as having a characteristic "average" deposition velocity (Hicks et al., 1987; Wesely, 1989; Ganzeveld and Lelieveld, 1995; Wang and Leuning, 1998; Zhang et al., 2002). However, Ganzeveld et al. (2002a) implemented a multi-layer column model in a global chemistry and general circulation model GCM-ECHAM (European Centre Hamburg Model) to study the role of canopy interactions in global atmosphere-biosphere NO_x exchange and demonstrated the importance of considering interactions within the canopy, particularly in pristine forest sites. More comprehensive treatments of atmosphere-biosphere exchange are thus needed in global models.

The deposition velocity of NO_2 to vegetation is largely regulated by stomatal conductance (Johansson, 1987; Thoene et al., 1991; Rondón and Granat, 1994; Teklemmariam and Sparks, 2006; Chaparro-Suarez et al., 2011; Breuninger et al., 2012; Delaria et al., 2018), which varies with tree species, photosynthetically active radiation (PAR), vapor pressure deficit (VPD), temperature (T), soil water potential (SWP) and seasonality of leaf phenology (Emberson et al., 2000; Zhang et al., 2003; Altimir et al., 2004; Hardacre et al., 2015; Kavassalis and Murphy, 2017). NO_2 deposition remains even more uncertain than deposition of O_3, where stomatal response has been shown to be the primary regulator of foliar deposition and mesophyllic resistance to deposition is negligible. Observations from leaf-level laboratory studies suggest the deposition of NO_2 is also controlled by stomatal aperture (Hanson and Lindberg, 1991; Rondón and Granat, 1994; Hereid and Monson, 2001; Teklemmariam and Sparks, 2006; Pape et al., 2009; Chaparro-Suarez et al., 2011; Breuninger et al., 2012; Delaria et al., 2018), however, reactions in the mesophyll may also be important for controlling the deposition velocity of NO_2 (Teklemmariam and Sparks, 2006; Breuninger et al., 2012). A failure to consider the effects of relevant meteorology on stomatal conductance, as well as our deficient

understanding of mesophyllic resistances and the diversity of ecosystem responses, severely limits our ability to understand dry-deposition processes and how they will be affected by feedbacks from changes in climate, land use, and air pollution. The importance of these considerations has recently been illustrated by Kavassalis and Murphy (2017), who found a significant correlation between VPD and ozone loss, and demonstrated that modeling using VPD-dependent parameterizations of deposition better predicted the correlation they observed. Previous work by Altimir et al. (2004) and Gunderson et al. (2002) have described the effects of VPD and other environmental parameters on the stomatal conductance to O_3 of *Pinus sylvestris* and *Liquidambar styraciflua*, respectively. More recent models, like the DO3SE model for estimating stomatal conductance to predict ozone deposition velocities, fluxes and damage to plants, incorporate the effects of VPD and SWP on stomatal conductance. No similar model exists for assessing these effects on NO_x deposition, although Ganzeveld et al. (2002a) included the effect of soil moisture availability for evaluating the role of canopy NO_x uptake on canopy NO_x fluxes. The DO3SE has successfully been implemented in the European Monitoring and Evaluation Program (EMEP) regional model (2012). Modelling studies by Büker et al. (2007) and Emberson et al. (2000) have also demonstrated the success of regional-scale parameterizations using observed relationships between meteorology and stomatal conductance for application to O_3. Such treatments of VPD and SWP were incorporated into a regional air quality model by Zhang et al. (2002, 2003).

In this study we present a simplified multi-layer atmosphere-biosphere exchange model and investigate the sensitivity of NO_x canopy fluxes, ozone production, NO_x vertical profiles, and NO_x lifetimes to different parameterizations of stomatal conductance and deposition velocity. We consider here both the Wesely model and the similarly simplistic approach of Emberson et al. (2000) that incorporates effects of VPD and SWP. We restrict our considerations to the effects of different stomatal resistance parameterizations on predicted deposition velocities, as the magnitude of the mesophyllic resistance remains uncertain and is assumed to be comparatively small in atmospheric models (Zhang et al., 2002). We also restrict our considerations to NO_2 deposition, as NO deposition has been shown to be negligible in comparison (Delaria et al., 2018). There have been many studies investigating the effects of dry-deposition parameterizations on deposition velocities—particularly of ozone—and the abilities of different modeling schemes to reproduce observational data for other molecules such as NO_2, NO, H_2O_2, HNO_3, hydroxy nitrates, alkyl nitrates, peroxyacyl nitrates, etc. Zhang et al. (1996); Wang et al. (1998); Emberson et al. (2000); Ganzeveld et al. (2002b); Büker et al. (2007); Wolfe et al. (2011); Hardacre et al. (2015); Nguyen et al. (2015). However, there has been little evaluation of how changes in dry deposition of NO_2 may affect surface mixing ratios and chemistry of important atmospheric species. Assessing the sensitivity to NO_2 deposition is crucial not only for evaluating the potential impact of uncertainties in dry-deposition parameterizations for global and regional models, but for understanding how a changing climate may influence NO_x, surface ozone, and the nitrogen cycle.

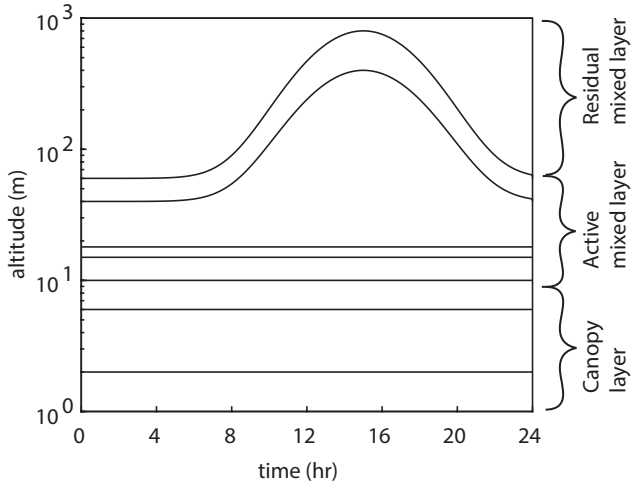

Figure 3.1: Planetary boundary dynamics in the 1D multibox model. The model domain consists of three boxes in the canopy layer, four in the active mixed layer, and one in the residual mixed layer. The lower five boxes have fixed heights, while the sixth and seventh boxes evolve throughout the day, in the form of a Gaussian function.

3.2 Model description

We have constructed a simple atmospheric model for investigating the influence of leaf-level NO_2 foliar deposition on canopy scale NO_x lifetimes and concentrations. The model consists of three canopy layers and a total of eight vertical boxes within the planetary boundary layer (PBL), taken to be 1000 m during the day and 60 m at night (Wolfe and Thornton, 2011; Wolfe et al., 2011). The increase in PBL height during the day is treated as a Gaussian function of time with 98% of the integrated area contained between sunrise and sunset, with the maximum height reached at the time of maximum daily temperature (Fig. 3.1). The first two boxes above the canopy were kept at a constant altitude, as the evolution of these layers was found to have a minimal effect on the model results discussed. The model was designed to be representative of a homogenous forest environment with the aim of simulating observations at forest tower sites. In each box, the change in concentration (C) of species i, is calculated using the time-dependent continuity equation:

$$\frac{\delta C_i(z)}{\delta t} = P(z) + L(z) + E(z) + D(z) + A(z) + \frac{\delta F(z)}{\delta z} \tag{3.1}$$

where the terms on the right are the chemical production, chemical loss, emission, deposition, advection, and turbulent flux, respectively. In each box ($k = 1 - 8$) the altitude (z) is considered as the average of the altitudes at the upper boundaries of boxes k and $k-1$ (the midpoint of box k). The change in concentration for species i is calculated for each time

step Δt = 2 s (3.1).

$$\Delta C_{i,k} = \left(P_{i,k} + L_{i,k} + E_{i,k} + D_{i,k} + A_{i,k} + \frac{F_{i,k}}{\Delta h_k} \right) \Delta t \tag{3.2}$$

where Δh_k is the width of box k. The only species not treated in this manner is the hydroxyl radical (OH), which is calculated using a steady-state approximation.

Deposition

The deposition flux (F_{dep}) of each depositing species i in the canopy is calculated according to:

$$F_{dep} = -V_d \cdot LAI \cdot C_i \tag{3.3}$$

where LAI is the leaf area index, and V_d is the deposition velocity. The deposition velocities are calculated according to:

$$V_d = \frac{1}{R} \tag{3.4}$$

where R is the total resistance to deposition.

$$R_{leaf} = \left(\frac{1}{R_{cut}} + \frac{1}{R_{st} + R_m} \right)^{-1} \tag{3.5}$$

$$R = R_a + R_b + R_{leaf} \tag{3.6}$$

where R_a, R_b, R_{cut}, R_{st}, and R_m are the aerodynamic, boundary layer, cuticular, stomatal, and mesophilic resistances, respectively. These resistances describe the turbulent transport of a gas to the surface (R_a), molecular transport through a thin layer of air above the leaf surface (R_b), and deposition to the leaf surface (R_{leaf}) (Baldocchi et al., 1987). R_{leaf} is dependent upon plant physiology and the chemical and physical properties of the deposition compounds. R_{leaf} is determined by deposition to the leaf cuticles (R_{cut}), diffusion through the stomata (R_{st}), and chemical processing within the mesophyll (R_m). We do not allow for emission of NO or NO_2 from leaves, consistent with recent laboratory observations that have observed negligible emission of these molecules (Chaparro-Suarez et al., 2011; Breuninger et al., 2013; Delaria et al., 2018).

All boundary, aerodynamic, cuticular, and soil resistances of O_3, HNO_3, CH_2O, alkyl nitrates (ANs) and acylperoxy nitrates (APNs), HC(O)OH, ROOH, and H_2O_2 are calculated according to Wolfe and Thornton (2011). The cuticular and mesophyllic resistances for NO_2 and NO are adjustable input parameters. Stomatal resistances are determined from the stomatal conductance to water vapor (g_s) calculated using either Eq. 3.7 (Wesely, 1989), or Eq. 3.8 (Jarvis, 1976; Emberson et al., 2000), hereafter referred to as the Wesely and Emberson schemes, respectively:

$$g_s = g_{max} \times \frac{T(40 - T)/400)}{(1 + (200(SR + 0.1)^{-1})^2} \tag{3.7}$$

Table 3.1: Parameters used in the model for comparison to observations from UMBS and BEARPEX-2009

Parameter	Symbol	UMBS	BEARPEX
Canopy height	h_{can}	[a]20 m	[b]10 m
Understory height	h_{us}	[c]4 m	[b]2 m
Total leaf area index	LAI	[c]3.5m^2 m^{-2}	[b]5.1 m2/m2
Radiation extinction coefficient	k_{rad}	[a]0.4	[a]0.4
Diffusion timescale ratio	τ/T_L	[a]2	[a]2
Friction velocity	u^*	[a]61 cm s-1	[a]61 cm s^{-1}
Maximum NO emission flux	eNO_{max}	[c]0.7 ppt m s^{-1}	[b]3 ppt m s^{-1}
Minimum NO emission flux	eNO_{min}	[c]0.3 ppt m s^{-1}	[b]1 ppt m s^{-1}
VOC basal emission flux	E_b	[d]5 ppb m s^{-1}	[b]11 ppb m s^{-1}
Integration interval	Δ t	2	2
OH + VOC rate constant (cm^3 molecules^{-1} s^{-1})	k_{OH}	[e]9.8$\times$ 10^{-11}	[e]8.7$\times$10^{-11}
NO_3 + VOC rate constant (cm^3 molecules^{-1} s^{-1})	k_{NO_3}	[e]7.0 $\times$ 10^{-13}	[e]1.7$\times$10^{-14}
Minimum daily temperature		15 °C	17 °C
Maximum daily temperature		23 °C	27 °C
Maximum daily relative humidity		85%	65%
Minimum daily relative humidity		65%	30%
Maximum daily soil water potential		[f]-0.05 MPa	[g]-0.8 MPa
Minimum daily soil water potential		[f]-0.25 MPa	[g]-1.0 MPa

a. Geddes and Murphy, 2014
b. Wolfe and Thornton, 2011
c. Seok et al., 2013
d. estimated from Bryan et al., 2015
e. See text, calculated assuming dominant VOC is MBO for Blodgett and isoprene for UMBS
f. Estimated from Matheny et al., 2015
g. Taken from Ishikawa and Bledsoe (2000) and Stern et al. (2018)

$$g_s = g_{max} \times f_{phen} \times f_{light} \times max\left[f_{min}, (f_{temp} \times f_{VPD} \times f_{SWP})\right] \tag{3.8}$$

where g_{max} is the species-specific maximum stomatal conductance, f_{min} is a species-specific scaling factor to the minimum stomatal conductance, SR is the solar radiation in W m^{-2}, and f_{phen}, f_{SWP}, f_{light}, f_{temp}, and f_{VPD} are functions representing modifications to the stomatal conductance due to leaf phenology, soil water content, irradiance, temperature, and vapor pressure deficit, respectively (Eq. 3.9—3.12).

$$f_{light} = 1 - \exp(-Light_a \times PPFD) \tag{3.9}$$

$$f_{temp} = 1 - \frac{(T - T_{opt})^2}{(T_{opt} - T_{min})^2} \tag{3.10}$$

$$f_{VPD} = min\left[1, \left((1 - f_{min}) \times \frac{(VPD_{min} - VPD)}{(VPD_{min} - VPD_{max})}\right) + f_{min}\right] \tag{3.11}$$

$$f_{SWP} = min\left[1, \left((1 - f_{min}) \times \frac{(SWP_{min} - SWP)}{(SWP_{min} - SWP_{max})}\right) + f_{min}\right] \tag{3.12}$$

T_{opt} and T_{min} are the optimal and minimum temperature required for stomatal opening. PPFD is the photosynthetic photon flux density and $Light_a$ is a species-specific light response parameter. VPD_{min} and VPD_{max} are the vapor pressure deficit at which stomatal opening reaches a minimum and maximum, respectively. SWP_{min} and SWP_{max} are the soil water potentials at which stomatal opening reaches a minimum and maximum, respectively. All model calculations represented the peak growing season when f_{phen}= 1. f_{temp}, f_{VPD}, and f_{light} were calculated according to Emberson et al. (2000) using parameters found in 3.2.

Site description

The model was evaluated with comparison to observations from the Biosphere Effects on Aerosols and Photochemistry 2009 (BEARPEX-2009) field campaign from 15 June – 31 July 2009 at Blodgett forest (Min et al., 2014), and the University of Michigan Biological Station (UMBS) during 5 August – 10 August 2012 (Geddes and Murphy, 2014). For the BEARPEX-2009 calculations, the modelled canopy included an overstory height of 10 m with a one-sided leaf area index (LAI) of 3.2 m^2m^{-2} (LAI_{os}), and an understory height of 2 m with a LAI of 1.9 m^2m^{-2} (LAI_{us}). Model simulations were run for June 30, 2009 using conditions from the BEARPEX-2009 ponderosa pine forest site located in the western foothills of the Sierra Nevada Mountains, CA (38°58'42.9"N, 120°57'57.9"W, elevation 1315 m) (3.1) (Fig. 3.2a). Meteorological conditions and soil NO emissions used in the model simulation were those reported by Min et al. (2014). Diurnal soil water potentials (SWP) were values reported in a geological survey of nearby Sierra sites in a comparatively wet year (Ishikawa and Bledsoe, 2000; Stern et al., 2018).

For UMBS-2012 calculations, the modelled canopy included an overstory height of 20 m with a one-sided LAI of 2.5 m^2m^{-2}, and an understory height of 4 m with a LAI of 1 m^2m^{-2} (Bryan et al., 2015). Model simulations were run for August 8, 2012 using conditions from

Table 3.2: Parameters used in the model for comparison to observations from UMBS and BEARPEX-2009

	UMBS	reference	BEARPEX	reference
g_{max} (cm s^{-1})	0.2	Büker et al. 2012	0.3	Altimir et al. 2003
f_{min}	0.05	Büker et al. 2012	0.03	Büker et al. 2012
$Light_a$	0.001	Büker et al. 2012	0.001	This study
T_{max} (°C)	33	Büker et al. 2012	35	Altimir et al. 2003
T_{min} (°C)	5	Büker et al. 2012	5	Altimir et al. 2003
T_{opt} (°C)	16	Büker et al. 2012	20	Altimir et al. 2003
VPD_{min} (kPa)	3.1	Büker et al. 2012	4	Hubbard et al. 2001, Ryan et al. 2000, Kolb and Stone 1999
VPD_{max} (kPa)	1.1	Büker et al. 2012	1.5	Hubbard et al. 2001, Ryan et al. 2000, Kolb and Stone 1999
SWP_{max} (MPa)	-1.0	Emberson et al. 2000	-1.0	Anderegg et al. 2017
SWP_{min} (MPa)	-1.9	Emberson et al. 2000	-2.0	Anderegg et al. 2017

the UMBS mixed hardwood forest located in northern Michigan (45°33'32" N, 84°42'52" W) (3.1) (Fig. 3.2b). Daily temperatures, VPDs, soil NO emissions and site-specific parameters used in the model simulations were those reported in Geddes and Murphy (2014), and Seok et al. (2013).

Temperature and relative humidity used in the model were sinusoidal fits to observations of minimum and maximum daily temperature and relative humidity from the corresponding field measurement site. The relative temperature decrease as a function of altitude was calculated using a fit to observations during BEARPEX-2007, as presented by Wolfe and Thornton (2011). Solar zenith angles (SZA) and photosynthetically active radiation (PAR) were calculated every 0.5 h for each location and time period using the National Center for Atmospheric Research TUV calculator (Madronich and Flocke, 1998) and fit using a smoothed spline interpolation. Within the canopy, extinction of radiation (ER) was calculated following Beer's law:

$$ER_k = \exp\left(\frac{-k_{rad} LAI_{cum}}{cos(SZA)}\right) \tag{3.13}$$

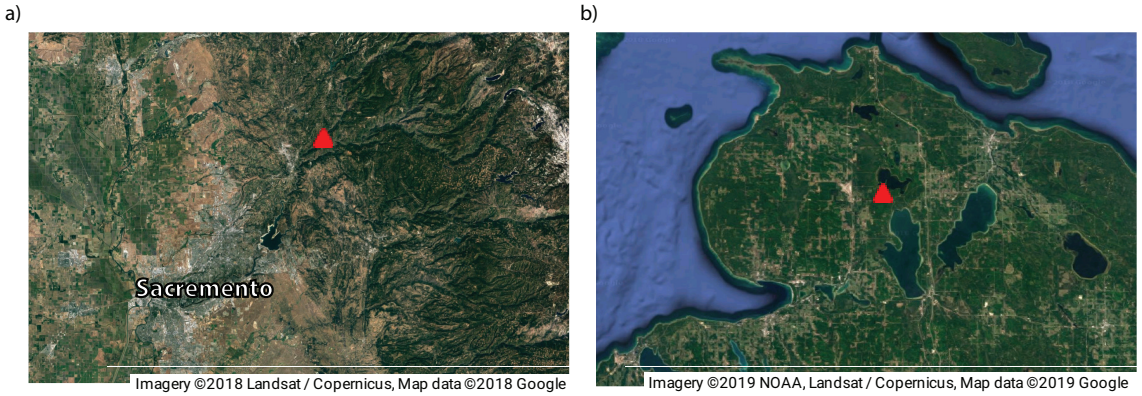

Figure 3.2: Satellite images showing the locations of (a) the BEARPEX-2009 campaign and (b) the University of Michigan Biological Station (UMBS). Red triangles show the specific site locations. Measurements of chemical species and local meteorological variables from the two campaigns were used to validate our 1D canopy multibox model.

where k_{rad} is the radiation extinction coefficient, SZA is the solar zenith angle,and LAI_{cum} is the cumulative LAI calculated as the sum of one-half the LAI in box k and the total LAI in the boxes above box k.

Vertical transport and advection

The turbulent diffusion flux ($F(z)$) is represented in the model using K-theory, according to the Chemistry of Atmosphere-Forest Exchange (CAFE) Model (Wolfe and Thornton, 2011).

$$F(z) = -K(z)\frac{\Delta C_{i,k}}{\Delta z} \tag{3.14}$$

where $\Delta C_{i,k}$ is the change of concentration of species i in box k during each timestep and Δz is the difference between the midpoints of boxes k and $k+1$. $K(z)$ above the canopy is based on the values from Gao et al. (1993) and below is a function of friction velocity calculated according to Wolfe et al. (2011) and is a function of the diffusion timescale ratio (τ/T_L)–defined as the ratio of the "time since emission" of a theoretical diffusing plume (τ) and the Lagrangian timescale (T_L)–and the friction velocity (u^*) (Wolfe and Thornton, 2011). The details of the parameterization of turbulent diffusion fluxes is documented elsewhere (Wolfe and Thornton, 2011) and based on the works of Raupach et al. (1996) and Makar et al. (1999). The height dependent friction velocity ($u(z)^*$) is attenuated from the above-canopy u^* according to Yi (2008). Although Finnigan et al. (2015) identified flaws in this treatment, we believe it is sufficient for our focus on illustrating generalizable qualitative trends.

The resulting residence time in the canopy is approximately 2—3 min for model conditions during the day. Our model is a simple parameterization of turbulent processes and as such will only capture mean vertical diffusion. Other works (Collineau and Brunet, 1993; Raupach et al., 1996; Brunet and Irvine, 2000; Thomas and Foken, 2007; Sörgel et al., 2011; Steiner et al., 2011) have shown that "near-field" effects of individual canopy elements and coherent turbulent structures can play an important role in canopy exchange. These more intricate processes are not captured explicitly by our simple model. Previous work (Gao et al., 1993; Makar et al., 1999; Stroud et al., 2005; Wolfe et al., 2011) have also utilized fairly simple representations of canopy exchange in local and regional models, and as such K-theory is likely sufficient to represent average vertical diffusion for the purposes of our study.

Advection in the model is treated as a simple mixing process in each model layer.

$$\frac{dC_i}{dt} = -k_{mix}(C_i - C_i(adv)) \tag{3.15}$$

where k_{mix}=0.3 h^{-1} (Wolfe and Thornton, 2011), and $C_i(adv)$ is the advection concentration of species i. Advection concentrations are set to fit with the observations during BEARPEX-2009 (Min et al., 2014) or UMBS-2012 (Geddes and Murphy, 2014; Seok et al., 2013) and are used to maintain reasonable background concentrations (Table 3.A1). Concentrations of NO_x, O_3, and some VOCs at both sites were influenced by emissions from nearby cities and consequently had sources outside the canopy. For the BEARPEX-2009 model runs, the maximum daily advection concentration was reached at around 17 hrs, based on field observations of higher NO_x plumes from near-by Sacramento in the afternoon (Wolfe and Thornton, 2011; Min et al., 2014). The diurnal advection concentrations of NO_x were modelled with a sinusoidal function in the range 0.1—0.35 ppb (Table 3.A1). For UMBS all advection concentrations were constant.

Chemistry

Chemistry in the model is based on reaction rate constants from the JPL Chemical Kinetics and Photochemical Data Evaluation No. 18 (Burkholder et al., 2014). Photolysis rates are calculated as a function of solar zenith angle (SZA), which was constructed using a smoothed spline interpolation fit of photolysis rates calculated with the TUV calculator (Madronich and Flocke, 1998) at every ten-degree interval of the zenith angle. The simplified reaction scheme included in the model is based on the model presented in Browne and Cohen (2012). The model includes both daytime and night-time NO_x chemistry and a simplified oxidation scheme. In this simplified case, oxidation of volatile organic compounds (VOCs) during the daytime results in the production of peroxy radicals (RO_2), treated as a uniform chemical family. To be applicable to a range of forest types, we also include adjustable parameters, k_{OH} and k_{NO_3} for the average rate constant for reaction of VOC with OH and NO_3, respectively. k_{OH} and k_{NO_3} are effective values adjusted in the model based on site-specific VOC composition and observations of OH reactivity. A complete list of reactions and rate constants included in the model is shown in Table 3.A2.

BVOC emissions

Emissions rates (molecules cm^{-3} s^{-1}) of biogenic volatile organic compounds (BVOCs) in the canopy are calculated via:

$$E(z) = \frac{E_b}{\Delta h} C_L(z) C_T(z) LAI(z) \tag{3.16}$$

(16) where E_b (molecules cm(leaf)$^{-2}$ s^{-1}) is the basal emission rate of VOC, Δh is the total height of the box, and C_L and C_T are corrections for light and temperature (Guenther et al., 1995).

Evaluation of NO_x fluxes and lifetimes

The model was used to assess the impact of NO_2 deposition parameters on the NO_x budget, lifetime, loss, and vertical profile within a forested environment. In each box, the rates of NO_x loss with respect to nitric acid formation, alkyl nitrate formation, and deposition were calculated from Eq. 3.17—3.19.

$$L_{NO_x \rightarrow HNO_3} = k_{OH+NO_2}[OH][NO_2] + k_{N_2O_5\ \text{hydrolosis}}[N_2O_5] + k_{NO_3+\text{aldehyde}}[\text{aldehyde}][NO_3] \tag{3.17}$$

$$L_{NO_x \rightarrow RONO_2} = \alpha k_{NO+RO_2}[NO][RO_2] + \beta k_{NO_3}[NO_3][BVOC] \tag{3.18}$$

$$L_{NO_x \rightarrow Dep} = \frac{F_{dep}}{\Delta h_k} \tag{3.19}$$

α is the fraction of the NO + RO_2 reaction that forms alkyl nitrates and β is the fraction of the NO_3 + BVOC reaction that forms alkyl nitrates. The NO_x lifetime was then scaled to the entire boundary layer by summing over the products of the lifetime and boundary layer fraction (Δh_k/PBL) in each box

$$\tau_{PBL} = \frac{\sum_{k=1}^{8} [NO_x]_k}{\sum_{k=1}^{8} L_{NO_x \rightarrow HNO_3} + L_{NO_x \rightarrow RONO_2} + L_{NO_x \rightarrow Dep}} \tag{3.20}$$

(20) NO_x was treated as the sum of NO, NO_2, and all short-lived products, including NO_3, $2N_2O_5$, and peroxyacetyl nitrate (PAN) (Romer et al., 2016). Deposition of PAN was not considered.

We also calculated the 24 h average vertical fluxes (Eq. 3.14) of NO_x , and used the flux through the canopy to estimate the fraction of soil emitted NO_x ventilated to the troposphere above. Because PAN formed during the nighttime is expected to re-release NO_x to the atmosphere during the day, in this calculation, PAN was included as part of the NO_x budget.

3.3 Sensitivity to parameterizations

We assessed the sensitivity of the model to τ/T_L, the radiation extinction coefficient (k_{rad}), the aerodynamic leaf width (l_w), LAI, soil NO emission (eNO), and α. These parameters are simplifications of complex physical processes and not always easily constrained by observations. The total deposition velocity of NO_2 chosen for these assessments was 0.2 cm s^{-1} during the daytime and 0.02 cm s^{-1} during the nighttime, based on values of g_{max} and g_{min} chosen for Blodgett forest (discussed above) and typical values for deposition velocity observed for a variety of species in the laboratory (Teklemmariam and Sparks, 2006; Chaparro-Suarez et al., 2011; Breuninger et al., 2013; Delaria et al., 2018).

The largest effects were observed for changes in α, LAI, and soil NO emission. LAI_{os} and LAI_{us} were scaled from their values of 1.9 m^2 m^{-2} and 3.2 m^2 m^{-2}, respectively by a factor of 0.25 and 1.5. Increasing the scaling factor from 0.25 to 1.5 resulted in a decrease of NO_x lifetimes, above canopy concentration, and average canopy flux of 24%, 27%, and 36%, respectively (Fig. 3.A1). Increasing α from 0.01 to 0.1 resulted in a decrease in NO_x lifetimes, above canopy concentrations, and average canopy fluxes of 75%, 38%, and 39%, respectively (Fig. 3.A2). For all other model runs an α of 0.075 was chosen, in accordance with observations from regions primarily influenced by BVOCs (eg. monoterpenes, isoprene, 2-methyl-3-buten-2-ol). Increasing the maximum soil NO emission from 1 to 10 ppt m s^{-1} increased the in-canopy enhancement from 28% to 140% relative to above-canopy NO_x concentrations (Fig. 3.A3b). The fraction of soil-emitted NO_x ventilated through the canopy also increased from 45% to 64% (Fig. 3.A3a). The large effect of soil NO emission on NO_x fluxes implies that this highly variable parameter (Vinken et al., 2014) is also important to constrain in chemical transport models. Further discussion of soil NO emission is, however, beyond the scope of this study.

Very small effects on NO_x were observed for changes in the parameters τ/T_L, k_{rad}, or l_w. The minor changes caused by variations in these parameters are listed below for completeness:

τ/T_L represents the diffusion timescale ratio, a full description of which can be found in Wolfe and Thornton (2011). Larger τ/T_L represents faster diffusion and vertical transport within the canopy layer, and shorter residence times in the canopy. We find that altering this parameter from 1.2 to 8 (representing a change in residence time from 650 s to 62 s) caused a 9.9%, 4.4%, and 8.7% increase in average canopy fluxes, NO_x lifetimes and above canopy concentration, respectively (Fig. 3.A4). For all subsequent model runs, a value of 2 for τ/T_L was chosen, resulting in a canopy residence time during the day of 152 s and 194 s for Blodgett Forest and UMBS, respectively, calculated using Eq.3.21.

$$\tau_{can} = h_{can} \sum_{k=1}^{3} \frac{\Delta h_k}{K(z_k)} \tag{3.21}$$

The boundary layer resistance, or laminar sublayer resistance, R_b, is dependent upon the

aerodynamic leaf width, l_w (Eq.3.22)

$$R_b = \frac{c\nu}{Du^*(z)} \left(\frac{l_w u^*(z)}{\nu} \right)^{1/2} \tag{3.22}$$

where $\nu = 0.146$ cm^2 s^{-1} is the kinematic viscosity of air, D is the species-dependent molecular diffusion coefficient, c is a tunable constant set to 1 for this study, and $u^*(z)$ is the height-dependent friction velocity that is a function of u^* and LAI_{cum} (Wolfe and Thornton, 2011). l_w depends upon the vegetation species. A value of 1 cm was chosen for the overstory and 2 cm for the understory, as these widths are characteristic of pine trees and understory shrubs in a poderosa pine forest (Wolfe and Thornton, 2011). Species with rapid deposition to the cuticles or the stomata are expected to be more sensitive to errors in l_w, such as HNO_3 or H_2O_2. An increase in NO_x lifetime, average canopy flux, and above canopy concentration of 1.4%, 2.4%, and 2.8%, respectively, was predicted for a change in l_w scaling factor from 0.1 to 2 (Fig. 3.A5). These changes are expected to be greater in forests with a larger average deposition velocity, where R_b makes a greater contribution to the total resistance.

The rates of stomatal gas exchange and photolysis are regulated by the intensity of light that penetrates the canopy. The extinction of radiation by the canopy, treated as a Beer's Law parameterization (Eq. 3.13), is exponentially proportional to the radiation extinction coefficient, k_{rad}. k_{rad} ranging from 0.4—0.65 has been measured for coniferous forests and understory shrubs (Wolfe and Thornton, 2011). The NO_x lifetime increased by 2.7% and the canopy fluxes, and above-canopy concentrations decreased by 0.7% and 0.6%, respectively, for a change in k_{rad} from 0 to 0.6 (Fig. 3.A6). This effect is expected to be greater for forests with larger LAI. The minimal effect of k_{rad} on model results was also observed for multiple canopy profile shapes of equivalent LAI.

3.4 Results

Model validation: comparison to field observations

To evaluate the applicability of our 1D multilayer canopy model for predicting NO_x concentrations and vertical fluxes in a variety of forest environments, we compared the model to observations from BEARPEX-2009 and UMBS-2012. Parameters used in each calculation are shown in 3.1. The model was run using both the Emberson and Wesely stomatal conductance models. Parameters for temperature, drought stress, and maximum and minimum stomatal conductances used in the Emberson model were input for the dominant tree species in the region (3.2). At the BEARPEX-2009 site, the dominant tree species was ponderosa pine. For this site, g_{max} and parameters for f_{SWP} and f_{VPD} were inferred from ponderosa pine stomatal conductance data (Kelliher et al., 1995; Ryan et al., 2000; Hubbard et al., 2001; Johnson et al., 2009; Anderegg et al., 2017), and f_{light} was inferred from measurements of the canopy conductance during BEARPEX-2009 (Fig. 3.3a). f_{temp} was represented by observations for Scots pine (Altimir et al., 2004; Emberson, 1996; Büker et al., 2012) and validated

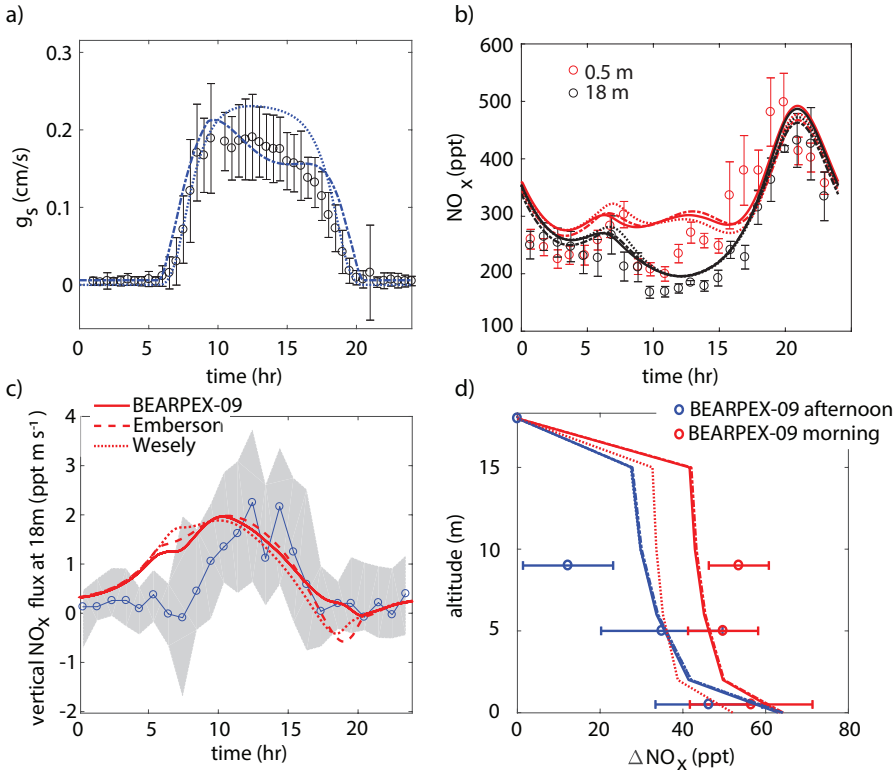

Figure 3.3: Comparison of model results to BEARPEX-2009 hourly averaged observations of (a) stomatal conductances, (b) NO_x mixing ratios at 18 m (black) and 0.5 m (red) and (c) vertical fluxes at 18 m. (d) Averaged observations of in-canopy NO_x enhancements from 09:00—12:00 (blue) and 13:00—16:00 (red) compared with modeled NO_x enhancements, defined as the difference between NO_x below the canopy and NO_x measured at 18 m. Observations from BEARPEX-2009 are from Min et al., (2014). In all panels solid lines, dotted lines, and dashed lines, represent results from our model with stomatal conductances parameterized using observed conductances, the Wesely model, and the Emberson model, respectively. Circles, error bars, and grey shaded regions represent observations, standard errors of the mean, and the interquartile range of data, respectively.

with comparison to stomatal conductance measured via sap-flow during BEARPEX-2009 (Fig. 3.3a). At UMBS the dominant species are quaking aspen and bigtooth aspen, with many birch, beech, and maple species also present (Seok et al., 2013). Data for a European beech tree species was used to represent stomatal conductance parameters (Büker et al., 2007, 2012) and SWP stress (Emberson et al., 2000). These parameters were validated with comparison to stomatal conductance calculated from water vapor and latent heat flux measurements during UMBS-2012 using an energy-balance method according to Mallick et al. (2013) (Fig. 3.4a).

The model replicates key features of the canopy fluxes and above-canopy NO_x daytime mixing ratios from the 2009 BEARPEX campaign (Fig. 3.3). The average daytime above-canopy NO_x mixing ratios during the duration of BEARPEX-2009 was 253 ppt, with observations ranging from 80—550 ppt of NO_2 and 10—100 ppt of NO (Min et al., 2014). The general daily trends in observations of NO_x mixing ratios are captured by both the Wesely and Emberson cases—with minimum NO_x mixing ratios occurring in the late morning, an increase of NO_x in the afternoon, and maximum NO_x concentrations of 450—500 ppt reached in the evenings, primarily as a result of high-NO_x plumes from near-by Sacramento in the afternoon (Wolfe et al., 2011; Min et al., 2014) (Fig. 3.3b). However, both model scenarios predict a slower than observed decrease in NO_x mixing ratios from the evening to the early morning, larger mid-morning fluxes than observed (by ∼0.5—1.5 ppt m s^{-1}), and fail to represent the in-canopy enhancement of NO_x (∼50 ppt), relative to above-canopy mixing ratios, observed in the evening (Fig. 3.3). The above-canopy vertical NO_x flux predicted in both model cases also agrees reasonably well with observations, with the Emberson case representing morning and midday NO_x fluxes slightly better than the Wesely case. This relatively good agreement between the Emberson case and observed fluxes is also demonstrated in Fig. 3.3d by the agreement between modelled and observed canopy NO_x enhancements. There is, however, generally little difference between Emberson and Wesely model cases for this site during the period considered (Fig. 3.3). This is likely due to the good agreement in both the Emberson and Wesely cases to observations of stomatal conductance (Fig. 3.3a). We also observe similar correspondence between the model and key features of the UMBS-2012 observations (Fig. 3.4). NO and NO_2 mixing ratios and canopy fluxes are both within the range of observations. The model predicts a maximum of ∼40% lower NO_2 in the morning and ∼30% higher NO_2 at night than what was observed (Fig. 3.4b). It should also be noted that this agreement was achieved without inclusion of an NO_2 compensation point, whereas Seok et al. (2013) had proposed the importance of considering foliar NO_2 emission at this location. Differences between the Wesely model and Emberson model were negligible for this site. This is likely due to a higher humidity in the summer in this region and larger soil moisture, reducing the prediction for midday and late afternoon VPD stress by the Emberson model, as can be seen by the similarity in the predicted g_s by the Emberson and Wesely models (Fig. 3.4a).

Effects of maximum stomatal conductance

The BEARPEX-2009 case was simulated using the Wesely model for different values of the maximum stomatal conductance (g_{max}) (Fig. 3.5), with advection concentrations of NO_x set to zero. The range of g_{max} currently represented in the literature during peak growing season for forested regions ranges from 0.2—0.8 cm s^{-1} (Kelliher et al., 1995; Emberson, 1996; Emberson et al., 2000; Ryan et al., 2000; Hubbard et al., 2001; Altimir et al., 2004; Fares et al., 2012). This range reflects differences in forest types and a wide variety of tree species. Global CTMs using the Wesely parameterization currently include g_{max} of 1.4, 0.77, and 1 cm s-1 for deciduous, coniferous, and mixed forests, respectively (Wesely, 1989; Wang

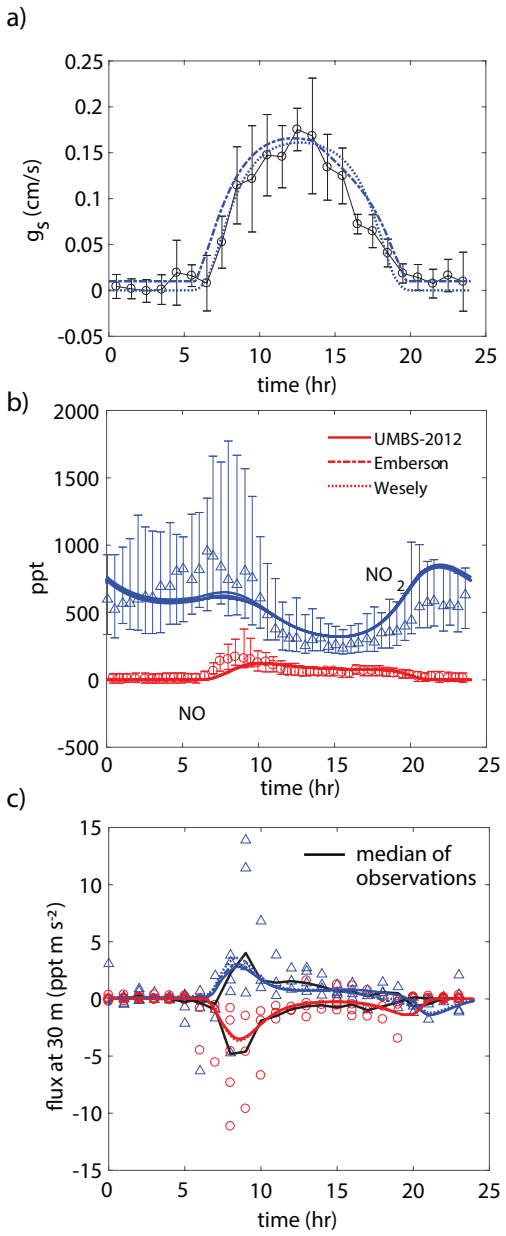

Figure 3.4: Comparison of model results to (a) hourly averaged observed stomatal conductances, (b) NO and NO_2 mixing ratios at 30 m, and (c) median (black lines) and hourly-averaged NO and NO_2 vertical fluxes at 30 m observed during UMBS-2012 for August 8, 2012. In all panels solid lines, dotted lines, and dashed lines, represent results from our model with stomatal conductances parameterized using observed conductances, the Wesely model, and the Emberson model, respectively. Blue triangles and red circles represent NO_2 and NO observations, respectively. Error bars represent the interquartile range of data.

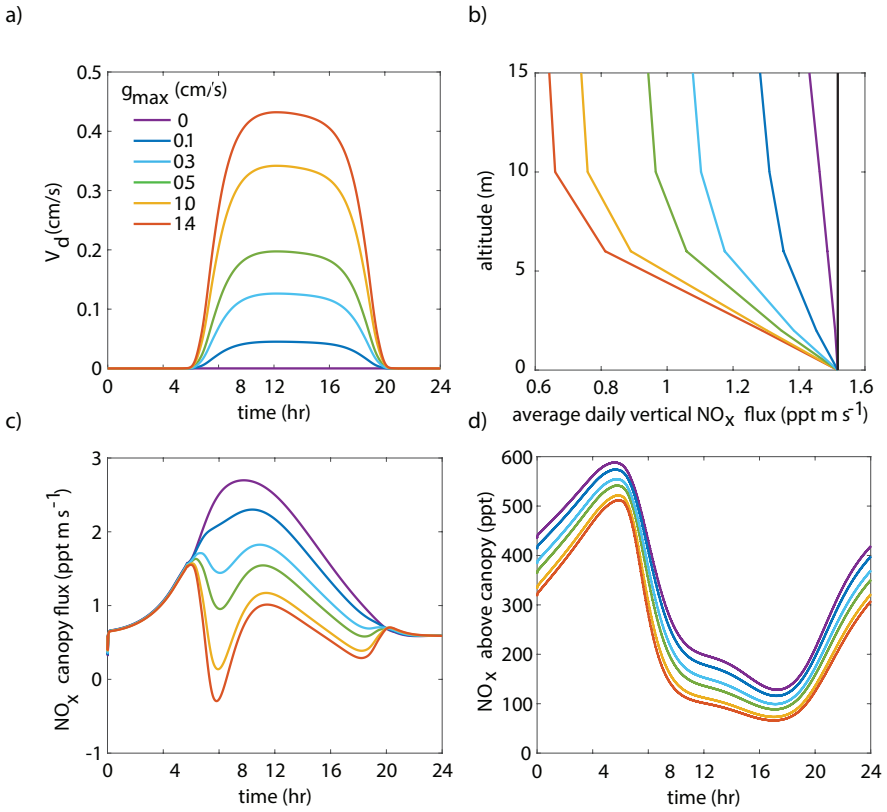

Figure 3.5: Model results of (a) diurnal NO_2 deposition velocities, (b) average daily vertical fluxes of NO_x and a conserved tracer (black line), (c) diurnal canopy fluxes at 10 m, and (d) diurnal above-canopy NO_x mixing ratios at 15 m for different values of maximum stomatal conductance (g_{max}) using the Wesely scheme to calculate stomatal conductance.

and Leuning, 1998). Figure 3.5b demonstrates the impact of g_{max} on the average daily vertical flux of NO_x through the canopy. 96% of soil emitted NO_x is ventilated through the canopy with no foliar deposition (g_{max}= 0 cm s^{-1}). In contrast, 44% of soil-emitted NO_x is taken up by the forest and 56% ventilated through the canopy when the maximum stomatal conductance is 1.4 cm s^{-1}. Figures 3.5c and 3.5d show the effects of g_{max} on the diurnal flux through the canopy and the diurnal above-canopy NO_x mixing ratio, respectively. Compared with no foliar deposition, a g_{max} of 1.4 cm s^{-1} results in ~60% reduction in the canopy flux and ~50% reduction in the above-canopy NO_x mixing ratio at noon. (Fig. 3.5c, d). In Figure 3.6a we show the fraction of soil-emitted NO_x ventilated through the canopy as a function of g_{max}. The model suggests a maximum foliar reduction of NO_x of ~60% for a canopy of 10 m and total LAI of 5.1 m^2 m^{-2}. Our model also predicts that changes in g_{max} have a greater overall impact on canopy NO_x fluxes at larger leaf resistances and slower foliar uptake. In the range for g_{max} of ~ 0—0.5 cm s^{-1}, variation in g_{max} can have a large impact on the predicted

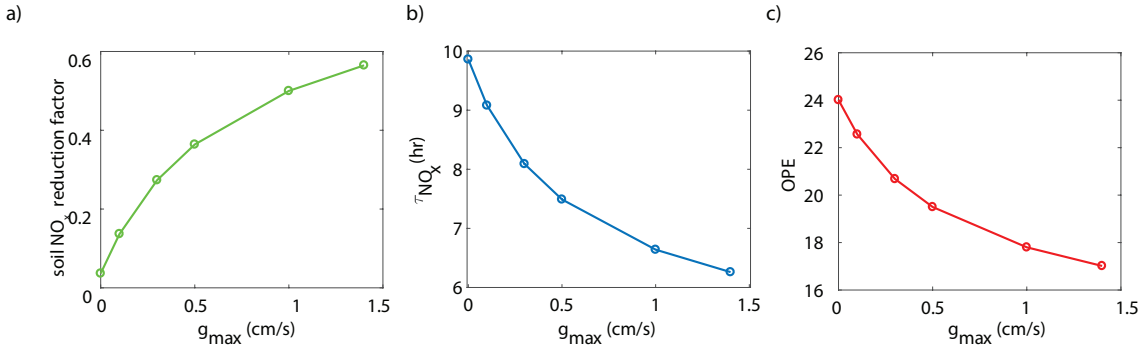

Figure 3.6: Model-predicted dependence of (a) the fraction of soil emitted NO_x removed in the canopy, (b) the average daily NO_x lifetime (τ_{NO_x}) in the planetary boundary layer, and (c) ozone production efficiency (OPE) on maximum stomatal conductance (g_{max}) using the Wesely scheme to calculate stomatal conductance.

canopy fluxes of NO_x, which would in turn have a large impact on concentrations and fluxes of O_3. These values of g_{max} result in deposition velocities in the range expected for most forests, based on laboratory measurements of leaf-level deposition (Hanson and Lindberg, 1991; Rondón and Granat, 1994; Hereid and Monson, 2001; Teklemmariam and Sparks, 2006; Pape et al., 2009; Chaparro-Suarez et al., 2011; Breuninger et al., 2013; Delaria et al., 2018) and global analysis suggesting 20—50% reductions in soil-emitted NO_x by vegetation (Jacob and Wofsy, 1990; Yienger and Levy, 1995; Ganzeveld et al., 2002b,a). Model calculations also predict a strong effect on the lifetimes of NO_x, as shown in Figure 3.6b, with maximum stomatal conductances of 0.1 cm s^{-1}, 0.3 cm s^{-1}, and 1.4 cm s^{-1} reducing the NO_x lifetime by ∼0.7 hrs (∼7%), ∼1.8 hrs (∼18%), and ∼3.6 hrs (∼36%), respectively compared with no deposition. Similar trends (not shown) were also observed using parameters for UMBS.

Emberson model vs. Wesely model comparison

The relative importance of including parameterizations of VPD and SWP in the calculation of stomatal conductance and overall deposition velocity is expected to be regionally variable, along with regional variations in dominant tree species, soil types, and meteorology. We ran the model using BEARPEX-2009 conditions using both the Wesely and Emberson stomatal conductance models under "dry" and "wet" conditions. Here we use "dry" to refer to conditions of low humidity and low soil moisture and "wet" to refer to conditions with high humidity and high soil moisture. Under the "dry" scenario the SWP daily minimum and maximum were ∼2.0 MPa and ∼1.7 MPa, respectively, with the daily minimum reached at sunset. A minimum daily RH of 40% occurred at noon, with a maximum at midnight of 65%. Summertime is often even drier in regions of the western United States, so these "dry" parameters are conservative estimates for many forests. Under the "wet" scenario the SWP daily minimum and maximum were -0.5 MPa and -0.1 MPa, respectively. The maximum

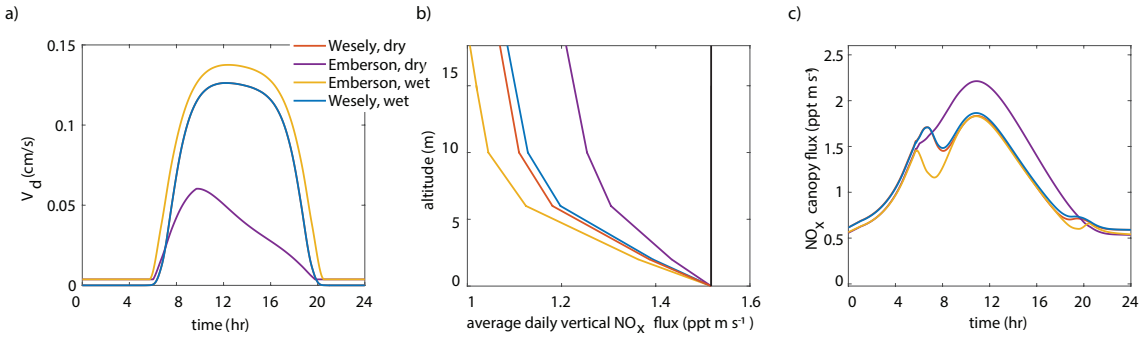

Figure 3.7: Modeled results of (a) diurnal NO_2 deposition velocities, (b) average daily vertical fluxes compared to a conserved tracer (black line), and (c) diurnal canopy fluxes at 10 m for "wet" and "dry" scenarios using either the Wesely or Emberson models to calculate stomatal conductance.

and minimum RH were 90% and 80%, respectively. The values for soil moisture and relative humidity chosen were based on observations of SWP by Ishikawa and Bledsoe (2000) and the long-term climate data record at Auburn Municipal Airport (38.9547° N, -121.0819° W) from NOAA National Centers for Environmental Information (noa).

The results of the Wesely and Emberson "wet" and "dry" model runs are shown in Figure 3.8. There was only a slight decrease of the in-canopy NO_x enhancement and the canopy flux in the Wesely "wet" case, presumably due to a slight increase in OH radicals at higher RH. Predictably, the difference in the modelled deposition velocities was quite dramatic between the Emberson "wet" and "dry" cases. In the "dry" scenario, the deposition velocity reached a maximum in the late morning, but rapidly declined after noon. The maximum deposition velocity reached was also substantially reduced (Fig. 3.7a). Using the "wet" Emberson stomatal conductance model, the NO_x flux out of the forest was reduced by 16% midday compared to the "dry" case, and the percent of soil NO_x removed within the canopy was increased from 18% to 30% (Fig. 3.7). The model calculates a substantial impact on above-canopy NO_x mixing ratios (Fig. 3.8), with a maximum of ∼30% difference in NO_x in the afternoon between "wet" and "dry" days using the Emberson parameterization, compared with ∼10% difference using the Wesely model. Using the Emberson parameterization of stomatal conductance, deposition during "wet" days is predicted to contribute substantially more to the total NO_x loss (∼40%), with only ∼15% contribution predicted for "dry" days (Fig. 3.9).

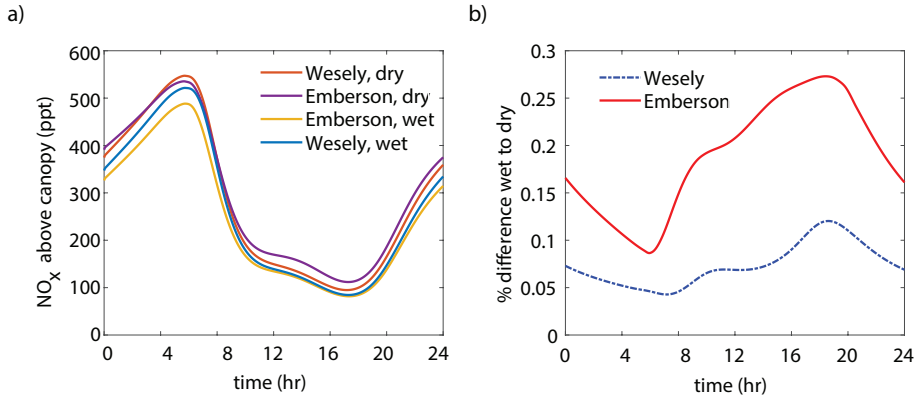

Figure 3.8: (a) Modeled NO_x mixing ratios above the canopy at 18 m for "wet" and "dry" scenarios using either the Wesely or Emberson models to calculate stomatal conductance. (b) Percent difference between NO_x mixing ratios on "wet" and "dry" days using either the Wesely (blue dashed line) or Emberson (red solid line) parameterization of stomatal conductance.

Under the Wesely model, where stomatal conductance is parameterized only with temperature and solar radiation, the predicted deposition velocity would be nearly identical between the spring and fall in the western United States and similar semi-arid regions (with comparatively minor temperature effects). While the Emberson model predicts large seasonal differences, the Wesely model fails to account for the dramatic decrease in stomatal conductance seen in the dry seasons in such regions caused by significant reductions in relative humidity and soil water potential (Prior et al., 1997; Panek and Goldstein, 2001; Chaves et al., 2002; Beedlow et al., 2013). We recognize that the multibox model presented in this work is a simplified representation of physical processes, and as such is not likely to (and is not intended to) provide quantitative exactitude for the trends described above. However, we argue for the necessity of incorporating these conceptual advances for accurately representing canopy processes and predicting their effect on the NO_x cycle.

3.5 Discussion

Implications for modelling NO_2 dry deposition

As in our multilayer canopy model, the most common current method of parameterizing stomatal and cuticular deposition in large-scale chemical transport models (CTMs) is through the resistance model framework of Baldocchi (1987). Many global (e.g. WRF-Chem and GEOS-Chem) and regional (e. g. MOZART and CAMx) CTMs calculate the stomatal component of the total deposition resistance using the representation of Wesely (1989), where stomatal conductance is dependent only on the type of vegetation, temperature, and solar

Lorem ipsum

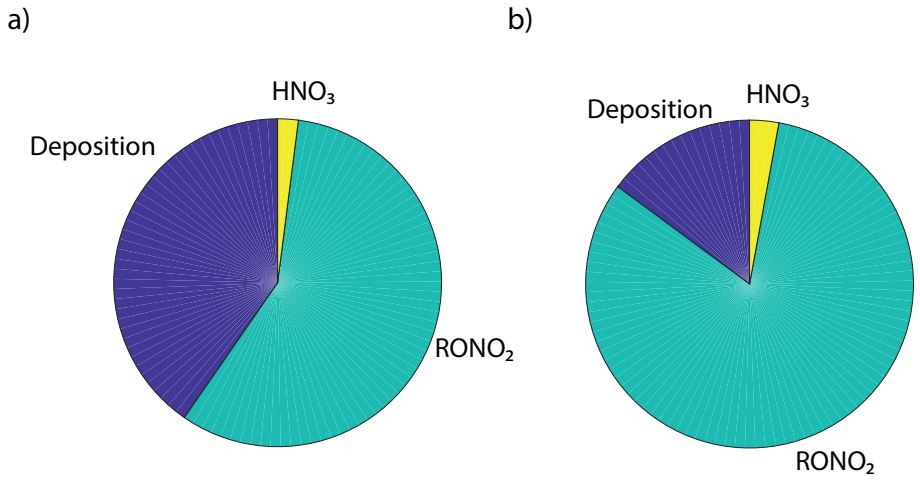

Figure 3.9: Model prediction for the daytime average fraction of NO_x removed by deposition, nitric acid formation, and alkyl nitrate formation using the Emberson parameterization of stomatal conductance for (a) "wet" and (b) "dry" conditions.

radiation. The limitations of this parameterization have been highlighted by observations of a strong dependence of foliar deposition on soil moisture and vapor pressure deficit (VPD) (Kavassalis and Murphy, 2017; Rydsaa et al., 2016). Inadequate descriptions of vegetative species, soil moisture, drought stress, etc., can have a dramatic impact on model results, and result in significant discrepancies between models and observations (Wesely and Hicks, 2000). Failure to account for effects of plant physiology on deposition may result in misrepresentation of deposition velocities, which, as we demonstrate, can have a substantial impact on NO_x lifetimes and mixing ratios above and within a forest canopy. This effect will be especially pronounced in areas, such as much of the western United States, where there are frequent periods of prolonged drought. Parameterizations of stomatal conductance, such as those presented in Emberson et al. (2000) and incorporated into some regional-scale CTMs (e.g. EMEP, MSC-W, and CHIMERE), if incorporated into global atmospheric models, could more accurately reflect the dependence of foliar deposition on meteorology and soil conditions. However, additional laboratory and field measurements on diverse plant species are also needed to determine appropriate, ecosystem-specific inputs to these parameterizations.

It should be noted that there have been significant recent advances in optimization approaches of stomatal modelling based on the theory that stomata maximize CO_2 assimilation

per molecule of water vapor lost via transpiration (Medlyn et al., 2011; Bonan et al., 2014; Franks et al., 2017; Lloyd Miner et al., 2016; Franks et al., 2018). Medlyn et al. (2011) reconciled the empirical widely utilized Ball-Berry model with a theoretical framework optimizing ribulose 1,5 bisphosphate (RuBP) regeneration-limited photosynthesis. However, such methods of water use efficiency optimization do not account for stomatal closure as a result of soil moisture stress. Bonan et al. (2014) further developed a model considering water use efficiency optimization and water transport between the soil, plant, and atmosphere. Such parameterizations are utilized in the Community Land Model (CLM)–a land surface model often incorporated into regional and global climate-chemistry models (Lombardozzi et al., 2015; Kennedy et al., 2019). Although this model provides a physiological and mechanistic basis for stomatal behaviour, it is heavily parameterized, relying on inputs of plant and soil parameters that could be expected to vary significantly across ecosystem types. For this reason, we view these methods as aspirational for incorporation into atmospheric global CTMs. We find the relative simplicity of the Emberson approach more useful for the purpose and scope of parameters for large-scale atmospheric models.

Implications for modelling ozone

NO_2, as well as O_3, deposition budgets are frequently calculated through inferential methods whereby the deposition velocity is constrained with ambient observations (Holland et al., 2005; Geddes and Murphy, 2014). These inferential models are often complicated by the fast reaction of the NO_2-NO-O_3 triad, making it difficult to separate chemical and physical processes. Further, these inferential models for determining dry deposition constrained with observations of chemical concentrations and eddy covariance measurements of fluxes are difficult to interpret because of similar chemical and turbulent timescales (Min et al., 2014; Geddes and Murphy, 2014). Emission of NO from soils, rapid chemical conversion to NO_2, and subsequent in-air reactions of NO_x must be evaluated accurately in in order to correctly infer NO_x and O_3 atmosphere-biosphere exchange from observations. Our multilayer canopy model applies a simple method of representing these processes and evaluating the separate effects of chemistry and dry deposition on the NO_x budget in forests.

Since the foliar deposition of NO_2 reduces the NO_x lifetime and NO_x that is transported out of the canopy, it will also reduce the amount of ozone that is produced both within and above the canopy. Ozone production efficiency (OPE) in the canopy is calculated using Eq.3.23—3.25:

$$L(NO_x) = L_{NO_x \to Dep} + L_{NO_x \to RONO_2} c + L_{NO_x \to HNO_3} \tag{3.23}$$

$$P(O_3) = k_{HO_2+NO}[HO_2][NO] + k_{CH_3O_2+NO}[CH_3O_2][NO] + (1-\alpha)k_{RO_2+NO}[RO_2][NO] \tag{3.24}$$

$$OPE = \frac{P(O_3)}{L(NO_x)} \tag{3.25}$$

where $P(O_3)$ is the ozone production rate and $L(NO_x)$ is the NO_x loss rate. The effect of stomatal conductance to NO_2 on OPE is shown in Figure 3.6c. An increase in g_{max} from

0 to 0.3 cm s^{-1} results in a decrease in OPE for the PBL from 24.0 to 20.7 (∼14%), and a decrease to 17.0 (∼30%) if g_{max} is 1.4 cm s^{-1}. This is similar to OPE calculations that have been reported for forests and environments with NO_x mixing ratios less than 1 ppb and heavily influenced by BVOC emissions (Marion et al., 2001; Browne and Cohen, 2012; Ninneman et al., 2017).

NO_2 deposition and the in-canopy chemistry of NO_2-NO-O_3 also impacts O_3 production and removal. O_3 deposition is frequently inferred from measurements of O_3 concentrations or eddy-covariance measurements (Wesely and Hicks, 2000; Kavassalis and Murphy, 2017). However, because NO_2 has a direct impact on ozone production, deposition of NO_2 can affect inferences of O_3 deposition from observations. The 14% reduction of OPE and more than a 20% reduction in daytime NO_x resulting from an increase in g_{max} from 0 to 0.3 cm s^{-1} can cause a parallel decrease in O_3 concentrations and fluxes independent of O_3 chemical loss or deposition. Thus, deposition of NO_2 must be taken into account when evaluating O_3 deposition losses from observed canopy fluxes.

Implications for near-urban forests

The analysis above suggests that the relative importance of chemical sinks and deposition will vary with NO_x concentration. To evaluate the relative importance of NO_2 foliar deposition and chemistry as a function of NO_x mixing ratio, a simplified 1-box model was also constructed with a simplified reaction scheme (Table 3.A3), VOC reactivity of 8 s^{-1}, α of 0.075, and a HO_x ($HO_x \equiv OH + HO_2$) production rate (P_{HO_x}) of 2×10^6 molecules cm^{-3} s^{-1} (similar to conditions observed at BEARPEX-09). RO_2, OH, and HO_2 were solved for steady-state concentrations and NO_x loss pathways were calculated via Eq. 3.26—3.29.

$$D_{NO_x} = LAI \cdot V_d \cdot \frac{h_{can}}{h_{PBL}}[NO_2] \tag{3.26}$$

where h_{can} is the canopy height (15m), h_{PBL} is the planetary boundary layer height (1000 m), and LAI is 5 m^2 m^{-2}.

$$P_{HNO_3} = k_{OH+NO_2}[OH][NO_2] \tag{3.27}$$

$$P_{ANs} = \alpha k_{RO_2+NO}[RO_2]fNO \tag{3.28}$$

where

$$fNO = \frac{k_{RO_2+NO}[NO]}{k_{RO_2+NO}[NO] + k_{RO_2+HO_2}[HO_2] + k_{RO_2+RO_2}[RO_2]} \tag{3.29}$$

The results from this simplified box model are shown in Figure 3.10 and agree well with our 1D multi-box model near 10 ppb NO_x (Fig. 3.A7). With deposition set to zero, nitric acid formation becomes a more significant sink of NO_x than alkyl nitrate formation at around 1 ppb, and nitric acid formation accounts for greater than 70% of the total loss at 100 ppb. With a deposition pathway included, deposition acts as the dominant NO_x sink above 30 ppb and at 10 ppb deposition and AN formation are each 20% of the NO_x sink. Deposition is approximately 10% of the sink over a wide range of concentrations. Forests in

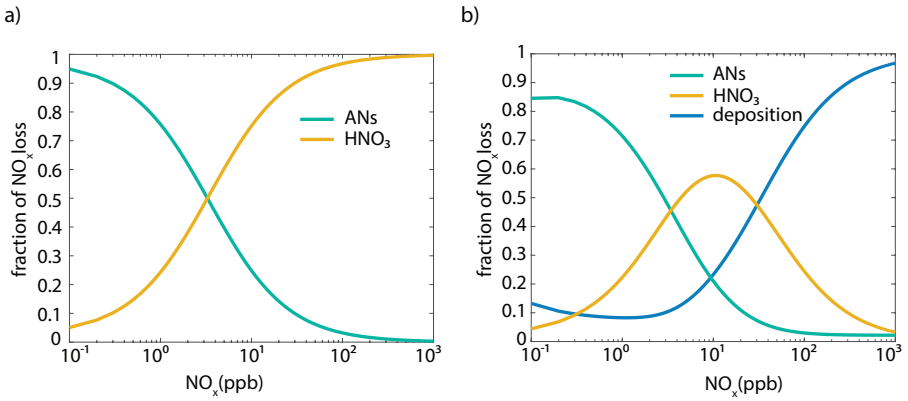

Figure 3.10: Fraction of NO_x loss to alkyl nitrate formation (green line), nitric acid formation (yellow line) with (a) no foliar uptake and (b) with foliar deposition (blue line) as a function of NO_x mixing ratio predicted by the simplified single-box model.

close proximity to urban centers (Fig. 3.A9) may result in a substantial local decrease in NO_x (Fig. 3.A8, Fig. 3.10). Although the influence of urban or near-urban trees on NO_x concentrations would be heavily dependent on meteorological factors (i.e. wind speed and direction), proximity to emission sources, and LAI, it may have some importance on a local or neighborhood scale. This effect may be relevant for understanding and predicting the effects of NO_x reduction policies within and near cities. It may also be useful in considering as a direct nitrogen input to the biosphere, not mediated by soil processes.

3.6 Conclusions

We have constructed a 1D multi-box model with representations of chemistry and vertical transport to evaluate the impact of leaf-level processes on canopy-scale concentrations, lifetimes, and canopy fluxes of NO_x. Our model is able to closely replicate canopy fluxes and above-canopy NO_x daytime mixing ratios during two field campaigns that took place in a Sierra Nevada pine forest (BEARPEX-2009) and a northern Michigan mixed hardwood forest (UMBS-2012). We conclude that the widely used canopy reduction factor approach to describing soil NO_x removal from the atmosphere within plant canopies is consistent with a process-based model that utilizes stomatal uptake and we recommend that the CRF parameter be replaced with stomatal models for NO_2 uptake.

We demonstrate with our 1D multi-box model that NO_2 deposition provides a mechanistic explanation behind canopy reduction factors (CRFs) that are widely used in CTMs. We

predict a maximum of ∼60% reduction in the fraction of soil-emitted NO_x ventilated through the canopy when stomatal conductances are greater than 0.075 cm s^{-1}, consistent with the range of global CRFs used in current CTMs (Jacob and Wofsy, 1990; Yienger and Levy, 1995). Our model also predicts that changes in g_{max} have a greater overall impact on canopy NO_x fluxes at larger leaf resistances to uptake (slower foliar uptake). In the range for g_{max} of ∼0–0.5 cm s^{-1}, errors or variability in stomatal conductance can have a large impact on the predicted canopy concentrations and fluxes of NO_x, which would in turn have large impact on concentrations and fluxes of O_3. This range of deposition velocities describes the range of uptake rates measured for many tree species and forest ecosystems (Hanson and Lindberg, 1991; Rondón and Granat, 1994; Hereid and Monson, 2001; Teklemmariam and Sparks, 2006; Pape et al., 2009; Chaparro-Suarez et al., 2011; Delaria et al., 2018). Model calculations also predict a similar trend on the lifetimes of NO_x, with a maximum reduction in the NO_x lifetime by ∼4 hrs (40%) compared with no deposition.

The large effect that small changes in stomatal conductance can have on NO_x lifetimes, concentrations, budget, and O_3 production makes it very important to accurately parameterize in atmospheric models. Most global scale chemical transport models parameterize stomatal conductance using the representation developed by Wesely (1989) (Jacob and Wofsy, 1990; Verbeke et al., 2015). These do no account for the effects of VPD, SWP, CO_2 mixing ratio, or other factors known to influence stomatal conductance (Hardacre et al., 2015). We show that incorporating vapor pressure deficit and soil water potential–using the parameterization of Emberson et al. (2000)–has a substantial impact on predicted NO_2 deposition, with the percent of soil NO_x removed within the canopy increasing from 18% to 30% in wet (low VPD and high SWP) conditions compared to dry conditions in the location of BEARPEX-2009. Under the Wesely model, where stomatal conductance is parameterized only with temperature and solar radiation, the predicted deposition velocity would be nearly identical between "wet" and "dry" days and between the spring and fall in semi-arid regions (e.g. much of the western United States, the Mediterranean Basin, the west coast of South America, parts of northwest Africa, parts of western and southern Australia, and parts of South Africa). The dominant effect of stomatal opening on NO_2 deposition causes an important time of day and seasonal behaviour that should be extensively explored with observations of NO_x fluxes and concurrent models to confirm the role of deposition in a wider range of environs and more thoroughly vet the conceptual model proposed here.

3.7 References

National Centers for Environmental Information, Auburn Municipal Airport, online database.

Altimir, N., Tuovinen, J.-P., Vesala, T., Kulmala, M., and Hari, P.: Measurements of ozone removal by Scots pine shoots: Calibration of a stomatal uptake model including

the non-stomatal component, Atmospheric Environment, 38, 2387–2398, https://doi.org/10.1016/j.atmosenv.2003.09.077, 2004.

Ammann, M., von Ballmoos, P., Stalder, M., Suter, M., and Brunold, C.: Uptake and assimilation of atmospheric NO2 — N by spruce needles (Picea abies): A field study, Water Air and Soil Pollution, 85, 1497–1502, https://doi.org/10.1007/BF00477193, 1995.

Anderegg, W. R. L., Wolf, A., Arango-Velez, A., Choat, B., Chmura, D. J., Jansen, S., Kolb, T., Li, S., Meinzer, F., Pita, P., Resco de Dios, V., Sperry, J. S., Wolfe, B. T., and Pacala, S.: Plant water potential improves prediction of empirical stomatal models, PLOS ONE, 12, 1–17, https://doi.org/10.1371/journal.pone.0185481, 2017.

Baldocchi, D. D., Hicks, B. B., and Camara, P.: A canopy stomatal resistance model for gaseous deposition to vegetated surfaces, Atmospheric Environment (1967), 21, 91 – 101, https://doi.org/10.1016/0004-6981(87)90274-5, 1987.

Beedlow, P., Lee, E., Tingey, D., Waschmann, R., and Burdick, C.: The importance of seasonal temperature and moisture patterns on growth of Douglas-fir in western Oregon, USA, Agricultural and Forest Meteorology, 169, 174–185, https://doi.org/10.1016/j.agrformet.2012.10.010, 2013.

Bonan, G., Williams, M., Fisher, R., and Oleson, K.: Modeling stomatal conductance in the Earth system: Linking leaf water-use efficiency and water transport along the soil-plant-atmosphere continuum, Geoscientific Model Development, 7, 2193–2222, https://doi.org/10.5194/gmd-7-2193-2014, 2014.

Breuninger, C., Oswald, R., Kesselmeier, J., and Meixner, F. X.: The dynamic chamber method: trace gas exchange fluxes (NO, NO_2, O_3) between plants and the atmosphere in the laboratory and in the field, Atmospheric Measurement Techniques, 5, 955–989, https://doi.org/10.5194/amt-5-955-2012, 2012.

Breuninger, C., Meixner, F. X., and Kesselmeier, J.: Field investigations of nitrogen dioxide (NO_2) exchange between plants and the atmosphere, Atmospheric Chemistry and Physics, 13, 773–790, https://doi.org/10.5194/acp-13-773-2013, 2013.

Browne, E. C. and Cohen, R. C.: Effects of biogenic nitrate chemistry on the NO_x lifetime in remote continental regions, Atmospheric Chemistry and Physics, 12, 11 917–11 932, https://doi.org/10.5194/acp-12-11917-2012, 2012.

Brunet, Y. and Irvine, M.: The Control Of Coherent Eddies In Vegetation Canopies: Streamwise Structure Spacing, Canopy Shear Scale And Atmospheric Stability, Boundary-Layer Meteorology, 94, 139–163, https://doi.org/10.1023/A:1002406616227, 2000.

Bryan, A., Cheng, S., Ashworth, K., Guenther, A., Hardiman, B., Bohrer, G., and Steiner, A.: Forest-atmosphere BVOC exchange in diverse and structurally complex canopies: 1-D

modeling of a mid-successional forest in northern Michigan, Atmospheric Environment, 120, https://doi.org/10.1016/j.atmosenv.2015.08.094, 2015.

Burkholder, J., Sander, S., Abbatt, J., Barker, J., Fleming, E., Friedl, R., Huie, R., Jackman, C., Kolb, C., Kurylo, M., Orkin, V., and Wine, P.: NASA Data Evaluation: Chemical Kinetics and Photochemical Data for Use in Atmospheric Studies, 2014.

Büker, P., Emberson, L., Ashmore, M., Cambridge, H., Jacobs, C., Massman, W., Müller, J., Nikolov, N., Novak, K., Oksanen, E., Schaub, M., and Llorente, D.: Comparison of different stomatal conductance algorithms for ozone flux modelling, Environmental pollution (Barking, Essex : 1987), 146, 726–35, https://doi.org/10.1016/j.envpol.2006.04.007, 2007.

Büker, P., Morrissey, T., Briolat, A., Falk, R., Simpson, D., Tuovinen, J.-P., Alonso, R., Barth, S., Baumgarten, M., Grulke, N., Karlsson, P., King, J., Lagergren, F., Matyssek, R., Nunn, A., Ogaya, R., Penuelas, J., Rhea, L., Schaub, M., and Emberson, L.: DO3SE modelling of soil moisture to determine ozone flux to European forest trees, Atmospheric Chemistry and Physics, 12, 5537–5562, https://doi.org/10.5194/acp-12-5537-2012, 2012.

Chaparro-Suarez, I., Meixner, F., and Kesselmeier, J.: Nitrogen dioxide (NO2) uptake by vegetation controlled by atmospheric concentrations and plant stomatal aperture, Atmospheric Environment, 45, 5742 – 5750, https://doi.org/10.1016/j.atmosenv.2011.07.021, 2011.

Chaves, M., Pereira, J., Maroco, J., Rodrigues, M., Ricardo, C., Osório, M., Carvalho, I., Faria, T., and Pinheiro, C.: How plants cope with water stress in the field. Photosynthesis and Growth, Annals of botany, 89 Spec No, 907–16, 2002.

Collineau, S. and Brunet, Y.: Detection of turbulent coherent motions in a forest canopy part I: Wavelet analysis, Boundary-Layer Meteorology, 65, 357–379, https://doi.org/10.1007/BF00707033, 1993.

Crutzen, P. J.: The Role of NO and NO2 in the Chemistry of the Troposphere and Stratosphere, Annual Review of Earth and Planetary Sciences, 7, 443–472, https://doi.org/10.1146/annurev.ea.07.050179.002303, 1979.

Delaria, E., Vieira, M., Cremieux, J., and Cohen, R.: Measurements of NO and NO2 exchange between the atmosphere and Quercus agrifolia, Atmospheric Chemistry and Physics, 18, 14 161–14 173, https://doi.org/10.5194/acp-18-14161-2018, 2018.

Emberson, L., Ashmore, M., Cambridge, H., Simpson, D., and Tuovinen, J.: Modelling stomatal flux across Europe, Environmental pollution (Barking, Essex : 1987), 109, 403–13, https://doi.org/10.1016/S0269-7491(00)00043-9, 2000.

Emberson, L. D.: Defining and mapping relative potential sensitivity of European vegetation to ozone., Ph.D. thesis, Imperial College, University of London, UK, 1996.

Fares, S., Matteucci, G., Mugnozza, G., Morani, A., Calfapietra, C., Salvatori, E., Fusaro, L., Manes, F., and Loreto, F.: Testing of models of stomatal ozone fluxes with field measurements in a mixed Mediterranean forest, Atmospheric Environment, 67, 242–251, https://doi.org/10.1016/j.atmosenv.2012.11.007, 2012.

Fenn, M., Poth, M., Aber, J., Baron, J., Bormann, B., Johnson, D., Lemly, D., Mcnulty, S., Ryan, D., and Stottlemyer, R.: Nitrogen Excess in North American Ecosystems: Predisposing Factors, Ecosystem Responses, and Management Strategies, Ecological Applications - ECOL APPL, 8, 706–733, https://doi.org/10.1890/1051-0761(1998)008[0706:NEINAE]2.0.CO;2, 1998.

Finnigan, J., Harman, I., Ross, A., and Belcher, S. E.: First-order turbulence closure for modelling complex canopy ows, Quarterly Journal of the Royal Meteorological Society, 141, https://doi.org/10.1002/qj.2577, 2015.

Franks, P., Berry, J., Lombardozzi, D., and Bonan, G.: Stomatal Function across Temporal and Spatial Scales: Deep-Time Trends, Land-Atmosphere Coupling and Global Models, Plant Physiology, 174, pp.00 287.2017, https://doi.org/10.1104/pp.17.00287, 2017.

Franks, P., Bonan, G., Berry, J., Lombardozzi, D., Holbrook, N., Herold, N., and Oleson, K.: Comparing optimal and empirical stomatal conductance models for application in Earth system models, Global change biology, 24, https://doi.org/10.1111/gcb.14445, 2018.

Galloway, J., Dentener, F., Boyer, E., Howarth, R., Seitzinger, S., Asner, G., Cleveland, C., Green, P., Holland, E., Karl, D., Michaels, A., Porter, J., Townsend, A., and Vöosmarty, C.: Nitrogen Cycles: Past, Present, and Future, Biogeochemistry, 70, 153–226, https://doi.org/10.1007/s10533-004-0370-0, 2004.

Ganzeveld, L. and Lelieveld, J.: Dry deposition parametrization in a chemistry general circulation model and its influence on the distribution of reactive trace gases, Journal of Geophysical Research 100 (1995) 20,999-21,012., 100, https://doi.org/10.1029/95JD02266, 1995.

Ganzeveld, L. N., Lelieveld, J., Dentener, F. J., Krol, M. C., Bouwman, A. J., and Roelofs, G.-J.: Global soil-biogenic NOx emissions and the role of canopy processes, Journal of Geophysical Research: Atmospheres, 107, ACH 9–1–ACH 9–17, https://doi.org/10.1029/2001JD001289, 2002a.

Ganzeveld, L. N., Lelieveld, J., Dentener, F. J., Krol, M. C., and Roelofs, G.-J.: Atmosphere-biosphere trace gas exchanges simulated with a single-column model, Journal of Geophysical Research: Atmospheres, 107, ACH 8–1–ACH 8–21, https://doi.org/10.1029/2001JD000684, 2002b.

Gao, W., Wesely, M., and Doskey, P.: Numerical modeling of the turbulent diffusion and chemistry of NOx, O3, isoprene, and other reactive trace gases in and above a forest canopy,

Journal of Geophysical Research, 981, 18 339–18 354, https://doi.org/10.1029/93JD01862, 1993.

Geddes, J. A. and Murphy, J. G.: Observations of reactive nitrogen oxide fluxes by eddy covariance above two midlatitude North American mixed hardwood forests, Atmospheric Chemistry and Physics, 14, 2939–2957, https://doi.org/10.5194/acp-14-2939-2014, 2014.

Guenther, A., Hewitt, C. N., Erickson, D., Fall, R., Geron, C., Graedel, T., Harley, P., Klinger, L., Lerdau, M., Mckay, W., Pierce, T., Scholes, B., Steinbrecher, R., Tallamraju, R., Taylor, J., and Zimmerman, P.: A global model of natural volatile organic compound emissions, Journal of geophysical research, 100, 8873–8892, https://doi.org/10.1029/94JD02950, 1995.

Gunderson, C., Sholtis, J., Wullschleger, S., Tissue, D., Hanson, P., and Norby, R.: Environmental and stomatal control of photosynthetic enhancement in the canopy of a sweetgum (Liquidambar styraciflua L.) plantation during 3 years of CO2 enrichment, Plant, Cell Environment, 25, 379 – 393, https://doi.org/10.1046/j.0016-8025.2001.00816.x, 2002.

Hanson, P. J. and Lindberg, S. E.: Dry deposition of reactive nitrogen compounds: A review of leaf, canopy and non-foliar measurements, Atmospheric Environment. Part A. General Topics, 25, 1615 – 1634, https://doi.org/10.1016/0960-1686(91)90020-8, 1991.

Hardacre, C., Wild, O., and Emberson, L.: An evaluation of ozone dry deposition in global scale chemistry climate models, Atmospheric Chemistry and Physics, 15, 6419–6436, https://doi.org/10.5194/acp-15-6419-2015, 2015.

Hereid, D. and Monson, R.: Nitrogen Oxide Fluxes between Corn (Zea mays L.) Leaves and the Atmosphere, Atmospheric Environment, 35, 975–983, https://doi.org/10.1016/S1352-2310(00)00342-3, 2001.

Hicks, B., Baldocchi, D., Meyers, T., Hosker, R., and Matt, D.: A Preliminary multiple resistance routine for deriving dry deposition velocities from measured quantities, Water Air and Soil Pollution, 36, 311–330, https://doi.org/10.1007/BF00229675, 1987.

Holland, E., Braswell, B., Lamarque, J.-F., Townsend, A., Sulzman, J., Müller, J.-F., Dentener, F., Brasseur, G., Levy, H., Penner, J., and G.-J, R.: Variation in the predicted spatial distribution of atmospheric nitrogen deposition and their impact on carbon uptake by terrestrial ecosystems, Journal of Geophysical Research, 1021, 15 849–15 866, https://doi.org/10.1029/96JD03164, 1997.

Holland, E., Braswell, B., Sulzman, J., and Lamarque, J.-F.: Nitrogen deposition onto the United States and Western Europe: Synthesis of observations and models, Ecological Applications, 15, 38–57, https://doi.org/10.1890/03-5162, 2005.

Hubbard, R., Ryan, M., Stiller, V., and Sperry, J.: Stomatal conductance and photosynthesis vary linearly with plant hydraulic conductance in ponderosa pine, Plant, Cell Environment, 24, https://doi.org/10.1046/j.1365-3040.2001.00660.x, 2001.

Ishikawa, C. and Bledsoe, C.: Seasonal and diurnal patterns of soil water potential in the rhizosphere of blue oaks: Evidence for hydraulic lift, Oecologia, 125, 459–465, https://doi.org/10.1007/s004420000470, 2000.

Jacob, D. J. and Wofsy, S. C.: Budgets of reactive nitrogen, hydrocarbons, and ozone over the Amazon forest during the wet season, Journal of Geophysical Research: Atmospheres, 95, 16 737–16 754, https://doi.org/10.1029/JD095iD10p16737, 1990.

Jarvis, P.: The Interpretation of the Variations in Leaf Water Potential and Stomatal Conductance Found in Canopies in the Field, Philosophical Transactions of the Royal Society of London. Series B, Biological Sciences, 273, 593–, https://doi.org/10.1098/rstb.1976.0035, 1976.

Johansson, C.: Pine forest: a negligible sink for atmospheric NOx in rural Sweden, Tellus B, 39B, 426–438, https://doi.org/10.1111/j.1600-0889.1987.tb00204.x, 1987.

Johnson, D., Woodruff, D., McCulloh, K., and Meinzer, F.: Leaf hydraulic conductance, measured in situ, declines and recovers daily: Leaf hydraulics, water potential and stomatal conductance in four temperate and three tropical tree species, Tree physiology, 29, 879–87, https://doi.org/10.1093/treephys/tpp031, 2009.

Kavassalis, S. and Murphy, J.: Understanding ozone-meteorology correlations: A role for dry deposition, Geophysical Research Letters, 44, https://doi.org/10.1002/2016GL071791, 2017.

Kelliher, F., Leuning, R., Raupach, M., and Schulze, E.-D.: Maximum Conductances for Evaporation from Global Vegetation Types, Agricultural and Forest Meteorology, 73, 1–16, https://doi.org/10.1016/0168-1923(94)02178-M, 1995.

Kennedy, D., Swenson, S., Oleson, K., Fisher, R., Lawrence, D., da Costa, A., and Gentine, P.: Implementing Plant Hydraulics in the Community Land Model, Version 5, Journal of Advances in Modeling Earth Systems, https://doi.org/10.1029/2018MS001500, 2019.

Lloyd Miner, G., Bauerle, W., and Baldocchi, D.: Estimating the sensitivity of stomatal conductance to photosynthesis: A review: The sensitivity of conductance to photosynthesis, Plant, Cell Environment, 40, https://doi.org/10.1111/pce.12871, 2016.

Lombardozzi, D., Bonan, G., Smith, N., Dukes, J., and Fisher, R.: Temperature acclimation of photosynthesis and respiration: A key uncertainty in the carbon cycle-climate feedback, Geophysical Research Letters, 42, https://doi.org/10.1002/2015GL065934, 2015.

Madronich, S. and Flocke, F.: The role of solar radiation in atmospheric chemistry, in Handbook of Environmental Chemistry, edited by P, Boule, pp. 1–26, 1998.

Makar, P., Fuentes, J., Wang, D., Staebler, R., and Wiebe, H.: Chemical processing of biogenic hydrocarbons within and above a temperate deciduous forest, Journal of Geophysical Research, 104, 3581–3603, https://doi.org/10.1029/1998JD100065, 1999.

Mallick, K., Jarvis, A., Fisher, J., Tu, K., Boegh, E., and Niyogi, D.: Latent Heat Flux and Canopy Conductance Based on Penman-Monteith, Priestley-Taylor Equation, and Bouchet's Complementary Hypothesis, Journal of Hydrometeorology, 14, 419–442, https://doi.org/10.1175/JHM-D-12-0117.1, 2013.

Marion, T., Perros, P., Losno, R., and Steiner, E.: Ozone Production Efficiency in Savanna and Forested Areas during the EXPRESSO Experiment, Journal of Atmospheric Chemistry, 38, 3–30, https://doi.org/10.1023/A:1026585603100, 2001.

Medlyn, B., Duursma, R., Eamus, D., and Ellsworth, D.: Reconciling the optimal and empirical approaches to modelling stomatal conductance, Global Change Biology, 2011.

Min, K.-E., Pusede, S. E., Browne, E. C., LaFranchi, B. W., and Cohen, R. C.: Eddy covariance fluxes and vertical concentration gradient measurements of NO and NO_2 over a ponderosa pine ecosystem: observational evidence for within-canopy chemical removal of NO_x, Atmospheric Chemistry and Physics, 14, 5495–5512, https://doi.org/10.5194/acp-14-5495-2014, 2014.

Nguyen, T., Crounse, J., Teng, A., Clair, J., Paulot, F., Wolfe, G., and Wennberg, P.: Rapid deposition of oxidized biogenic compounds to a temperate forest, Proceedings of the National Academy of Sciences, 112, E392–E401, https://doi.org/10.1073/pnas.1418702112, 2015.

Ninneman, M., Lu, S., Lee, P., McQueen, J., Huang, J., Demerjian, K., and Schwab, J.: Observed and Model-Derived Ozone Production Efficiency over Urban and Rural New York State, Atmosphere, 8, https://doi.org/10.3390/atmos8070126, 2017.

Oren, R., Ellsworth, D., Johnsen, K., Phillips, N., Ewers, B., Maier, C., Schäfer, K., Mccarthy, H., Hendrey, G., Mcnulty, S., and Katul, G.: Soil fertility limits carbon sequestration by forest ecosystems in a CO2-enriched atmosphere, Nature, 411, 469–72, https://doi.org/10.1038/35078064, 2001.

Panek, J. and Goldstein, A.: Response of stomatal conductance to drought in ponderosa pine: Implications for carbon and ozone uptake, Tree physiology, 21, 337–44, https://doi.org/10.1093/treephys/21.5.337, 2001.

Pape, L., Ammann, C., Nyfeler-Brunner, A., Spirig, C., Hens, K., and Meixner, F. X.: An automated dynamic chamber system for surface exchange measurement of non-reactive and

reactive trace gases of grassland ecosystems, Biogeosciences, 6, 405–429, https://doi.org/10.5194/bg-6-405-2009, 2009.

Prior, L., Eamus, D., and Duff, G.: Seasonal and Diurnal Patterns of Carbon Assimilation, Stomatal Conductance and Leaf Water Potential in Eucalyptus tetrodonta Saplings in a Wet–Dry Savanna in Northern Australia, Australian Journal of Botany - AUST J BOT, 45, https://doi.org/10.1071/BT96017, 1997.

Raupach, M., Finnigan, J., and Brunet, Y.: Coherent Eddies and Turbulence in Vegetation Canopies: The Mixing-Layer Analogy, Boundary-Layer Meteorology, 78, 351–382, https://doi.org/10.1007/978-94-017-0944-$6_1$5, 1996.

Romer, P. S., Duffey, K. C., Wooldridge, P. J., Allen, H. M., Ayres, B. R., Brown, S. S., Brune, W. H., Crounse, J. D., de Gouw, J., Draper, D. C., Feiner, P. A., Fry, J. L., Goldstein, A. H., Koss, A., Misztal, P. K., Nguyen, T. B., Olson, K., Teng, A. P., Wennberg, P. O., Wild, R. J., Zhang, L., and Cohen, R. C.: The lifetime of nitrogen oxides in an isoprene-dominated forest, Atmospheric Chemistry and Physics, 16, 7623–7637, https://doi.org/10.5194/acp-16-7623-2016, 2016.

Rondón, A. and Granat, L.: Studies on the dry deposition of NO2 to coniferous species at low NO2 concentrations, Tellus B: Chemical and Physical Meteorology, 46, 339–352, https://doi.org/10.3402/tellusb.v46i5.15809, 1994.

Ryan, M., Bond, B., Law, B., Hubbard, R., Woodruff, D., Cienciala, E., and Kučera, J.: Transpiration and whole-tree conductance in ponderosa pine trees of different heights, Oecologia, 124, 553–560, https://doi.org/10.1007/s004420000403, 2000.

Rydsaa, J., Stordal, F., Gerosa, G., Finco, A., and Hodnebrog, : Evaluating stomatal ozone fluxes in WRF-Chem: Comparing ozone uptake in Mediterranean ecosystems, Atmospheric Environment, 143, https://doi.org/10.1016/j.atmosenv.2016.08.057, 2016.

Seok, B., Helmig, D., Ganzeveld, L., Williams, M. W., and Vogel, C. S.: Dynamics of nitrogen oxides and ozone above and within a mixed hardwood forest in northern Michigan, Atmospheric Chemistry and Physics, 13, 7301–7320, https://doi.org/10.5194/acp-13-7301-2013, 2013.

Steiner, A., Pressley, S., Botros, A., Jones, E., Chung, S., and Edburg, S.: Analysis of coherent structures and atmosphere-canopy coupling strength during the CABINEX field campaign, Atmos. Chem. Phys., 11, 11 921–11 936, https://doi.org/10.5194/acp-11-11921-2011, 2011.

Stern, M., Anderson, F., Flint, L., and Flint, A.: Soil moisture datasets at five sites in the central Sierra Nevada and northern Coast Ranges, California, Data Series, https://doi.org/10.3133/ds1083, 2018.

Stroud, C., Makar, P., Karl, T., Guenther, A., Geron, C., Turnipseed, A., Nemitz, E., Baker, B., Potosnak, M., and Fuentes, J.: Role of canopy-scale photochemistry in modifying biogenic-atmosphere exchange of reactive terpene species: Results from the CELTIC field study, Journal of Geophysical Research-Atmospheres, 110, https://doi.org/10.1029/2005jd005775, 2005.

Sörgel, M., Trebs, I., Serafimovich, A., Moravek, A., Held, A., and Zetzsch, C.: Simultaneous HONO measurements in and above a forest canopy: influence of turbulent exchange on mixing ratio differences, Atmospheric Chemistry and Physics, 11, https://doi.org/10.5194/acp-11-841-2011, 2011.

Teklemmariam, T. and Sparks, J.: Leaf fluxes of NO and NO2 in four herbaceous plant species: The role of ascorbic acid, Atmospheric Environment, 40, 2235–2244, https://doi.org/10.1016/j.atmosenv.2005.12.010, 2006.

Thomas, C. and Foken, T.: Flux contribution of coherent structures and its implications for the exchange of energy and matter in a tall spruce canopy, Boundary-Layer Meteorology, 123, 317–337, https://doi.org/10.1007/s10546-006-9144-7, 2007.

Thoene, B., Schröder, P., Papen, H., Egger, A., and Rennenberg, H.: Absorption of atmospheric NO2 by spruce (Picea abies L. Karst.) trees, New Phytologist, 117, 575–585, https://doi.org/10.1111/j.1469-8137.1991.tb00962.x, 1991.

Townsend, A., Braswell, B., Holland, E., and Penner, J.: Spatial and Temporal Patterns in Terrestrial Carbon Storage Due to Deposition of Fossil Fuel Nitrogen, Ecological Applications, 6, 806—-814, https://doi.org/10.2307/2269486, 1996.

Verbeke, T., Lathière, J., Szopa, S., and de NOBLET, N.: Impact of future land-cover changes on HNO3 and O3 surface dry deposition, Atmospheric Chemistry and Physics, 15, 13 555–13 568, https://doi.org/10.5194/acp-15-13555-2015, 2015.

Vinken, G. C. M., Boersma, K. F., Maasakkers, J. D., Adon, M., and Martin, R. V.: Worldwide biogenic soil NO_x emissions inferred from OMI NO_2 observations, Atmospheric Chemistry and Physics, 14, 10 363–10 381, https://doi.org/10.5194/acp-14-10363-2014, 2014.

Vitousek, P., Aber, J., Howarth, R., Likens, G., Matson, P., Schindler, D., Schlesinger, W., and Tilman, D.: Human alteration of the global nitrogen cycle: Source and consequences, Ecological Applications, 7, 739–750, 1997.

Wang, Y., Logan, J., and Jacob, D.: Global simulation of tropospheric O 3 NO x -hydrocarbon chemistry 2. Model evaluation and global ozone budget, Journal of Geophysical Research, 103, 10 727–10 755, https://doi.org/10.1029/98JD00157, 1998.

Wang, Y.-P. and Leuning, R.: A two-leaf model for canopy conductance, photosynthesis and partitioning of available energy I:: Model description and comparison with a multi-layered

model, Agricultural and Forest Meteorology, 91, 89 – 111, https://doi.org/10.1016/S0168-1923(98)00061-6, 1998.

Wesely, M.: Parameterization of surface resistances to gaseous dry deposition in regional-scale numerical models, Atmospheric Environment, 23, 1293–1304, https://doi.org/10.1016/0004-6981(89)90153-4, 1989.

Wesely, M. and Hicks, B.: A review of the current status of knowledge on dry deposition, Atmospheric Environment, 34, 2261–2282, https://doi.org/10.1016/S1352-2310(99)00467-7, 2000.

Wild, O.: Modelling the global tropospheric ozone budget: Exploring the variability in current models, Atmospheric Chemistry and Physics, 7, https://doi.org/10.5194/acp-7-2643-2007, 2007.

Williams, M., RASTETTER, E., Fernandes, D., GOULDEN, M., Wofsy, S., Shaver, G., Melillo, J., Munger, J., Fan, S.-M., and Nadelhoffer, K.: Modelling the soil-plant-atmosphere continuum in a Quercus-Acer stand at Harvard Forest: The regulation of stomatal conductance by light, nitrogen and soil/plant hydraulic properties, Plant Cell and Environment - PLANT CELL ENVIRON, 19, 911–927, https://doi.org/10.1111/j.1365-3040.1996.tb00456.x, 1996.

Wolfe, G., Thornton, J., Bouvier-Brown, N., Goldstein, A., Park, J., McKay, M., Matross, D., Mao, J., Brune, W., Lafranchi, B., Browne, E., Min, K.-E., Wooldridge, P., Cohen, R., Crounse, J., Faloona, I., Gilman, J., Kuster, W., de Gouw, J., and Keutsch, F.: The Chemistry of Atmosphere-Forest Exchange (CAFE) Model Part 2: Application to BEARPEX-2007 observations, Atmos. Chem. Phys., 11, 1269–1294, https://doi.org/10.5194/acpd-10-21791-2010, 2011.

Wolfe, G. M. and Thornton, J. A.: The Chemistry of Atmosphere-Forest Exchange (CAFE) Model Part 1: Model description and characterization, Atmospheric Chemistry and Physics, 11, 77–101, https://doi.org/10.5194/acp-11-77-2011, 2011.

Yi, C.: Momentum Transfer within Canopies, Journal of Applied Meteorology and Climatology, 47, 262–275, https://doi.org/10.1175/2007JAMC1667.1, 2008.

Yienger, J. J. and Levy, H.: Empirical model of global soil-biogenic NO emissions, Journal of Geophysical Research: Atmospheres, 100, 11 447–11 464, https://doi.org/10.1029/95JD00370, 1995.

Zhang, L., Padro, J., and Walmsley, J.: A multi-layer model vs single-layer models and observed O 3 dry deposition velocities, Atmospheric Environment - ATMOS ENVIRON, 30, 339–345, https://doi.org/10.1016/1352-2310(95)00286-8, 1996.

Zhang, L., Moran, M., Makar, P., Brook, J., and Gong, S.: Modelling gaseous dry deposition in AURAMS – A Unified Regional Air-quality Modelling System, Atmospheric Environment, 36, 537–560, https://doi.org/10.1016/S1352-2310(01)00447-2, 2002.

Zhang, L., Brook, J., and R, V.: A revised parameterization for gaseous dry deposition in air-quality models, Atmospheric Chemistry and Physics, 3, https://doi.org/10.5194/acpd-3-1777-2003, 2003.

3.8 Appendix

Table 3.A1: Advection concentrations for the UMBS and BEARPEX-2009 scenarios

[a]Species	UMBS (ppb)	BEARPEX-2009 (ppb)
NO_2	0.6	0.1—0.35[b]
O_3	30	50
CH_2O	1	1
CH_3CHO	0.5	0.5

a. Species not shown have advection concentrations of zero.
b. For the BEARPEX-2009 case this was the maximum daily advection concentration reached around 17 hrs, based on field observations of higher NO_x plumes from near-by Sacramento in the afternoon.

Table 3.A2: Reactions and rate constants used in the 1D multibox model

Reaction	Rate constant
$NO + O_3 \longrightarrow NO_2 + O_2$	$3.0 \times 10^{-12} \exp(-1500/T)$
$NO_2 + hv \xrightarrow{O_2} NO + O_3$	See Text
$O_3 + hv \xrightarrow{H_2O} O_2 + 2\,OH$	See Text
$OH + O_3 \longrightarrow HO_2 + O_2$	$1.7 \times 10^{-12} \exp(-940/T)$
$HO_2 + O_3 \longrightarrow OH + 2\,O_2$	$1.0 \times 10^{-14} \exp(-490/T)$
$OH + OH \xrightarrow{M} H_2O_2$	$k_0 = 6.9 \times 10^{-31}(T/300)^{-1}$ $k_\infty = 2.6 \times 10^{-11}$

Continued on next page

Table 3.A2 – continued from previous page

Reaction	Rate constant
$OH + HO_2 \longrightarrow H_2O + O_2$	$4.8 \times 10^{-11} \exp(250/T)$
$HO_2 + HO_2 \xrightarrow{M} H_2O_2 + O_2$	$3.5 \times 10^{-13} \exp(430/T)$ $+1.7 \times 10^{33}(M - [H_2O])e^{1000/T}$ $\times[1 + 1.4 \times 10^{-21}[H_2O]e^{2200/T}]$
$H_2O_2 + OH \longrightarrow HO_2 + H_2O$	1.8×10^{-12}
$H_2O_2 + hv \longrightarrow 2\,OH$	See Text
$NO_2 + OH \xrightarrow{M} HNO_3$	$k_0 = 1.49 \times 10^{-30}(T/300)^{-1.8}$ $k_\infty = 2.58 \times 10^{-11}$
$HO_2 + NO \longrightarrow OH + NO_2$	$3.5 \times 10^{-12} \exp(250/T)$
$NO_2 + O_3 \longrightarrow NO_3 + O_2$	$1.2 \times 10^{-13} \exp(-2450/T)$
$NO_3 + NO_2 \xrightarrow{M} N_2O_5$	$k_0 = 2.0 \times 10^{-30}(T/300)^{-4.4}$ $k_\infty = 1.4 \times 10^{-12}(T/300)^{-0.7}$
$N_2O_5 + H_2O \longrightarrow 2\,HNO_3$	2.0×10^{-21}
$NO + NO_3 \longrightarrow 2\,NO_2$	$1.5 \times 10^{-11} \exp(170/T)$
$N_2O_5 \longrightarrow NO_2 + NO_3$	$K_{eq} = 2.7 \times 10^{-27} \exp(1100/T)$
$NO_3 + hv \longrightarrow NO + O_2$	See Text
$NO_3 + hv \xrightarrow{2\,O_2} NO_2 + O_3$	See Text
$CO + OH \xrightarrow{M,\,O_2} CO_2 + HO_2$	$k_0 = 5.9 \times 10^{-33}(T/300)^{-1.4}$ $k_\infty = 1.1 \times 10^{-12}(T/300)^{1.3}$
$CH_4 + OH \longrightarrow CH_3O_2 + H_2O$	$2.45 \times 10^{-12} \exp(-1775/T)$
$CH_3O_2 + HO_2 \longrightarrow CH_3OOH + O_2$	$4.1 \times 10^{-13} \exp(750/T)$
$CH_3O_2 + NO \xrightarrow{O_2} CH_2O + HO_2 + NO_2$	$2.8 \times 10^{-12} \exp(300/T)$
$CH_3OOH + OH \longrightarrow CH_2O + OH + H_2O$	$0.3 \times 3.8 \times 10^{-12} \exp(200/T)$
$CH_3OOH + OH \longrightarrow CH_3O_2 + H_2O$	$0.7 \times 3.8 \times 10^{-12} \exp(200/T)$
$CH_3OOH + hv \xrightarrow{O_2} CH_2O + H_2O + OH$	See Text
$CH_2O + OH \longrightarrow CO + HO_2 + H_2O$	$5.5 \times 10^{-12} \exp(125/T)$

Continued on next page

Table 3.A2 – continued from previous page

Reaction	Rate constant
$CH_2O + hv \xrightarrow{O_2} CO + 2\,HO_2$	See Text
$CH_3CHO + OH \xrightarrow{O_2} CH_3C(O)O_2 + H_2O$	$5.4 \times 10^{-12} \exp(135/T)$
$CH_3C(O)O_2 + NO_2 \longrightarrow PAN$	$k_0 = 9.7 \times 10^{-29}(T/300)^{-5.6}$ $k_\infty = 9.3 \times 10^{-12}(T/300)^{-1.5}$
$CH_3C(O)O_2 + NO \xrightarrow{O_2} NO_2 + CO_2 + CH_3O_2$	$8.1 \times 10^{-12} \exp(270/T)$
$CH_3C(O)O_2 + CH_3O_2 \longrightarrow CH_2O + O_2 + CH_3OOH$	$1.3 \times 10^{-12} \exp(640/T)$
$CH_3C(O)O_2 + HO_2 \longrightarrow O_3 + CH_3COOH$	$4.3 \times 10^{-13} \exp(1040/T)$
$CH_3C(O)O_2 + CH_3C(O)O_2 \longrightarrow O_2 + 2\,CO_2 + 2\,CH_3$	$2.9 \times 10^{-12} \exp(500/T)$
$CH_3CHO + NO_3 \longrightarrow HNO_3 + CH_3COO_2$	$1.4 \times 10^{-12} \exp(-1900/T)$
$PAN \longrightarrow CH_3COO_2 + NO_2$	$K_{eq} = 9.0 \times 10^{-29} \exp(14000/T)^{-1}$
$VOC + OH \longrightarrow RO_2$	k_{OH}
$RO_2 + NO \longrightarrow (1-\alpha)HO_2 + (1-\alpha)NO_2 + \alpha RONO_2$	$2.7 \times 10^{-12} \exp(360/T)$
$RO_2 + HO_2 \longrightarrow 0.5\,ROOH + 0.5\,O_2 + 0.5\,HO_2 + 0.5\,OH$	$2.06 \times 10^{-13} \exp(1300/T)$
$RO_2 + RO_2 \xrightarrow{O_2} 1.2\,CH_3O_2 + products$	9×10^{-14}
$RO_2 + CH_3O_2 \xrightarrow{O_2} 0.6\,CH_3O_2 + 0.6\,HO_2 + products$	9×10^{-14}
$VOC + NO_3 \longrightarrow \beta\,RONO_2 + (1-\beta)\,NO_2 + products$	k_{NO_3}

Table 3.A3: Reactions and rate constants used in the simplified single box model

Reaction	Rate constant
$HO_2 + HO_2 \xrightarrow{M} H_2O_2{}^+O_2$	2.74×10^{-12}
$NO_2 + OH \xrightarrow{M} HNO_3$	9.2×10^{-12}
$RO_2 + NO \longrightarrow (1-\alpha)HO_2 + (1-\alpha)NO_2 + \alpha\, RONO_2$	9.0×10^{-12}
$RO_2 + HO_2 \longrightarrow ROOH + O_2$	8.0×10^{-12}
$RO_2 + RO_2 \xrightarrow{O_2} 1.2\, CH_3O_2 + \text{products}$	6.8×10^{-14}

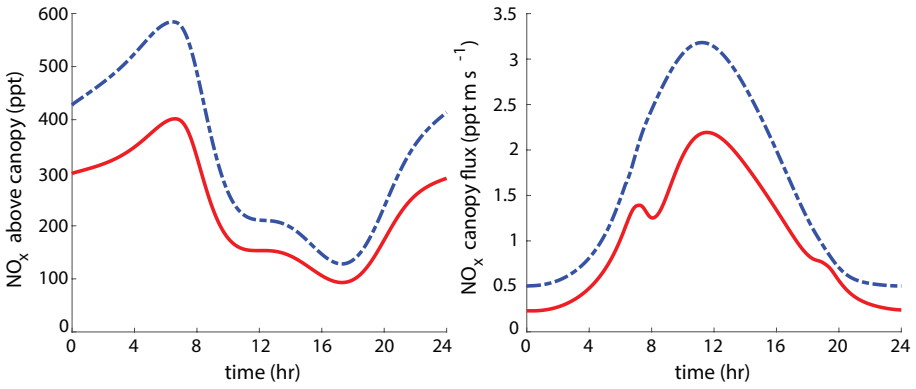

Figure 3.A1: Model predictions for the above canopy NO_x mixing ratios (a) and fluxes (b) for a LAI scaling factor of 0.25 (blue dash) and 1.5 (red solid).

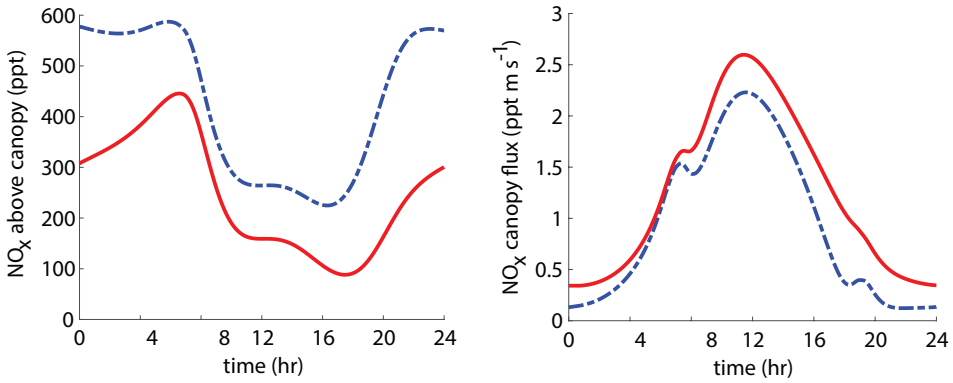

Figure 3.A2: Model predictions for the above canopy NO_x mixing ratios (a) and fluxes (b) for $\alpha = 0.01$ (blue dash) and $\alpha = 0.1$ (red solid).

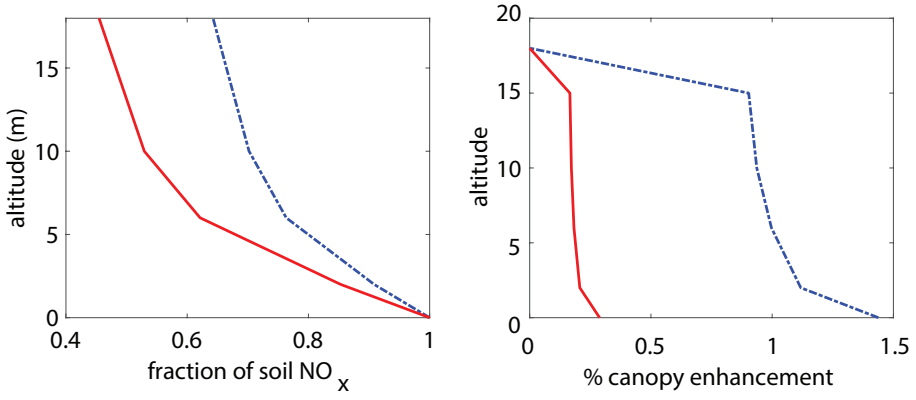

Figure 3.A3: Model predictions for the fraction of soil NO_x ventilated vertically (a) percent of NO_x within the canopy relative to above-canopy concentrations (b) for an NO emission rate of 10 ppt m s^{-1} (blue dash) and 1 ppt m s^{-1} (red solid).

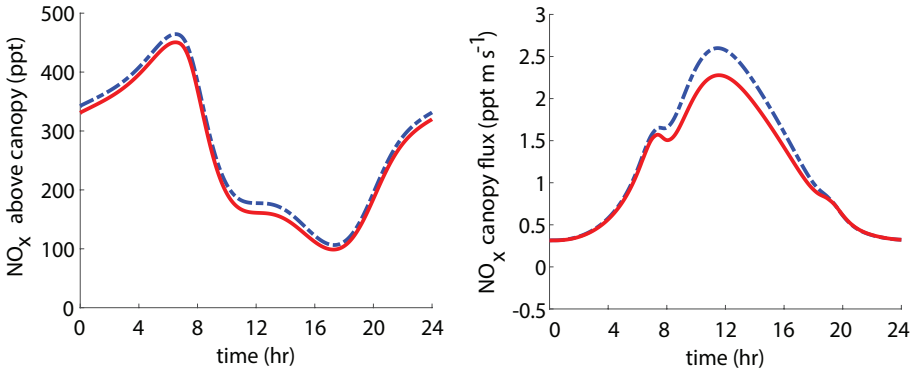

Figure 3.A4: Model predictions for the above canopy NO_x mixing ratios (a) and fluxes (b) for $\tau/T_L = 8$ (blue dash) and $\tau/T_L = 1.2$ (red solid).

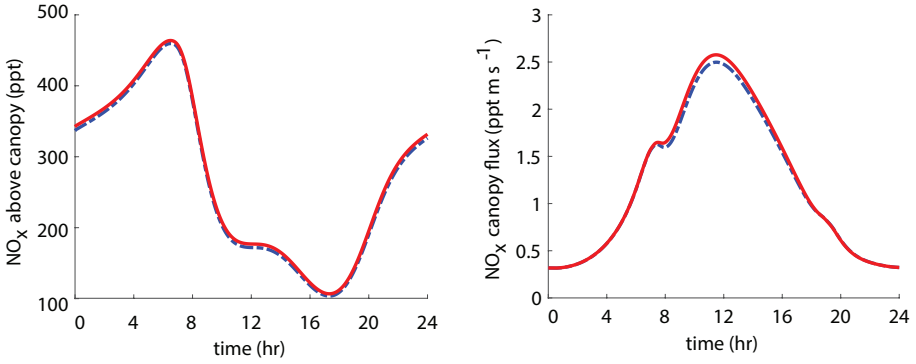

Figure 3.A5: Model predictions for the above canopy NO_x mixing ratios (a) and fluxes (b) for an l_w scaling factor of 0.1 (blue dash) and 2 (red solid).

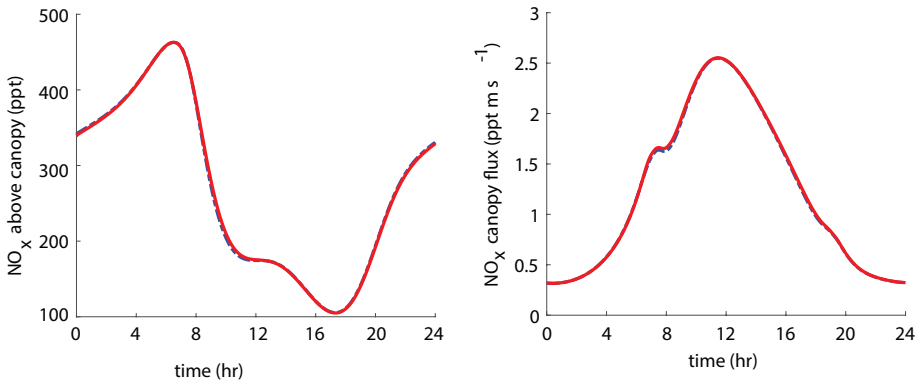

Figure 3.A6: Model predictions for the above canopy NO_x mixing ratios (a) and fluxes (b) for $k_{rad} = 0.6$ (blue dash) and $k_{rad} = 0$ (red solid).

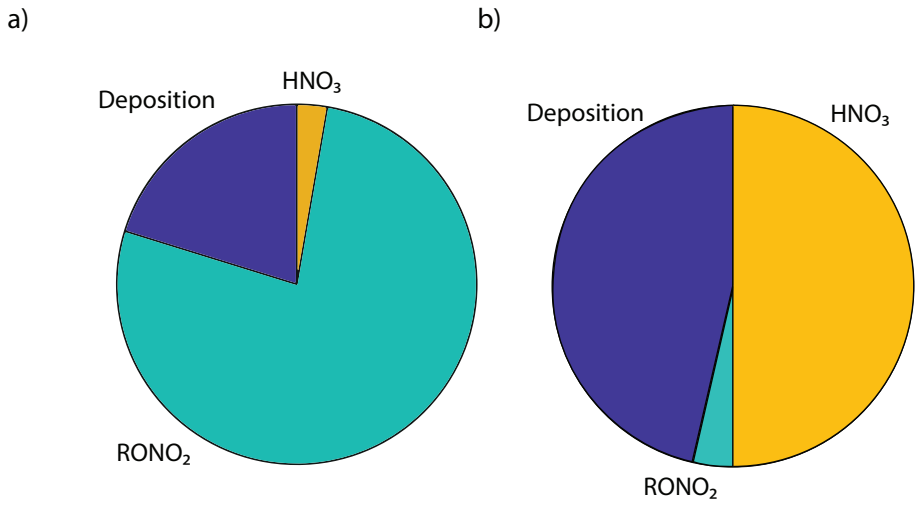

Figure 3.A7: Multi-box model prediction of the average daily fraction of NO_x lost to nitric acid formation, alkyl nitrate formation, and deposition in an environment with 0.1—0.2 ppb NO_x (a) and 20—30 ppb NO_x (b).

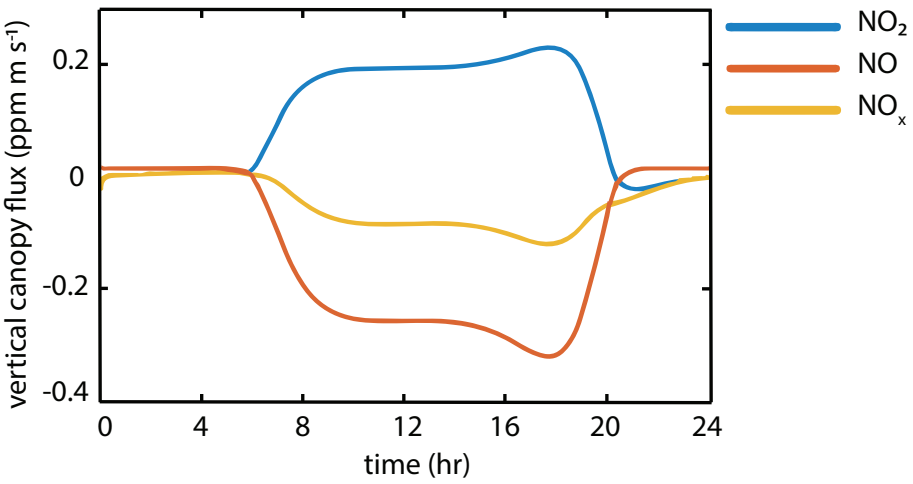

Figure 3.A8: Multi-box model prediction of the diurnal canopy flux in an environment with daily minimum NO_x concentrations of 20 ppb during the day and maximum concentrations of 50 ppb at night. Model was run using parameters for Blogett Forest.

Figure 3.A9: Satellite image of east San Francisco Bay Area

Chapter 4

Laboratory measurements of NO_2 deposition to native California trees and the role of forests in the NO_x cycle

Adapted from E. R. Delaria et al., Laboratory measurements of stomatal NO_2 deposition to native California trees and the role of forests in the NO_x cycle, *Atmos. Chem. Phys. Discuss.*, 2020, 1–32, https://doi.org/10.5194/acp-2020-240, 2020.

4.1 introduction

Nitrogen oxides ($NO_x \equiv NO + NO_2$) are a form of reactive nitrogen that plays a major role in the chemistry of the atmosphere. NO_x catalyzes tropospheric ozone formation, contributes to the production of photochemical smog, and influences the oxidative capacity of the atmosphere (Crutzen, 1979). NO_x is primarily emitted as NO through fossil fuel burning, lighting, and soil microbial activity. The latter source is of particular importance in remote, forested, and agricultural regions.

Understanding the fate of atmospheric NO_x, in addition to its emission sources, is essential for interpreting the impact of NO_x on atmospheric chemistry. Prior studies have demonstrated that NO_2 can directly deposit to foliage via diffusion through stomata (e.g., Teklemmariam and Sparks, 2006; Chaparro-Suarez et al., 2011; Breuninger et al., 2013; Delaria et al., 2018). The currently understood mechanism of this uptake process is as follows: NO_2 enters through the stomatal cavity and dissolves into the apoplastic fluid, forming nitrate, which then is reduced to ammonium by the enzyme nitrate reductase (Park and Lee, 1988; Ammann et al., 1995; Tischner, 2000; Lillo, 2008; Heidari et al., 2011). There is evidence that NO_2 may also be directly scavenged by antioxidants, most notably ascorbate (Ramge et al., 1993; Teklemmariam and Sparks, 2006). These processes may be impacted

by the leaf pH, which is known to change under conditions of limited water availability (Bahrun et al., 2002). Experiments using ^{15}N as an isotopic tracer have demonstrated that absorbed NO_2 is eventually assimilated into amino acids (Rogers et al., 1979; Okano and Totsuka, 1986). Although the role of stomatal conductance (g_s) in controlling the deposition of NO_2 is well-documented, the impact of the processes in the mesophyll–processes taking place between the intercellular air space and the ultimate nitrogen assimilation site–on the rate of uptake remains poorly resolved. The question of whether and how much mesophyllic processes affect NO_x budgets at the canopy scale thus persists.

The most divisive example of the mesophyll quandry is the sometimes-reported emission of NO_x from plants, mostly in the form of NO, at low NO_x mixing ratios that would be relevant to remote forested regions (Johansson, 1987; Rondón and Granat, 1994; Hereid and Monson, 2001; Sparks et al., 2001; Teklemmariam and Sparks, 2006). This would, under many conditions, indicate that trees instead serve as a constant source, rather than sink, of NO_x. However, this idea has been called into question by a number recent studies including Lerdau et al. (2000), Chaparro-Suarez et al. (2011), Breuninger et al. (2013) and Delaria et al. (2018). It is possible that the magnitude and direction of the NO_x flux to leaves may vary depending on the species and conditions. One such factor that has been suggested to impact foliar emission and deposition of NO_x is elevated soil nitrogen. Soil nitrate fertilization has been documented to lead to an increase in nitrate reductase activity in the needles of scots pine seedlings (Andrews, 1986; Pietilainen and Lahdesmaki, 1988; Sarjala, 1991). It is possible that as a result of abundant nitrate fertilization, nitrate accumulates in leaves, leading to emission or a reduction in uptake. For example, Chen et al. (2012) observed an increase in NO emission and Teklemmariam and Sparks (2006) detected an increase of NO_2 emission under conditions of elevated soil nitrate. *Per contra*, Joensuu et al. (2014) found no evidence of fertilization-induced NO_x emissions. No influence of soil nitrogen on either NO_2 or NO uptake has been documented at atmospherically relevant conditions (Okano and Totsuka, 1986; Teklemmariam and Sparks, 2006; Joensuu et al., 2014).

In this study we present results from laboratory measurements of NO_2 fluxes on ten native California tree species–six conifers and four broadleaf trees–using a branch enclosure system and laser-induced fluorescence (LIF) detection of NO_2. Here we investigate the relative influence of stomatal and mesophyllic processes on the total uptake rate of NO_2 under atmospherically relevant conditions. Our aim is to assess the factors controlling NO_2 foliar deposition and their ultimate impact on the NO_x cycle. To test this, we measured the NO_2 deposition velocity over a range of stomatal conductances and considered evidence for additional limits on the uptake rate. We also conducted experiments under drought and elevated soil nitrogen and tested for indications of an NO_2 compensation point or changes in the apparent mesophyllic uptake limit.

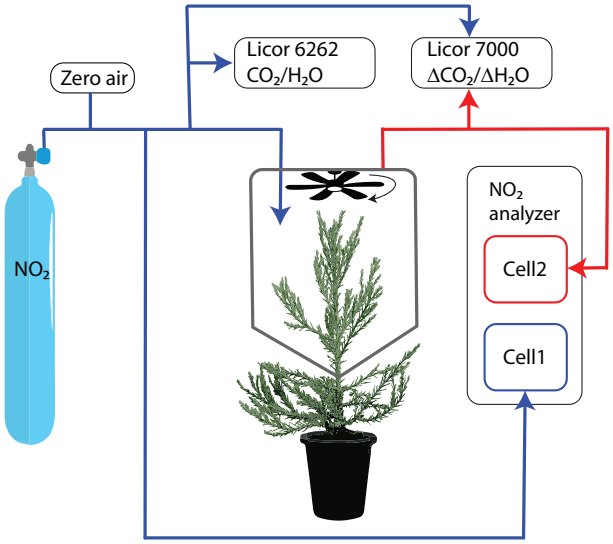

Figure 4.1: Figure of instrumental setup. Blue lines show the flow of gas that enters the chamber and red lines show the flow of gas sampled from the chamber.

4.2 Methods

Tree specimens

Foliar deposition of NO_2 was investigated in the laboratory using ten native California tree species–*Pinus sabiniana, Pinus ponderosa, Pinus contorta, Pseudotsuga menziesii, Calocedrus decurrens, Sequoia sempervirens, Arbutus menziesii, Acer macrophyllum, Quercus agrifolia, and Quercus douglasii.* Three to six individuals of each species were purchased from a local native California plant nursery (Native Here Nursery) or Forestfarm, where the plants were grown from seeds and cuttings. The tree specimens were grown in a nutrient-rich commercial soil mixture of Sun Gro Sunshine #4 and Supersoil potting soil in 20—40 liter pots in an outdoor section of the Oxford facility greenhouse at the University of California, Berkeley. The trees were 2—3 years old when measurements were taken. No additional fertilizers or pesticides were used on the plants. Trees were transported into the lab for experimentation, where they were exposed to a 12 h light/dark cycle. Trees were illuminated with an LED diode array of 430—475 and 620—670 nm lights (Apollo Horticulture). For the deciduous trees (*Q. douglassi, and A. macrophyllum*) experiments were run between May and September 2019. For all other species experiments were conducted year-round, between October 2018 and November 2019.

LIF measurement of NO_2 deposition fluxes

Measurements were made with a dynamic chamber and Laser-Induced Fluorescence (LIF) detection of NO_2. A full description of our apparatus can be found in Delaria et al. (2018). Briefly, an NO_2 standard was mixed with humidified zero air (air filtered to remove NO_x and reactive species) and delivered to a ∼10 L chamber enclosing the branch of a tree at a total flow rate of ∼6000 cm^3 min^{-1} (Fig.4.1). The lifetime of air within the chamber was ∼ 2 min. Humidity was adjusted by controlling the fraction of zero air that passed through a bubbler filled with distilled water. The mixing ratios of NO_2 entering the chamber were typically 0—10 ppb. Some of the air entering the chamber was diverted to cell #1 of the NO_2 LIF analyzer and two Licor instruments (6262 and 7000) for measuring the mixing ratios of NO_2 and H_2O/CO_2, respectively in the in-flowing air stream, such that the flow rate of air directly into the chamber was ∼5000 cm^3 min^{-1}. Air from the chamber was simultaneously pumped out to cell #2 of the NO_2 LIF analyzer and the Licor-7000 instrument for measuring the mixing ratio of NO_2 within the chamber and the change in CO_2 and water vapor between the in- and outgoing air streams, respectively (Fig. 4.1). A slight positive pressure was maintained within the chamber to ensure lab air did not leak into the chamber.

Fluxes of NO_2 to leaves were calculated according to (Eq.4.1—4.2):

$$Flux = \frac{Q}{A}([NO_2]_{in} - [NO_2]_{out}) \tag{4.1}$$

$$Flux = V_d([NO_2]_{out} - [NO_2]_{comp}) \tag{4.2}$$

where $[NO_2]_{in}$ and $[NO_2]_{out}$ are concentrations of NO_2 entering and exiting the chamber, respectively, $[NO_2]_{comp}$ is the compensation point concentration, Q is the flow rate (cm^3/s), A is the enclosed one-sided leaf area, and V_d is the deposition velocity. The leaf area was determined using the ImageJ software package (Schneider and Eliceiri, 2012) and the flow rate was measured at the beginning of each experimental run (Mesa Laboratories 510-M Bios Defender). Peroxyacetyl nitrate (PAN) and acetone were also delivered to the chamber for simultaneous measurements of PAN stomatal deposition. Negligible thermal production of NO_2 was observed. The results of PAN deposition experiments will be discussed elsewhere. The NO_2 mixing ratio was also corrected for the differences in collisional quenching of the excited state NO_2 by water vapor in cells #1 and #2, caused by transpiration of the tree within the chamber (Thornton et al., 2000).

$$[NO_2]_{out,actual} = [NO_2]_{out,measured} \times (1 + 5\Delta X_{H_2O}) \tag{4.3}$$

where ΔX_{H_2O} is the difference in the water vapor mole fraction between the chamber and the incoming air stream.

Deposition velocities were determined using the method described in Delaria et al. (2018): a weighted orthogonal distance linear regression was performed on NO_2 fluxes (determined using Eq. 4.1) against $[NO_2]_{out}$ to obtain a slope equal to V_d. A positive x-intercept was interpreted as evidence for a possible compensation point. During each day of experimentation we stepped through at least 8 different NO_2 concentrations, with each concentration

step lasting for 40 minutes. Uncertainty in V_d was obtained through propagating uncertainty in measured NO_2 concentrations, Q, and A. The uncertainty in NO_2 concentrations was estimated as one standard deviation of variation in measurements during the last 10 minutes of each concentration step. The uncertainty in Q was estimated as <1 % and a 10% uncertainty was estimated for the enclosed one-sided leaf area.

The deposition velocities measured can be related to the resistance-model framework for deposition of trace gases developed by Baldocchi et al. (1987) (Eq.4.4—4.6).

$$V_d = \frac{1}{R} \tag{4.4}$$

$$R = R_a + R_b + R_{leaf} \tag{4.5}$$

$$\frac{1}{R_{leaf}} = \frac{1}{R_{cut}} + \frac{1}{R_s + R_m} \tag{4.6}$$

R is the total resistance to deposition, R_a is the aerodynamic resistance, R_b is the boundary layer resistance and R_{leaf} is resistance to uptake by the leaf. R_a was assumed to be negligible under our chamber conditions (Pape et al., 2009; Breuninger et al., 2012; Delaria et al., 2018). R_{leaf} is made up of R_{cut}, R_s, and R_m. Respectively, these refer to the cuticular resistance (resistance to deposition to the surface of the leaf), stomatal resistance ($1/g_s$), and mesophyllic resistance (resistance associated with all processes taking place within the leaf that limit uptake).

Measurement of stomatal conductance

CO_2 and water vapor exchanges were measured using the Licor 6262 and Licor 7000 instruments. Measurements of water vapor exchange were used to calculate the transpiration rate (E) and total conductance to water vapor (g_t^w) using Eq. 4.7 and Eq. 4.8, according to von Caemmerer and Farquhar (1981).

$$E = \frac{Q}{A}\frac{w_a - w_e}{1 - w_a} \tag{4.7}$$

$$g_t^w = \frac{E(1 - (w_i + w_a)/2)}{w_i - w_a} \tag{4.8}$$

where w_a and w_e are the mole fractions of water vapor of the outgoing and incoming airstreams, respectively, and ω_i is the internal leaf water vapor mole fraction. ω_e was measured with the Licor-6262 with dry air as a reference and $\Delta\omega$ ($\omega_a - \omega_e$) was measured with the Licor-7000 with incoming air as the reference. ω_i was assumed to be the saturation vapor pressure at the leaf temperature, which was measured with a thermocouple at the surface of an enclosed leaf. The chamber temperature was measured with a second thermocouple and was typically 20±3°C. The photosynthetic photon flux density (PPFD) was monitored outside the chamber with a LiCor quantum sensor (LiCor LI-190SA) and was 1190μmol m^2

s^1, approximately the PPFD for Berkeley, California, at noon during the month of October. We performed calculations based on von Caemmerer and Farquhar (1981) to confirm this is above the photon flux required to achieve maximal stomatal aperture for tree types relevant to this study. Total conductance was calculated as the average over the light or dark period of an experiment. The uncertainty in our calculation of total conductance to water vapor was primarily influenced by uncertainty in the leaf temperature and the assumption of leaf water vapor saturation. We observed fluctuations in the temperature of enclosed leaves of ±2°C. Total uncertainty in g_t^w was determined by propagating this uncertainty in leaf temperature, which resulted in larger estimated uncertainties at larger chamber humidities, usually coinciding with higher stomatal conductances. Chamber relative humidity was maintained at less than 90% to minimize this effect. Variations in stomatal conductance were achieved by varying the mole fraction of water vapor in the air delivered to the chamber. The Licor-6262 instrument was calibrated weekly using standard CO_2 cylinders and the Licor-610 dewpoint generator. The Licor-7000 instrument was calibrated daily.

The stomatal conductance (g_s^w) could then be calculated from Eq. 4.9:

$$\frac{1}{g_s^w} = \frac{1}{g_t^w} - \frac{1}{g_b^w} \tag{4.9}$$

where $1/g_b^w$ is the boundary layer resistance to water vapor. The boundary layer resistance to water vapor was estimated to be negligible under our experimental conditions, with an upper bound of 0.6 s cm^{-1} determined using the methods described by Delaria et al. (2018). Stomatal (g_s) and total (g_t) conductances to NO_2 were calculated by scaling the values for water vapor by the ratio of diffusivities in air (D_{NO_2}/D_{H_2O}) according to Massman (1998).

Nitrogen measurements

To test the influence of excess soil nitrogen on the ability of trees to take up nitrogen through their stomata in the form of NO_2, we fertilized three individuals of both *Quercus agrifolia* and *Pseudotsuga menziesii* with a 20 mM ammonium nitrate solution. The trees were watered with 250 ml of this ammonium nitrate solution three days per week. Three individuals of each species were watered with DI water as the control group. The trees underwent this fertilization treatment for 120 days before beginning dynamic chamber measurements on NO_2 foliar deposition. NO_2 deposition experiments were conducted for 70 days, during which time the soil fertilization treatments were continued.

Soil nitrogen

Approximately 5 mg of a soil core sample was taken each day from the individual on which we conducted an NO_2 deposition experiment. The soil was sifted through a mesh 2 mm sieve. Soil nitrate and ammonium were extracted by shaking ≈2.5 mg of the soil sample in 30 ml of ≈ 2M KCl for one hour, followed by filtering the samples through a Whatman No.1 filter paper. The other ≈2.5 mg was dried in a drying oven at 60°C for at least 48

hours. The mass of the soil after drying was measured to determine the percentage dry mass of the extracted soil sample. Six KCl blanks, 3 KCl samples spiked with 5 mL (low QC), and 3 KCl samples spiked with 10 mL KCl (high QC) were carried through the extraction process to serve as quality controls (QC samples). NH_4^+ and NO_3^- were measured using a colorimetric synthesis following the method of Sims et al. (1995) and Decina et al. (2017). Briefly, a standard 1 ppm stock solution of ammonium nitrate was made from ammonium nitrate solid dissolved in milli-q water, and was diluted to 0, 0.1, 0.2, 0.3, 0.4, and 0.5 mg/L in 1 cm, 2.5 mL cuvettes. These standard solutions served as the calibration standards; we made three sets of calibration standards for both ammonium and nitrate analysis. All glassware was acid washed in a 1M solution of HCl prior to all measurements and extractions to prevent contamination.

For ammonium analysis, 160 μL of each soil extraction sample from the control group, 10 μL from the fertilizer-treated group, and 1.6 mL of the QC samples were pipetted into individual cuvettes. 100, 200, 100, and 500 μL of 0.2 M citrate, 5 mM nitroprusside, 0.3 M hypochlorite reagents, and milli-q water, respectively, were then added sequentially into each cuvette. The cuvettes were filled to a final volume of 2.5 mL with KCl, and the samples were allowed to sit for 30 min. For nitrate measurements, 320 μL and 10 μL of soil samples from the the control and fertilized groups, respectively, and 1550 μL of the QC samples, were pipetted into separate cuvetts. 950 μL of a regent containing 1g/L vanadium chloride and 25 mg/L N-(1-Naphthyl)ethylenediamine (NEDD) was subsequently added to each cuvette, which were then filled to a final volume of 2.5 mL with KCl and allowed to sit for 24 hrs. 160 μL and 320 μL of a control *Q. agrifolia* soil extraction sample were added to one set of calibration standards for ammonium and nitrate analysis, respectively, to test the effects of the soil matrix on the calibration.

Concentrations of ammonium and nitrate in each sample were determined with colorimetric measurements using a custom built spectrophotometer. The spectrophotometer light source was a broad spectrum quartz tungsten-halogen lamp (QTH10 Thorlabs Inc.). The absorption of each sample and standard was measured with the light source passing through a 540 $\pm$ 2 nm bandpass filter (FB570-10 Thorlabs Inc.) for nitrate analysis or a 670 $\pm$ 2 nm bandpass filter (FB540-10 Thorlabs Inc.) for ammonium analysis.

Uncertainty analysis

Concentrations of ammonium and nitrate in the soil extraction samples were determined from the slope in their respective calibration curves. The calibrations for ammonium and nitrate analysis had respective uncertainties of 7% and 5%. The slopes of the calibration curves with added sample from a *Q. agrifolia* soil extraction were not statistically different from those containing only standards, allowing us to exclude the possibility of interference from the soil matrix.

The accuracy uncertainty in the high and low QC samples were 3% and 11%, respectively for anmmonium measurements, and 3% and 12% for nitrate measurements. We estimated the resulting uncertainty for cuvette samples with less than 0.15 mg/L NH_4^+ or NO_3^- ($\approx$ 1.8

μg/mg soil NH_4^+ or NO_3^-) to be 15%. Samples with larger concentrations were estimated to have 5% uncertainty. The blank quality control standards contained 0.04 mg/L ammonium and nitrate. This was blank-subtracted from each sample.

Leaf nitrogen

After deposition experiments were completed the leaves were removed from the trees and dried for 48 hours in a drying oven. The leaves were then ground to a fine powder and the percent nitrogen, hydrogen, and carbon content were measured with a ICP Optima 7000 DV instrument.

Drought stress

Calocedrus decurrens and *Pinus ponderosa* were drought stressed to study the impact of drought on NO_2 deposition. Three individuals of each species were watered daily (control group) and three individuals of each species were watered with 250 mL once every four weeks (drought group). Limited-water treatment of the drought group was carried out for 60 days before conducting dynamic chamber experiments for NO_2 foliar deposition. NO_2 deposition experiments were run for 30-40 days. During the experiments, the control group was watered 50 mL daily and the experimental group was watered 50 mL once every two weeks. The *P. ponderosa* drought-stress experiments took place between March and June 2019. The *C. decurrens* drought stress spanned from August to December 2019.

The xylem water potential (Ψ_p) of the trees were monitored to measure the drought stress level of the trees using a Scholander pressure chamber (Model 670 PMS Instr. Comp.). Leaves were cut, wrapped in aluminum foil, and then inserted into the pressure bomb. The Ψ_p of cuttings were measured around 11:00AM each day. A Ψ_p measurement lower than -1.0 MPa indicated signs of drought stress in the *P. ponderosa*. The *C. decurrens* did not show evidence of drought stress in Ψ_p measurements while in the greenhouse, however, early signs of embolism were observed.

4.3 Results

V_d was calculated for each day of measurements with a weighted linear regression of measured fluxes and chamber NO_2 concentrations (Delaria et al., 2018). No statistically significant compensation point was observed under any experimental condition for the majority of the species studied, in agreement with previous work (Chaparro-Suarez et al., 2011; Breuninger et al., 2013; Delaria et al., 2018). Only *P. menziesii* was found to have a compensation point, estimated to be 20 ppt, but this concentration is below the limit of quantification for our instrument and we believe this measurement to be consistent with a compensation point of zero. V_d and g_s measurements allowed for consideration of whether the deposition of NO_2 is exclusively stomatally controlled, or is also affected by the internal processing in the

mesophyll. We rarely observed total closing of the stomata when the chamber lights were turned off at night. All of the deposition observed at night could be explained by deposition to these partially open stomata. This is consistant with previous studies observing only partial closing of stomata at night in a variety of plant species (Dawson et al., 2007; Drake et al., 2013) . The results of experiments are show in (Table 4.1).

Measurements of mesophyllic resistance

We utilized two methods of examining the importance of the mesophyllic resistance on the deposition of NO_2. Figure 4.2 shows the predicted stomatal-limited NO_2 deposition fluxes, assuming negligible R_b and R_m ($Flux = g_t[NO_2]_{out}$) plotted vs. the measured NO_2 fluxes. Our upper bound measurement of R_b for NO_2 is 1 s cm^{-1} (0.6 s cm^{-1} for water vapor). This was calculated by measuring the deposition of NO_2 to a 30 cm^2 tray of activated charcoal. R_b decreases with the enclosed leaf area according to Pape et al. (2009), which at a minimum was 200 cm^2. The maximum R_b in the chamber should thus be ≈0.1 s cm^{-1}. Assuming $g_s = g_t$ would lead to a maximum of a 6% error in the calculated g_s assuming a g_t of 0.6 cm s^{-1} and R_b of 0.1 s cm^{-1}. Any deviation from unity in the observed slope of predicted vs. measured fluxes can thus be attributed to R_m. Significant deviations from unity can be seen in several species, most notably *S. sempervirens* (Table 4.1 and Fig. 4.2). Slopes were calculated using a weighted average of the slopes obtained from a least squares cubic weighted fit of each individual experiment (Table 4.1). Some experiments were excluded (shown in red in Fig. 4.2), as they were determined to be outliers by a generalized extreme studentized deviate test for outliers. Identified outliers were excluded to account for potentially erroneous deviations in the V_d/g_t ratio due to systematic error in the daily calibration of the Licor-7000 instrument, which we believe to be the primary cause of the relationships observed above the 1:1 line. The only physical explanation of points above the 1:1 line would be substantial cuticular deposition, which we did not observe any evidence for at low stomatal conductances in our experiments. Outliers were also excluded and to avoid over-weighting of days with abnormally large stomatal conductances. These instances normally coincided with low V_d/g_t ratios, and if these data were also subject to some systematic error, would bias our analysis of R_m.

R_m was also explicitly calculated using the relationship of V_d and g_t. Figure 4.3 shows V_d from each day of experiments plotted against the measured g_t. Deviations from the 1:1 line are attributable to the mesophyllic resistance. R_m was calculated with a weighted fit of the resistance model:

$$V_d = \frac{1}{R_c} + \frac{1}{(\frac{1}{g_s} + R_m)} \tag{4.10}$$

No significant cuticular resistances were observed so only results of R_m are recorded (Table 4.1). R_m was calculated both assuming negligible R_b ($g_s = g_t$) and $R_b = 1$ s cm^{-1}. There were no significant differences between these two calculations (Table 4.1).

Table 4.1: Summary of species-dependent foliar deposition results

species	R_m s cm^{-1}	R_m (g_s)^f s cm^{-1}	max^d V_d cm s^{-1}	max^e g_t^w cm s^{-1}	median dark V_d mmol $m^{-2}s^{-1}$	slope^a	r g_t vs. slope	$[NO_2]_{comp}$ ppb
P. sabiniana	0.43± 0.06	0.46± 0.06	0.51 ± 0.04	500 ± 100	0.087	0.79±0.04	-0.37^c	-0.03 ±0.03
P.ponderosa	0.7 ± 0.1	0.69 ± 0.09	0.26 ± 0.01	230 ± 25	0.038	0.91 ± 0.05	-0.72^c	0.00±0.02
P.contorta	0.5 ± 0.2	0.5 ± 0.2	0.24 ± 0.03	180 ± 30	0.018	0.99 ± 0.03	-0.36^c	0.00±0.01
P. menziesii	0.30 ± 0.07	0.30 ± 0.06	0.26 ± 0.02	230 ± 20	0.044	0.91 ± 0.04	-0.26	0.02±0.02^b
C. decurrens	0.4 ± 0.1	0.4 ± 0.1	0.21 ± 0.03	160 ± 20	0.009	0.91 ± 0.02	-0.36^c	0.00±0.02
S. sempervirens	0.9 ± 0.1	0.9 ± 0.1	0.27 ± 0.04	330 ± 80	0.009	0.60 ± 0.04	-0.43^c	-0.01±0.02
A. menziesii	0.4 ± 0.1	0.4 ± 0.1	0.26 ± 0.05	210 ± 10	0.037	0.93 ± 0.03	-0.38^c	-0.02±0.01
A. macrophyllum	0.5 ± 0.1	0.54 ± 0.09	0.47 ± 0.08	400 ± 100	0.017	0.84 ± 0.03	-0.21	-0.02±0.01
Q.agrifolia	1.3 ± 0.3	1.3 ± 0.2	0.15± 0.01	90 ±20	0.008	0.89 ± 0.04	-0.22	0.00±0.01
Q. douglasii	0.2 ± 0.1	0.2 ± 0.1	0.30 ± 0.03	180 ± 20	0.004	0.89 ± 0.04	0.23	-0.01±0.02

a. Slope of measured vs. predicted fluxes (Fig. 4.2).

b. Statistically significant ($\alpha = 0.01$) compensation point. Compensation point listed is at limit of detection for the instrument.

c. Statistically significant ($\alpha = 0.05$) correlation.

e. Maximum stomatal conductance that was observed during our experiments and the error associated with that measurement.

e. Listed maximum g_t^w the maximum stomatal conductance to water vapor that was observed during our experiments and the error associated with that measurement. Units in mmol $m^{-2}s^{-1}$ for ease of comparison with other stomatal conductance studies.

f. R_m calculated assuming R_b is at the upper bound (R_b=1 s cm^{-1})

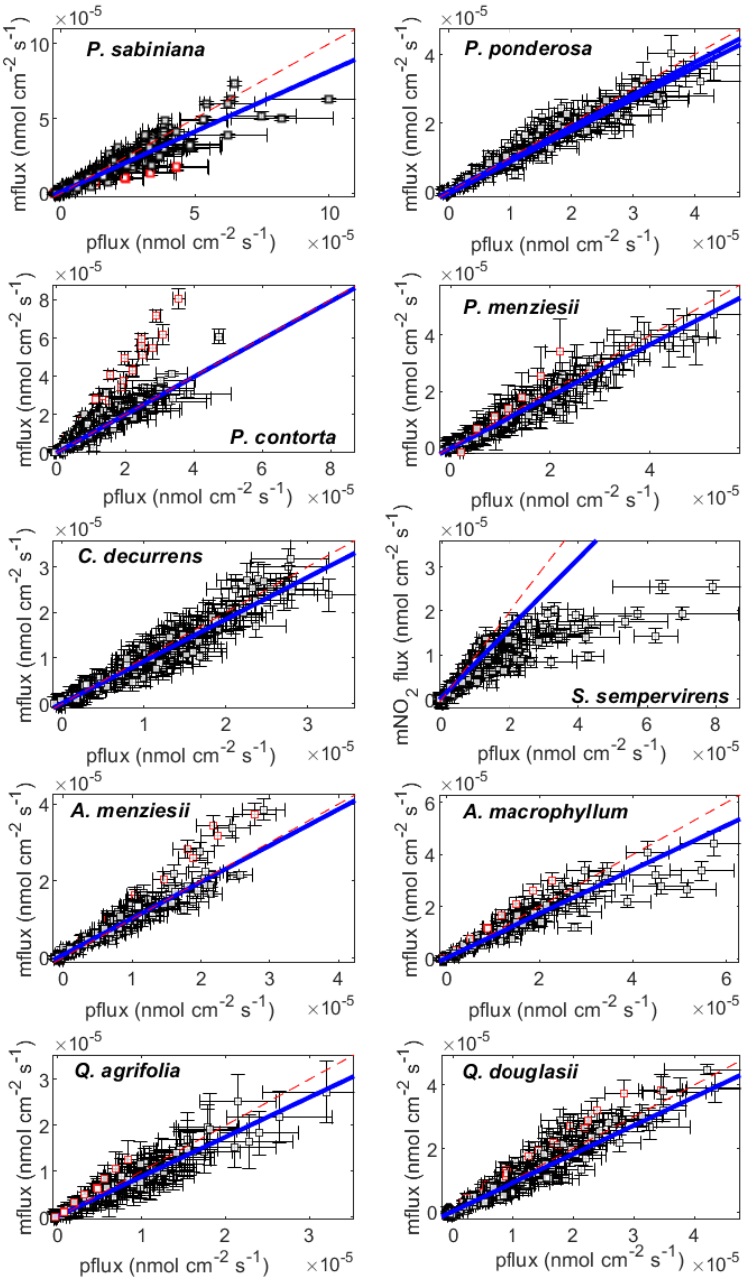

Figure 4.2: Measured fluxes (mflux) plotted against stomatal-limited predicted fluxes (pflux). Blue solid lines are the linear fit to data. Red lines are the 1:1 line. Error bars for the measured fluxes are calculated by propagating uncertainty in the measured NO_2 mixing ratios, the flow rate, and the leaf area (Eq. 4.1). Error bars for the predicted fluxes are calculated by propagating uncertainties in the measured NO_2 mixing ratios and the total conductance (Eq. 4.8). Red markers indicate data determined to be outliers by a generalized extreme studentized deviate test for outliers.

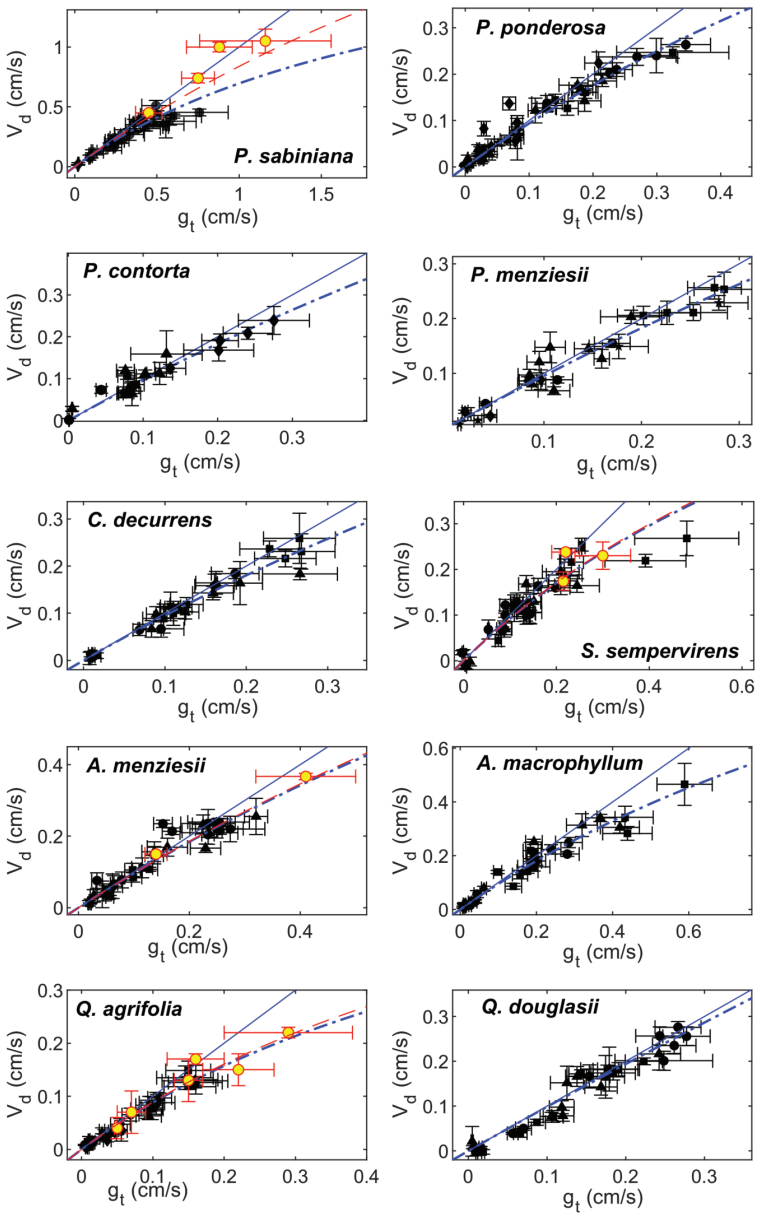

Figure 4.3: Deposition velocities plotted against measured stomatal conductances to NO_2. Black markers represent measurements in zero air and red-yellow markers are measurements in helium. Solid blue lines are the 1:1 line and dashed blue lines are error weighted fits to the resistance model using only measurements in zero air (Eq. 4.4). Fits to the resistance model including data from helium measurements are shown as dashed red lines.

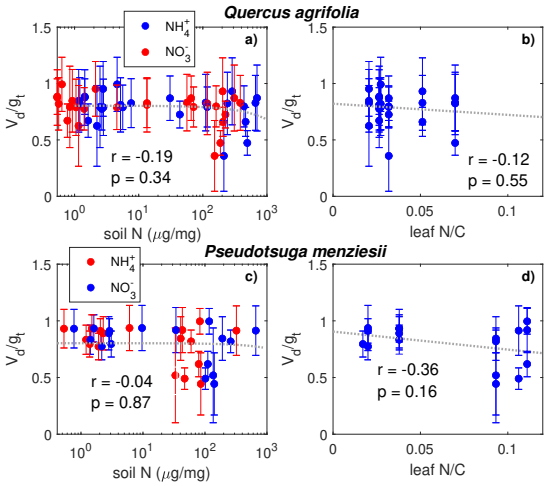

Figure 4.4: The V_d/g_t ratio is plotted against soil nitrogen concentration in the form of NH_4^+ and NO_3^- for (a) *Q. agrifolia* and (c) *P. menziesii*. The V_d/g_t ratio is plotted against the leaf nitrogen:carbon ratio for (b) *Q. agrifolia* and (d) *P. menziesii*. On each pannel the Pearson's correlation coefficient and the p-value for the slope are shown. The amount of soil and leaf nitrogen has no significant impact on the V_d/g_t ratio.

Table 4.2: Average soil and leaf nitrogen

tree[a]	soil NH_4^+ μg/mg	soil NO_3^- μg/mg	leaf N %	leaf C %
QA control	3.0± 0.5	3 ± 1	1.1 ± 0.1	47.7 ± 0.2
QA high N	300± 60	170 ± 30	2.4 ± 0.5	48.1 ± 0.2
PM control	2.7 ± 0.8	2.0 ± 0.5	1.3 ± 0.2	56 ± 9
PM high N	190± 43	80 ± 20	4.7 ± 0.2	45.9 ± 0.4

a. QA is *Q. agrifolia* and PM is *Pseudotsuga menziesii*.

Effects of excess soil nitrogen

The impact of soil fertilzation on the foliar uptake of NO_2 by two tree species, *Q. agrifolia* and *P. menziesii*, was examined by watering a control group of both species with deionized water and a fertilized group with 20 ppm ammonium nitrate. On average, the soil nitrogen concentrations of NH_4^+ and NO_3^- were 100x larger for the fertilized groups than the control groups (Table 4.2). The percentage of leaf nitrogen content approximately doubled between the control groups and the fertilized groups (Table 4.2).

The effect of soil nitrogen fertilization and leaf nitrogen content on the ratio of V_d/g_t is shown in Fig. 4.4. No significant relationship ($\alpha = 0.01$) was observed for either *Q.*

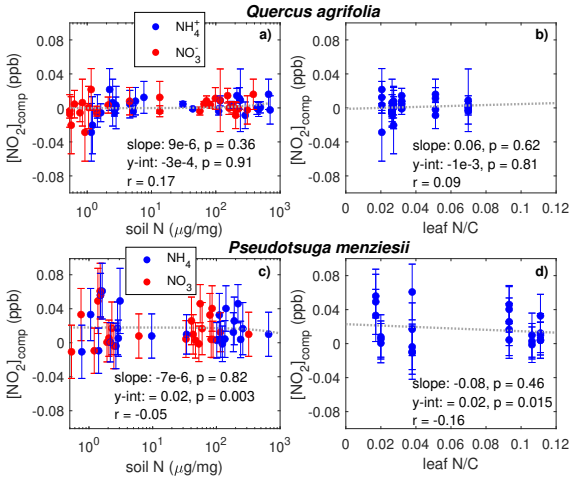

Figure 4.5: $[NO_2]_{comp}$ is plotted against soil nitrogen concentration in the form of NH_4^+ and NO_3^- for (a) *Q. agrifolia* and (c) *P. menziesii*. $[NO_2]_{comp}$ is plotted against the leaf nitrogen:carbon ratio for (b) *Q. agrifolia* and (d) *P. menziesii*. On each pannel the Pearson's correlation coefficient, the slope, the intercept, and their p-values are shown. The amount of soil and leaf nitrogen has no significant impact on the compensation point.

agrifolia of *P. menziesii*, suggesting the mesophyllic processing of NO_2 is unaffected by soil or leaf nitrogen content. We also observe no increase in the compensation point of NO_2 as a result of higher leaf nitrogen content or elevated soil nitrogen (Fig. 4.5). The trees on which we conducted these experiments were observed to behave consistently up to the point of embolism.

Drought stress measurements

The impact of drought stress on NO_2 foliar uptake for *C. decurrens* and *P. ponderosa* was observed by regularly watering a control group and watering an experimental, drought group at much lower frequency (once every 4 weeks in the greenhouse, and once every 2 weeks in lab). The median Ψ_p measured was lower for the drought groups than the control groups (Table 4.3), *C. decurrens* drought median Ψ_p was -0.80 MPa compared to control median of -0.30 MPa, and *P. ponderosa* drought median was -1.05 MPa compared to control median of -0.60 MPa. The first quartiles of the control groups and third quartiles of the drought groups do not overlap, reflecting a significant difference between the Ψ_p measurements of the two groups. We also observed a strong correlation between measured Ψ_p and stomatal conductance. We find a more substantial impact of drought on the water potentials, and of the water potentials on the stomatal conductance, in *P. ponderosa* trees than *C. decurrens*. Both these California conifer species are quite drought resistant (Pharis, 1966; Kolb and Robberecht, 1996; Maherali and DeLucia, 2000), but these results may indicate *C. decurrens* is particularly protected against water loss.

Table 4.3: Summary of drought stress results

tree[a]	med Ψ_p (IQR) MPa	med g_t (IQR) cm s^{-1}	med V_d (IQR) cm s^{-1}	R_m s cm^{-1}	slope[b]	r^c g_t vs V_d/g_t	r^c Ψ_p vs g_t
PP control	-0.60 (0.35)	0.23 (0.17)	0.21 (0.13)	0.69 ± 0.09	0.89 ± 0.02	-0.59[d]	0.651[d]
PP drought	-1.05 (0.53)	0.07 (0.12)	0.06 (0.12)	0.0 ± 0.3	1.0 ± 0.1	-0.10	
CD control	-0.30 (0.30)	0.13 (0.09)	0.12 (0.09)	0.37 ± 0.15	0.95 ± 0.02	-0.11	0.357[d]
CD drought	-0.80 (0.45)	0.06 (0.05)	0.06 (0.05)	1.17 ± 0.38	0.88 ± 0.03	-0.23	

a. PP is *Pinus ponderosa* and CD is *Calocedrus decurrens*
b. Slope of measured vs. predicted fluxes.
c. Pearson correlation coefficients.
d. Statistically significant ($\alpha = 0.05$ correlation).

The mesophyllic resistance (R_m) calculated showed a statistically significant difference for both *C. decurrens* and *P. ponderosa*. R_m in drought-stressed *C. decurrens* increased from 0.37 s cm^{-1} to 1.17 s cm^{-1}, while in *P. ponderosa* R_m decreased from 0.86 s cm^{-1} to 0 s cm^{-1}. The effects on calculated R_m are also reflected in the relationship of measured conductance (g_t) and deposition velocity (V_d) (Fig. 4.A4).

4.4 Discussion

Effects of mesophyll resistance on the lifetime of NO_x

The mesophyllic resistances (R_m) for each of the ten tree species measured are calculated from Fig. 4.3 and Eq. 4.10 and are tabulated in Table 4.1, assuming either $g_s = g_t$ or the upper bound for R_b. The slopes of predicted fluxes vs. measured fluxes, calculated in Fig. 4.2, are also tabulated in Table 4.1. The importance of the mesophyllic resistance and internal processing of NO_2 can be evaluated by examining both R_m and the slope of measured vs. predicted fluxes. We also examined the potential impact of the mesophyllic processing of NO_2 by considering the Pearson's correlation coefficient between g_t and the slope of measured vs. predicted fluxes measured on each day an experiment was run. These correlation coefficients can be found in Table 4.1. The more negative this correlation, the greater the deviation in the slope from unity for higher values of g_t, consistent with larger impact of the mesophyll on the NO_2 uptake rate. All tree species except for *C. decurrens*, *Q. agrifolia*, and *Q. douglasii* show statistically significant correlations ($\alpha = 0.05$) (Table 4.1). R_m becomes more important at larger stomatal conductances (lower stomatal resistances), as can be seen with the increasing deviations from 1:1 in some species at higher values of g_t in Fig. 4.3. Thus, even for trees with higher calculated R_m, the impact of mesophyllic processing is unlikely to be large if the maximum stomatal conductance observed is relatively small, resulting in a slope in the measured vs predicted flux that does not deviate greatly from unity. This is the case for *Q. agrifolia* and *P. ponderosa*. Alternatively, *P. sabiniana* demonstrates a case of a relatively small R_m, but also a smaller slope in measured vs. predicted fluxes, driven by consistently larger stomatal conductances (lower R_s) (Fig. 4.3). However, the greater uncertainty in measurements of stomatal conductance at a larger chamber humidity calls in to question the accuracy of many g_t measurements larger than approximately 0.4 cm s^{-1}.

To evaluate with greater certainty the relationship of V_d and g_t, we conducted a set of experiments in helium to raise the stomatal conductance by increasing the gas diffusivities while maintaining relatively lower chamber humidity. These experiments were conducted on four of the tree species: *P. sabiniana, S. sempervirens, Q. agrifolia, A. macrophyllum* and *A. menziesii*. In these experiments the V_d/g_t ratio for *A. menziesii* and *P. sabiniana* remained close to 1:1 up to 0.4 and 1.3 cm s^{-1} stomatal conductance, respectively (Fig. 4.3). We therefore suspect negligible contribution of the mesophyll to deposition to these two species. The only sizable impact of mesophyllic NO_2 processing is seen in *S. sempervirens*, with a large calculated R_m and a frequently high g_t (Fig. 4.3), resulting in a slope of measured vs.

predicted fluxes of 0.6–considerably below unity.

Currently, atmospheric models incorporate a mesophyllic resistance to NO_2 of 0.1 s cm^{-1} (Zhang et al., 2002). This would result in slope of measured vs. predicted fluxes of 0.94, even with a relatively large average g_t of 0.6 cm s^{-1}. The median slope measured in our study was 0.89. Using the model presented in Delaria and Cohen (2020), we investigated whether our results could possibly imply a more important impact of the mesophyllic resistance on the atmospheric fate of NO_x at the canopy level. The model was run using meteorological conditions for June measured during the BEARPEX-2009 campaign, located at a ponderosa pine forest in the western foothills of the Sierra Nevada mountain range (38°58'42.9"N, 120°57'57.9"W, elevation 1315 m). The model was initialized over two days and data from the third day was analyzed. We conducted two model runs at a stomatal conductance (g_s) to NO_2 deposition of 0.3 cm s^{-1}–the median measured maximum stomatal conductance excluding *P.sabiniana*–with an R_m of either 0.1 or 0.6 s cm^{-1}–the median measured R_m excluding *P. sabiniana*. For a stomatal conductance to NO_2 of 0.3 cm s^{-1} ($\approx$ 0.5 cm s^{-1} to water vapor) the model predicts only a 2.5% decrease in NO_x lost to deposition with an R_m of 0.6 compared with an R_m of 0.1 s cm^{-1}. The lifetime to deposition with an R_m of 0.1 and 0.6 s cm^{-1} was 30.5 hr and 32.2 hr, respectively, representing only a 6% difference. The total atmospheric lifetime of NO_x in the boundary layer with an R_m of 0.1 and 0.6 s cm^{-1} was 4.86 hr and 4.89 hr, respectively, representing only a 0.6% difference. Even the observed seemingly significant mesophyllic resistance of *S. sempervirens* is therefore likely to be irrelevant at the canopy-scale. Contributions from mesophyllic processing, though mechanistically important at a cellular level, are likely to not matter at the canopy-scale. We therefore suggest that on canopy, regional, and global scales, mesophyllic processes within leaves represent a negligible contribution to NO_x budgets and lifetimes.

Effects of excess soil nitrogen

We observed no effects of soil nitrogen, in the form of NH_4^+ and NO_3^-, or the leaf nitrogen content on the ratio of V_d/g_t (Fig. 4.4) for either *Q. agrifolia* or *P. menziesii*. Changes in this ratio would indicate an effect on the mesophyllic resistance. All variation in the uptake rates (V_d) could be explained exclusively with deviations in g_t. We did observe declines in g_t in the fertilized group relative to the control group during the later stages of experimentation, which coincided with observable evidence of plant stress (e.g., browning, wilting, and beginning signs of embolism). These results are supported by previous studies which have also found a negligible impact of nitrogen fertilization on NO_2 uptake (Teklemmariam and Sparks, 2006; Joensuu et al., 2014). This suggests that the mechanism of NO_2 uptake via dissolution and subsequent reduction of NO_3^- and NO_2^- is likely not bidirectional, nor influenced by accumulation of NO_3^- and NO_2^- within the mesophyll. It seems likely that either the disproportionation step and scavenging by antioxidants (e.g. ascorbate) are the rate limiting steps in the mesophyllic processing of NO_2, or that under biologically relevant conditions nitrate reductase is not saturated. This finding further supports that reactions within the mesophyll are atmospherically unimportant.

We also did not observe any evidence for a relationship between the NO_2 compensation point and the soil nitrogen content nor the leaf nitrogen content (Fig 4.5) for either *Q. agrifolia* or *P. menziesii*. In general, we only observed uptake and no emission of NO_2. We also conducted measurements of NO uptake and emission, but the fluxes measured were so small they were below the limit of quantifcation for our instrument. Chen et al. (2012) observed a strong relationship between NO emissions from stomata and soil nitrate fertilization. However, the maximum NO emissions they measured were a factor of 50 lower than the deposition of NO_2 measured here. NO emission from leaves is therefore not likely to be a significant source of atmospheric NO_x. *P. menziessi* was the only tree examined in our experiments that demonstrated any evidence for emission of NO_2 at low mixing ratios, with a compensation point of ≈ 20 ppt. This concentration is much lower than has been observed in previous studies that have detected an NO_2 compensation point (Hereid and Monson, 2001; Teklemmariam and Sparks, 2006). However, this concentration is near the limit of detection for our instrument (Delaria et al., 2018) so should be taken *cum grano salis*. A possible cause for discrepancy between our study and those that have measured significant NO_2 compensation points is that our experiments are conducted only using photosynthetically active radiation. Some past work has demonstrated that UV light may cause photolysis of nitrate at the leaf surface and subsequent emission of NO_x (Hari et al., 2003; Raivonen et al., 2006). The lack of a relationship between NO_x emission and soil N fertilization contrasts with the results of Teklemmariam and Sparks (2006), but is consistent with the nitrogen fertilization experiments conducted by Joensuu et al. (2014).

Effects of drought stress

Although there was a statistically significant impact of drought stress on R_m, this is unlikely to be atmospherically relevant for reasons stated above. Additionally, in the case of *P. ponderosa*, the lack of measurements at larger g_t is likely to mask any existing mesophyllic effects, leading to minimal deviation in V_d/g_t from unity (Fig. S4). Despite a calculation of significant mesophyllic resistance in both drought and control *C. decurrens* individuals, the lack of a statistically significant ($\alpha = 0.05$) correlation between g_t and V_d/g_t casts doubt on this relationship. The impact of drought on NO_2 uptake at the leaf-level is thus exclusively its affect on the stomatal conductance. At the canopy-level, documented affects of drought on leaf area also requires consideration (Pharis, 1966; Kolb and Robberecht, 1996; Maherali and DeLucia, 2000).

Effects of nighttime stomatal deposition

Most atmospheric chemical transport models, such as the abundantly utilized WRF-Chem and GEOS-Chem, use the Wesley model for parameterizing dry deposition of gaseous species (e.g., Skamarock and Powers, 2008; Fast et al., 2014; Amnuaylojaroen et al., 2014; Ng et al., 2017). These models implicitly assume the stomata are fully closed at night, despite more recent studies demonstrating many species of vegetation maintain partially open stomata

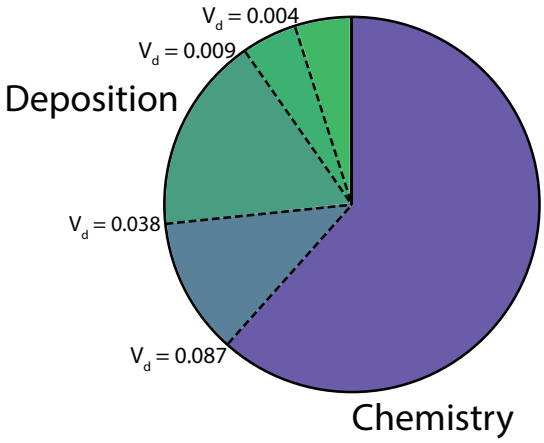

Figure 4.6: Fraction of NO_x loss to deposition and chemistry (nitric acid, alkyl nitrate, and peroxyacyl nitrate). The four dashed lines between the deposition and chemistry fractions show NO_x loss with a nighttime NO_2 deposition velocity of 0.004, 0.009, 0.038, and 0.087 cm s^{-1}. These deposition velocities respectively represent the minimum, first quartile, third quartile, and maximum of the median nighttime deposition velocities measured for the native California trees examined in this study.

at night (Musselman and Minnick, 2000; Dawson et al., 2007; Fisher et al., 2007; Drake et al., 2013). We find minimal cuticular deposition of NO_2, in agreement with several other studies (Sparks et al., 2001; Chaparro-Suarez et al., 2011). However, field observations have shown that substantial nighttime deposition of NO_2 is necessary to explain nighttime levels of NO_x (Jacob and Wofsy, 1990). The same phenomenon has been seen with other gaseous molecules, most notably PAN, which has also been observed to have a non-zero deposition at night (Wolfe et al., 2009; Crowley et al., 2018). Laboratory studies have measured zero PAN cuticular deposition (Sparks et al., 2003).

To assess the impact of nighttime stomatal opening on the atmospheric fates and lifetimes of NO_x at night, we ran our 1-D multibox canopy model, under the conditions described above, at the minimum, maximum, 25th percentile, and 75th percentile of the median nighttime deposition velocities measured in this study (0.004, 0.087, 0.009, and 0.038 cm s^{-1}, respectively). At such a low degree of stomatal opening, we found these deposition velocities to be statistically equivalent to the stomatal conductance to NO_2. The fractions of NO_x loss to deposition and chemistry to these levels of stomatal opening at night are shown in Fig. 4.6. Here chemistry represents loss to HNO_3, $RONO_2$, and PAN, and nighttime is defined from 20:00 — 05:00. The range between the first and third quartile of the nighttime deposition observed results in a range in the fraction of NO_x loss to deposition from 13% to 25% and a range in lifetime from $\approx$ 7.5—5 hrs (Fig 4.6).

The relatively large impact of the nighttime stomatal conductance on the fate of NO_x, coupled with the large degree of inter-species variation in nighttime stomatal opening, indicates a need for more extensive studies of the nighttime deposition of NO_2. Deposition is

a permanent sink of atmospheric NO_x, contrasting with the major chemical nighttime sink of NO_x to PAN formation. The relative fractions of nighttime NO_x loss to deposition and PAN formation would thus be likely to have a substantial impact on the fate of atmospheric NO_x and the cycling of NO_x.

Impacts on the nitrogen cycle in California

To our knowledge, this is the first study conducted on NO_2 stomatal deposition to native California tree species, except for *Q. agrifolia* (Delaria et al., 2018). However, there are many measurements of the stomatal conductance of Californian trees. Murray et al. (2019) examined patterns in maximum g_s^w ($max\ g_s^w$) across bioclimatic zones. Among the species they looked at were *A. menziesii*, *A. macrophyllum* and *Q. agrifolia*, for which they measured an average $max\ g_s^w$ of 550 mmol m^{-2} s^{-1}, 420 mmol m^{-2} s^{-1}, and 390 mmol m^{-2} s^{-1}, respectively. In comparison, our measurements of $max\ g_s^w$ for these species were, respectively, 210 ± 10 mmol m^{-2} s^{-1}, 400 ± 100 mmol m^{-2} s^{-1}, and 90 ± 20 mmol m^{-2} s^{-1}. Our estimates of $max\ g_s^w$ for *A. menziesii* and *Q. agrifolia* are substantially lower. A possible explanation of this is that measurements of these tree species Murray et al. (2019) were collected from subspecies near the California coast, which has a considerably more humid climate, compared to our trees, which were grown from seeds sourced from the much drier inland Mt. Diablo foothills region. Murray et al. (2019) also selected a single leaf on several individuals of the species measured, whereas our $max\ g_s^w$ measurement were conducted at the branch level. Maire et al. (2015) determined a maximum stomatal conductance for *A. menziesii* of 150 mmol m^{-2} s^{-1}, much closer to our measurements. For *Quercus* and *Acer* species in similar climate regions to where our trees were sourced from, Maire et al. (2015) calculated $max\ g_s^w$ ranging from 103—890 mmol m^{-2} s^{-1} and 112—320 mmol m^{-2} s^{-1}, respectively. Henry et al. (2019) measured a similar maximum stomatal conductance of *Q. agrifolia* to our study of 95 mmol m^{-2} s^{-1}. Maire et al. (2015) also measured a maximum stomatal conductance to water vapor for *P. ponderosa* and *S. sempervirens* of 124 mmol m^{-2} s^{-1} and 91 mmol m^{-2} s^{-1}, respectively–considerably smaller than the values measured in this study. Ambrose et al. (2010) measured a $max\ g_s^w$ for *S. sempervirens* of 240 mmol m^{-2} s^{-1}, in better agreement with our measurements. *P. ponderosa* stomatal conductance measurements reported in this study were in very good agreement with the stomatal conductance measured during the BEARPEX-2009 campaign in a ponderosa pine dominated forest during a wet year (Min et al., 2014; Delaria and Cohen, 2020). The median of $max\ g_s^w$ for all four angiosperms we measured was 200 mmol m^{-2} s^{-1} , in good agreement with the 250 mmol m^{-2} s^{-1} median of all angiosperms in Mediterranean climate regions found by Murray et al. (2019) and the 215 mmol m^{-2} s^{-1} median found by Maire et al. (2015). Our median for the six gymnosperms measured was 230 mmol m^{-2} s^{-1}, considerably larger than the median 100 mmol m^{-2} s^{-1} $max\ g_s^w$ found by Maire et al. (2015) in Meditteranean climate regions (defined as warm temperature steppe regions as classified by Kottek et al. (2006)). This may have been because our trees were well-watered and grown under optimal conditions, and it is possible the $max\ g_s^w$ values measured in the field did not adequately reflect the true species $max\ g_s^w$.

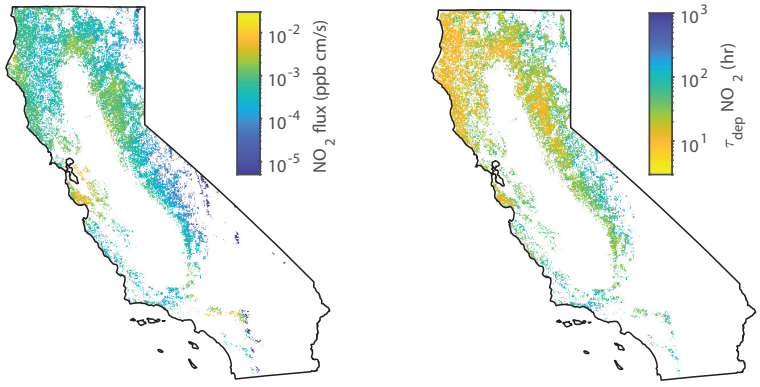

Figure 4.7: (left) Average midday deposition fluxes of NO_2 to forests in June throughout California. (right) Average midday deposition lifetimes of NO_x assuming a uniform 1 km boundary layer height in June throughout California. White areas are non-forested areas.

Overall, the stomatal conductances to water vapor measured in our laboratory experiments falls within the ranges of $max\ g_s^w$ measured in previous studies–although significant inconsistencies exist in the current literature. Possible discrepancies may have resulted from the location each species were measured, growing conditions, ages of the trees, etc. Nevertheless, our NO_2 deposition results–and their applicability to mature trees in California forests–are bolstered by the fact that our $max\ g_s^w$ measurements fall within the ranges measured for for mature trees in the field. To assess the impact of the lab-measured deposition velocities on the NO_x cycle in California, we used our measurements of $maxV_d$ and $medV_d$(night) to estimate the flux and lifetime of NO_x to deposition in forests throughout the state during the day and night, respectively (Fig. 4.7, Fig.4.8).

The average deposition flux to trees in California was calculated via Eq.4.11

$$F_{dep} = [NO_2] \times V_d eff \times LAI \times \text{land cover} \tag{4.11}$$

Leaf area index (LAI) data was obtained from MCD15A2H Version 6 Moderate Resolution Imaging Spectroradiometer (MODIS) Level 4 product (Myneni et al., 2015) (Fig. S3). The NO_2 surface concentration over California was obtained from the OMI satelite using the BEHR product (Laughner et al., 2018) (Fig. S3). Land cover data was obtained from NLCD Land Cover (CONUS) for 2016 (Yang et al., 2018) (Fig. S1). The land cover data set was modified such that there were only two land categories: forest and not forest. Only forested sites were considered. Tree counts were obtained from the USDA Forest Service Forestry Inventory Analysis Database (for, 2014) (Fig. S2). For each plot in the Forest Service Inventory that contained more than 50% of the trees measured in our study, a weighted averaged effective deposition velocity to NO_2 ($V_d eff$) was calculated from the max V_d listed in Table 4.1 (Fig. S3). Data was interpolated to a 500m grid. The resulting midday fluxes

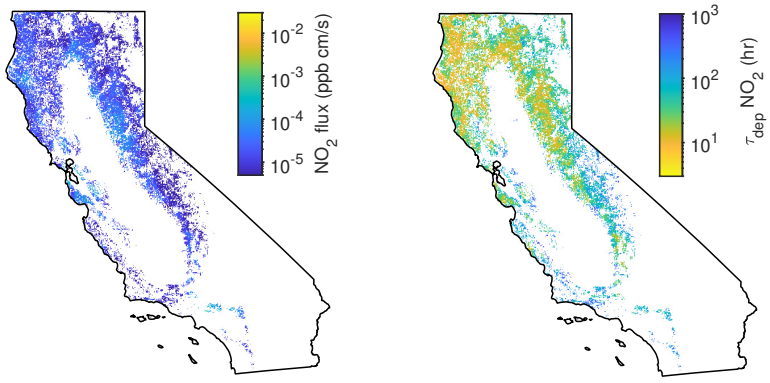

Figure 4.8: (left) Average midnight deposition fluxes of NO_2 to forests in June throughout California. (right) Average midnight deposition lifetimes of NO_x assuming a uniform 100 m boundary layer height in June throughout California. White areas are non-forested areas.

throughout California are shown in Fig. 4.7 and midnight fluxes are shown in Fig. 4.8. The greatest fluxes predicted are near the San Francisco Bay Area, where there are high NO_x concentrations, and also a relatively high forest LAI for an urban region (Fig. S3). Similar hotspots can be seen near Los Angeles in the inland chaparral regions. Large fluxes are also predicted in the foothill forest region of the Sierra Nevada mountain range, where there is a a large LAI, and frequent occurances of *P. sabiniana*, the tree having the largest V_d (Fig. S2, Fig. S3). Relatively large fluxes occur in this region particularly during the nighttime.

The resulting lifetime of NO_2 to deposition is calculated via Eq. 4.12

$$\tau_{dep} = PBL\,(V_deff \times LAI \times \text{land cover})^{-1} \tag{4.12}$$

where PBL is the planetary boundary layer height. The lifetimes to deposition during the day for a uniform PBL height of 1 km are shown in Fig. 4.7. In forested regions the lifetime to deposition is approximately 10 hrs. This is especially significant in the near-urban San Francisco Bay, where deposition is competitive with the chemical sinks of HNO_3 and $RONO_2$ formation, which typically represent a lifetime to NO_x loss of 2-11 hrs (e.g., Nunnermacker et al., 2000; Dillon et al., 2002; Alvarado et al., 2010; Valin et al., 2013; Romer et al., 2016; Laughner and Cohen, 2019). The lifetimes to deposition during the day for a uniform PBL height of 100 m are shown in Fig. 4.8. With a reduced boundary layer during the night, the lifetime to NO_x to deposition is on the same order as the deposition lifetime during the day (10—100 hr), representing a very significant permanent loss of NO_x from the atmosphere when compared with the overall NO_x lifetime at night (Brown et al., 2004, 2006; Crowley et al., 2010).

4.5 Conclucions

We present measurements assessing the relative effects of stomatal diffusion and mesophyllic processing of NO_2 on the uptake rate of NO_2. We find that the deposition velocity of NO_2 is essentially equal to the stomatal conductance to NO_2 under conditions of drought, excess soil nitrogen, variations in vapor pressure deficit, and in both the day and night. We find no evidence of any emission of NO_2 from leaves. NO_2 foliar exchange is thus uni-directional and variations are driven–from an atmospheric perspective–nearly entirely by the rate of diffusion through open stomata. This opens the possibility of using direct measurements of stomatal conductance, known relationships of the effects of environmental conditions on stomatal opening, as well as indirect measurements, such as satellite solar-induced fluorescence data to infer NO_x foliar exchange. Additionally, we find significant differences in deposition velocities between species, reflecting differences in maximum stomatal conductance measurements that have been found by a number of previous studies (e.g., Ambrose et al., 2010; Maire et al., 2015; Henry et al., 2019; Murray et al., 2019). This diversity is not reflected in current atmospehric models, and may have a meaningful impact on estimates of regional NO_x fluxes and lifetimes. Our observations of stomatal opening in the absence of light also suggests foliar deposition serves as a large and important sink of NO_x during the night. These findings not only have important implications for NO_x chemistry, but are also relevant for the atmosphere-biosphere exchange of other gasses, such as CO_2 and biogenic volatile organic compounds.

4.6 References

Forest Inventory and Analysis. 2014. The Forest Inventory and Analysis Database: Database description and user guide version 6.0.1 for Phase 3, URL http://www.fia.fs.fed.us/library/database-documentation/, 2014.

Alvarado, M. J., Logan, J. A., Mao, J., Apel, E., Riemer, D., Blake, D., Cohen, R. C., Min, K.-E., Perring, A. E., Browne, E. C., Wooldridge, P. J., Diskin, G. S., Sachse, G. W., Fuelberg, H., Sessions, W. R., Harrigan, D. L., Huey, G., Liao, J., Case-Hanks, A., Jimenez, J. L., Cubison, M. J., Vay, S. A., Weinheimer, A. J., Knapp, D. J., Montzka, D. D., Flocke, F. M., Pollack, I. B., Wennberg, P. O., Kurten, A., Crounse, J., Clair, J. M. S., Wisthaler, A., Mikoviny, T., Yantosca, R. M., Carouge, C. C., and Le Sager, P.: Nitrogen oxides and PAN in plumes from boreal fires during ARCTAS-B and their impact on ozone: an integrated analysis of aircraft and satellite observations, Atmospheric Chemistry and Physics, 10, 9739–9760, https://doi.org/10.5194/acp-10-9739-2010, 2010.

Ambrose, A. R., Sillett, S. C., Koch, G. W., Van Pelt, R., Antoine, M. E., and Dawson, T. E.: Effects of height on treetop transpiration and stomatal conductance in coast redwood (Sequoia sempervirens), Tree Physiology, 30, 1260–1272, https://doi.org/10.1093/treephys/tpq064, 2010.

Ammann, M., von Ballmoos, P., Stalder, M., Suter, M., and Brunold, C.: Uptake and assimilation of atmospheric NO2 — N by spruce needles (Picea abies): A field study, Water Air and Soil Pollution, 85, 1497–1502, https://doi.org/10.1007/BF00477193, 1995.

Amnuaylojaroen, T., Barth, M. C., Emmons, L. K., Carmichael, G. R., Kreasuwun, J., Prasitwattanaseree, S., and Chantara, S.: Effect of different emission inventories on modeled ozone and carbon monoxide in Southeast Asia, Atmospheric Chemistry and Physics, 14, 12 983–13 012, https://doi.org/10.5194/acp-14-12983-2014, 2014.

Andrews, M.: The partitioning of nitrate assimilation between root and shoot of higher plants, Plant, Cell & Environment, 9, 511–519, https://doi.org/10.1111/1365-3040.ep11616228, 1986.

Bahrun, A., Jensen, C. R., Asch, F., and Mogensen, V. O.: Drought-induced changes in xylem pH, ionic composition, and ABA concentration act as early signals in field-grown maize (Zea mays L.), Journal of Experimental Botany, 53, 251–263, https://doi.org/10.1093/jexbot/53.367.251, 2002.

Baldocchi, D. D., Hicks, B. B., and Camara, P.: A canopy stomatal resistance model for gaseous deposition to vegetated surfaces, Atmospheric Environment (1967), 21, 91 – 101, https://doi.org/10.1016/0004-6981(87)90274-5, 1987.

Breuninger, C., Oswald, R., Kesselmeier, J., and Meixner, F. X.: The dynamic chamber method: trace gas exchange fluxes (NO, NO_2, O_3) between plants and the atmosphere in the laboratory and in the field, Atmospheric Measurement Techniques, 5, 955–989, https://doi.org/10.5194/amt-5-955-2012, 2012.

Breuninger, C., Meixner, F. X., and Kesselmeier, J.: Field investigations of nitrogen dioxide (NO_2) exchange between plants and the atmosphere, Atmospheric Chemistry and Physics, 13, 773–790, https://doi.org/10.5194/acp-13-773-2013, 2013.

Brown, S. S., Dibb, J. E., Stark, H., Aldener, M., Vozella, M., Whitlow, S., Williams, E. J., Lerner, B. M., Jakoubek, R., Middlebrook, A. M., DeGouw, J. A., Warneke, C., Goldan, P. D., Kuster, W. C., Angevine, W. M., Sueper, D. T., Quinn, P. K., Bates, T. S., Meagher, J. F., Fehsenfeld, F. C., and Ravishankara, A. R.: Nighttime removal of NOx in the summer marine boundary layer, Geophysical Research Letters, 31, https://doi.org/10.1029/2004GL019412, 2004.

Brown, S. S., Ryerson, T. B., Wollny, A. G., Brock, C. A., Peltier, R., Sullivan, A. P., Weber, R. J., Dubé, W. P., Trainer, M., Meagher, J. F., Fehsenfeld, F. C., and Ravishankara, A. R.: Variability in Nocturnal Nitrogen Oxide Processing and Its Role in Regional Air Quality, Science, 311, 67–70, https://doi.org/10.1126/science.1120120, 2006.

Chaparro-Suarez, I., Meixner, F., and Kesselmeier, J.: Nitrogen dioxide (NO2) uptake by vegetation controlled by atmospheric concentrations and plant stomatal aperture, Atmospheric Environment, 45, 5742 – 5750, https://doi.org/10.1016/j.atmosenv.2011.07.021, 2011.

Chen, J., Wu, F.-H., Liu, T.-W., Chen, L., Xiao, Q., Dong, X.-J., He, J.-X., Pei, Z.-M., and Zheng, H.-L.: Emissions of nitric oxide from 79 plant species in response to simulated nitrogen deposition, Environmental Pollution, 160, 192 – 200, https://doi.org/10.1016/j.envpol.2011.09.007, 2012.

Crowley, J. N., Schuster, G., Pouvesle, N., Parchatka, U., Fischer, H., Bonn, B., Bingemer, H., and Lelieveld, J.: Nocturnal nitrogen oxides at a rural mountain-site in southwestern Germany, Atmospheric Chemistry and Physics, 10, 2795–2812, https://doi.org/10.5194/acp-10-2795-2010, 2010.

Crowley, J. N., Pouvesle, N., Phillips, G. J., Axinte, R., Fischer, H., Petäjä, T., Nölscher, A., Williams, J., Hens, K., Harder, H., Martinez-Harder, M., Novelli, A., Kubistin, D., Bohn, B., and Lelieveld, J.: Insights into HO_x and RO_x chemistry in the boreal forest via measurement of peroxyacetic acid, peroxyacetic nitric anhydride (PAN) and hydrogen peroxide, Atmospheric Chemistry and Physics, 18, 13 457–13 479, https://doi.org/10.5194/acp-18-13457-2018, 2018.

Crutzen, P. J.: The Role of NO and NO2 in the Chemistry of the Troposphere and Stratosphere, Annual Review of Earth and Planetary Sciences, 7, 443–472, https://doi.org/10.1146/annurev.ea.07.050179.002303, 1979.

Dawson, T. E., Burgess, S. S. O., Tu, K. P., Oliveira, R. S., Santiago, L. S., Fisher, J. B., Simonin, K. A., and Ambrose, A. R.: Nighttime transpiration in woody plants from contrasting ecosystems, Tree Physiology, 27, 561–575, https://doi.org/10.1093/treephys/27.4.561, 2007.

Decina, S. M., Templer, P. H., Hutyra, L. R., Gately, C. K., and Rao, P.: Variability, drivers, and effects of atmospheric nitrogen inputs across an urban area: Emerging patterns among human activities, the atmosphere, and soils, Science of The Total Environment, 609, 1524 – 1534, https://doi.org/10.1016/j.scitotenv.2017.07.166, 2017.

Delaria, E., Vieira, M., Cremieux, J., and Cohen, R.: Measurements of NO and NO2 exchange between the atmosphere and Quercus agrifolia, Atmospheric Chemistry and Physics, 18, 14 161–14 173, https://doi.org/10.5194/acp-18-14161-2018, 2018.

Delaria, E. R. and Cohen, R. C.: A model-based analysis of foliar NOx deposition, Atmospheric Chemistry and Physics, 20, 2123–2141, https://doi.org/10.5194/acp-20-2123-2020, 2020.

Dillon, M. B., Lamanna, M. S., Schade, G. W., Goldstein, A. H., and Cohen, R. C.: Chemical evolution of the Sacramento urban plume: Transport and oxidation, Journal of Geophysical Research: Atmospheres, 107, ACH 3–1–ACH 3–15, https://doi.org/10.1029/2001JD000969, 2002.

Drake, P. L., Froend, R. H., and Franks, P. J.: Smaller, faster stomata: scaling of stomatal size, rate of response, and stomatal conductance, Journal of Experimental Botany, 64, 495–505, https://doi.org/10.1093/jxb/ers347, 2013.

Fast, J. D., Allan, J., Bahreini, R., Craven, J., Emmons, L., Ferrare, R., Hayes, P. L., Hodzic, A., Holloway, J., Hostetler, C., Jimenez, J. L., Jonsson, H., Liu, S., Liu, Y., Metcalf, A., Middlebrook, A., Nowak, J., Pekour, M., Perring, A., Russell, L., Sedlacek, A., Seinfeld, J., Setyan, A., Shilling, J., Shrivastava, M., Springston, S., Song, C., Subramanian, R., Taylor, J. W., Vinoj, V., Yang, Q., Zaveri, R. A., and Zhang, Q.: Modeling regional aerosol and aerosol precursor variability over California and its sensitivity to emissions and long-range transport during the 2010 CalNex and CARES campaigns, Atmospheric Chemistry and Physics, 14, 10 013–10 060, https://doi.org/10.5194/acp-14-10013-2014, 2014.

Fisher, J. B., Baldocchi, D. D., Misson, L., Dawson, T. E., and Goldstein, A. H.: What the towers don't see at night: nocturnal sap flow in trees and shrubs at two AmeriFlux sites in California, Tree Physiology, 27, 597–610, https://doi.org/10.1093/treephys/27.4.597, 2007.

Hari, P., Raivonen, M., Vesala, T., Munger, J., Pilegaard, K., and Kulmala, M.: Ultraviolet light and leaf emission of NOx, Nature, 422, 134–134, https://doi.org/10.1038/422134a, 2003.

Heidari, B., Matre, P., Nemie-Feyissa, D., Meyer, C., Rognli, O. A., Møller, S. G., and Lillo, C.: Protein Phosphatase 2A B55 and A Regulatory Subunits Interact with Nitrate Reductase and Are Essential for Nitrate Reductase Activation, Plant Physiology, 156, 165–172, https://doi.org/10.1104/pp.111.172734, 2011.

Henry, C. L., John, G. P., Pan, R., Bartlett, M. K., Fletcher, L. R., Scoffoni, C., and Sack, L.: A stomatal safety-efficiency trade-off constrains responses to leaf dehydration, in: Nature Communications, 2019.

Hereid, D. and Monson, R.: Nitrogen Oxide Fluxes between Corn (Zea mays L.) Leaves and the Atmosphere, Atmospheric Environment, 35, 975–983, https://doi.org/10.1016/S1352-2310(00)00342-3, 2001.

Jacob, D. J. and Wofsy, S. C.: Budgets of reactive nitrogen, hydrocarbons, and ozone over the Amazon forest during the wet season, Journal of Geophysical Research: Atmospheres, 95, 16 737–16 754, https://doi.org/10.1029/JD095iD10p16737, 1990.

Joensuu, J., Raivonen, M., Kieloaho, A.-J., Altimir, N., Kolari, P., Sarjala, T., and Bäck, J.: Does nitrate fertilization induce nox emission from scots pine (p. sylvestris) shoots?, Plant and Soil, 388, 283–295, https://doi.org/10.1007/s11104-014-2328-x, 2014.

Johansson, C.: Pine forest: a negligible sink for atmospheric NOx in rural Sweden, Tellus B, 39B, 426–438, https://doi.org/10.1111/j.1600-0889.1987.tb00204.x, 1987.

Kolb, P. and Robberecht, R.: High temperature and drought stress effects on survival of Pinus ponderosa seedlings, Tree physiology, 16, 665–72, https://doi.org/10.1093/treephys/16.8.665, 1996.

Kottek, M., Grieser, J., Beck, C., Rudolf, B., and Rubel, F.: World Map of the Köppen-Geiger Climate Classification Updated, Meteorologische Zeitschrift, 15, 259–263, https://doi.org/10.1127/0941-2948/2006/0130, 2006.

Laughner, J., Zhu, Q., and Cohen, R.: Berkeley High Resolution (BEHR) OMI NO2 - Gridded pixels, daily profiles, v5, UC Berkeley, Dataset, https://doi.org/10.6078/D12D5X, 2018.

Laughner, J. L. and Cohen, R. C.: Direct observation of changing NOx lifetime in North American cities, Science, 366, 723–727, https://doi.org/10.1126/science.aax6832, 2019.

Lerdau, M. T., Munger, J. W., and Jacob, D. J.: The NO2 Flux Conundrum, Science, 289, 2291–2293, https://doi.org/10.1126/science.289.5488.2291, 2000.

Lillo, C.: Signalling cascades integrating light-enhanced nitrate metabolism, Biochemical Journal, 415, 11–19, https://doi.org/10.1042/BJ20081115, 2008.

Maherali, H. and DeLucia, E. H.: Xylem conductivity and vulnerability to cavitation of ponderosa pine growing in contrasting climates, Tree Physiology, 20, 859–867, https://doi.org/10.1093/treephys/20.13.859, 2000.

Maire, V., Wright, I. J., Prentice, I. C., Batjes, N. H., Bhaskar, R., van Bodegom, P. M., Cornwell, W. K., Ellsworth, D., Niinemets, , Ordonez, A., Reich, P. B., and Santiago, L. S.: Global effects of soil and climate on leaf photosynthetic traits and rates, Global Ecology and Biogeography, 24, 706–717, https://doi.org/10.1111/geb.12296, 2015.

Massman, W.: A review of the molecular diffusivities of H2O, CO2, CH4, CO, O3, SO2, NH3, N2O, NO, and NO2 in air, O2 and N2 near STP, Atmospheric Environment, 32, 1111 – 1127, https://doi.org/https://doi.org/10.1016/S1352-2310(97)00391-9, 1998.

Min, K.-E., Pusede, S. E., Browne, E. C., LaFranchi, B. W., and Cohen, R. C.: Eddy covariance fluxes and vertical concentration gradient measurements of NO and NO_2 over a ponderosa pine ecosystem: observational evidence for within-canopy chemical removal of NO_x, Atmospheric Chemistry and Physics, 14, 5495–5512, https://doi.org/10.5194/acp-14-5495-2014, 2014.

Murray, M., Soh, W. K., Yiotis, C., Batke, S., Parnell, A. C., Spicer, R. A., Lawson, T., Caballero, R., Wright, I. J., Purcell, C., and McElwain, J. C.: Convergence in Maximum Stomatal Conductance of C3 Woody Angiosperms in Natural Ecosystems Across Bioclimatic Zones, Frontiers in Plant Science, 10, 558, https://doi.org/10.3389/fpls.2019.00558, 2019.

Musselman, R. C. and Minnick, T. J.: Nocturnal stomatal conductance and ambient air quality standards for ozone, Atmospheric Environment, 34, 719 – 733, https://doi.org/https://doi.org/10.1016/S1352-2310(99)00355-6, 2000.

Myneni, R., Knyazikhin, Y., and Park, T.: MCD15A2H MODIS/Terra+Aqua Leaf Area Index/FPAR 8-day L4 Global 500m SIN Grid V006 [Data set].NASA EOSDIS Land Processes DAAC, https://doi.org/10.5067/MODIS/MCD15A2H.006, 2015.

Ng, N. L., Brown, S. S., Archibald, A. T., Atlas, E., Cohen, R. C., Crowley, J. N., Day, D. A., Donahue, N. M., Fry, J. L., Fuchs, H., Griffin, R. J., Guzman, M. I., Herrmann, H., Hodzic, A., Iinuma, Y., Jimenez, J. L., Kiendler-Scharr, A., Lee, B. H., Luecken, D. J., Mao, J., McLaren, R., Mutzel, A., Osthoff, H. D., Ouyang, B., Picquet-Varrault, B., Platt, U., Pye, H. O. T., Rudich, Y., Schwantes, R. H., Shiraiwa, M., Stutz, J., Thornton, J. A., Tilgner, A., Williams, B. J., and Zaveri, R. A.: Nitrate radicals and biogenic volatile organic compounds: oxidation, mechanisms, and organic aerosol, Atmospheric Chemistry and Physics, 17, 2103–2162, https://doi.org/10.5194/acp-17-2103-2017, 2017.

Nunnermacker, L. J., Kleinman, L. I., Imre, D., Daum, P. H., Lee, Y.-N., Lee, J. H., Springston, S. R., Newman, L., and Gillani, N.: NO y lifetimes and O3 production efficiencies in urban and power plant plumes: Analysis of field data, Journal of Geophysical Research: Atmospheres, 105, 9165–9176, https://doi.org/10.1029/1999JD900753, 2000.

Okano, K. and Totsuka, T.: Absorption of nitrogen dioxide by sunflower plants grown at various levels of nitrate, New Phytologist, 102, 551–562, https://doi.org/10.1111/j.1469-8137.1986.tb00831.x, 1986.

Pape, L., Ammann, C., Nyfeler-Brunner, A., Spirig, C., Hens, K., and Meixner, F. X.: An automated dynamic chamber system for surface exchange measurement of non-reactive and reactive trace gases of grassland ecosystems, Biogeosciences, 6, 405–429, https://doi.org/10.5194/bg-6-405-2009, 2009.

Park, J. Y. and Lee, Y. N.: Solubility and decomposition kinetics of nitrous acid in aqueous solution, The Journal of Physical Chemistry, 92, 6294–6302, https://doi.org/10.1021/j100333a025, 1988.

Pharis, R.: Comparative Drought Resistance of Five Conifers and Foliage Moisture Content as a Viability Index, Ecology, 47, 211, https://doi.org/10.2307/1933767, 1966.

Pietilainen, P. and Lahdesmaki, P.: Effect of various concentrations of potassium nitrate and ammonium sulphate on nitrate reductase activity in the roots and needles of Scots pine seedlings in N Finland, Annales Botanici Fennici, 25, 201–206, URL http://www.jstor.org/stable/23725723, 1988.

Raivonen, M., Bonn, B., Sanz, M. J., Vesala, T., Kulmala, M., and Hari, P.: UV-induced NOy emissions from Scots pine: Could they originate from photolysis of deposited HNO3?, Atmospheric Environment, 40, 6201 – 6213, https://doi.org/10.1016/j.atmosenv.2006.03.063, 2006.

Ramge, P., Badeck, F.-W., Plochl, M., and Kohlmaier, G. H.: Apoplastic antioxidants as decisive elimination factors within the uptake process of nitrogen dioxide into leaf tissues, New Phytologist, 125, 771–785, https://doi.org/10.1111/j.1469-8137.1993.tb03927.x, 1993.

Rogers, H. H., Jeffries, H. E., and Witherspoon, A. M.: Measuring Air Pollutant Uptake by Plants: Nitrogen Dioxide, Journal of Environmental Quality, 8, 551–557, https://doi.org/10.2134/jeq1979.00472425000800040022x, 1979.

Romer, P. S., Duffey, K. C., Wooldridge, P. J., Allen, H. M., Ayres, B. R., Brown, S. S., Brune, W. H., Crounse, J. D., de Gouw, J., Draper, D. C., Feiner, P. A., Fry, J. L., Goldstein, A. H., Koss, A., Misztal, P. K., Nguyen, T. B., Olson, K., Teng, A. P., Wennberg, P. O., Wild, R. J., Zhang, L., and Cohen, R. C.: The lifetime of nitrogen oxides in an isoprene-dominated forest, Atmospheric Chemistry and Physics, 16, 7623–7637, https://doi.org/10.5194/acp-16-7623-2016, 2016.

Rondón, A. and Granat, L.: Studies on the dry deposition of NO2 to coniferous species at low NO2 concentrations, Tellus B: Chemical and Physical Meteorology, 46, 339–352, https://doi.org/10.3402/tellusb.v46i5.15809, 1994.

Sarjala, T.: Effect of mycorrhiza and nitrate nutrition on nitrate reductase activity in Scots pine seedlings, Physiologia Plantarum, 81, 89–94, https://doi.org/10.1111/j.1399-3054.1991.tb01718.x, 1991.

Schneider, C. A., R. W. S. and Eliceiri, K. W.: A Preliminary multiple resistance routine for deriving dry deposition velocities from measured quantities, Nature Methods, 9, 671–675, https://doi.org/10.1038/nmeth.2089, 2012.

Sims, G. K., Ellsworth, T. R., and Mulvaney, R. L.: Microscale determination of inorganic nitrogen in water and soil extracts, Communications in Soil Science and Plant Analysis, 26, 303–316, https://doi.org/10.1080/00103629509369298, 1995.

Skamarock, W. C., K. J. B. D. J. G. D. O. B. D. M. D. M. G. H. X.-Y. W. W. and Powers, J. G.: A Description of the Advanced Research WRF Version 3, Tech. rep., National Center for Atmospheric Res., https://doi.org/10.5065/D68S4MVH, 2008.

Sparks, J., Monson, R., Sparks, K., and Lerdau, M.: Leaf uptake of nitrogen dioxide (NO2) in a tropical wet forest: Implications for tropospheric chemistry, Oecologia, 127, 214–221, https://doi.org/10.1007/s004420000594, 2001.

Sparks, J. P., Roberts, J. M., and Monson, R. K.: The uptake of gaseous organic nitrogen by leaves: A significant global nitrogen transfer process, Geophysical Research Letters, 30, https://doi.org/10.1029/2003GL018578, 2003.

Teklemmariam, T. and Sparks, J.: Leaf fluxes of NO and NO2 in four herbaceous plant species: The role of ascorbic acid, Atmospheric Environment, 40, 2235–2244, https://doi.org/10.1016/j.atmosenv.2005.12.010, 2006.

Thornton, J. A., Wooldridge, P. J., and Cohen, R. C.: Atmospheric NO2: In Situ Laser-Induced Fluorescence Detection at Parts per Trillion Mixing Ratios, Analytical Chemistry, 72, 528–539, https://doi.org/10.1021/ac9908905, pMID: 10695138, 2000.

Tischner, R.: Nitrate uptake and reduction in higher and lower plants, Plant, Cell & Environment, 23, 1005–1024, https://doi.org/10.1046/j.1365-3040.2000.00595.x, 2000.

Valin, L. C., Russell, A. R., and Cohen, R. C.: Variations of OH radical in an urban plume inferred from NO2 column measurements, Geophysical Research Letters, 40, 1856–1860, https://doi.org/10.1002/grl.50267, 2013.

von Caemmerer, S. and Farquhar, G. D.: Some relationships between the biochemistry of photosynthesis and the gas exchange of leaves, Planta, 153, 376–387, https://doi.org/10.1007/BF00384257, 1981.

Wolfe, G. M., Thornton, J. A., Yatavelli, R. L. N., McKay, M., Goldstein, A. H., LaFranchi, B., Min, K.-E., and Cohen, R. C.: Eddy covariance fluxes of acyl peroxy nitrates (PAN, PPN and MPAN) above a Ponderosa pine forest, Atmospheric Chemistry and Physics, 9, 615–634, https://doi.org/10.5194/acp-9-615-2009, 2009.

Yang, L., Jin, S., Danielson, P., Homer, C., Gass, L., Bender, S. M., Case, A., Costello, C., Dewitz, J., Fry, J., Funk, M., Granneman, B., Liknes, G. C., Rigge, M., and Xian, G.: A new generation of the United States National Land Cover Database: Requirements, research priorities, design, and implementation strategies, ISPRS Journal of Photogrammetry and Remote Sensing, 146, 108 – 123, https://doi.org/10.1016/j.isprsjprs.2018.09.006, 2018.

Zhang, L., Moran, M., Makar, P., Brook, J., and Gong, S.: Modelling gaseous dry deposition in AURAMS – A Unified Regional Air-quality Modelling System, Atmospheric Environment, 36, 537–560, https://doi.org/10.1016/S1352-2310(01)00447-2, 2002.

4.7 Appendix

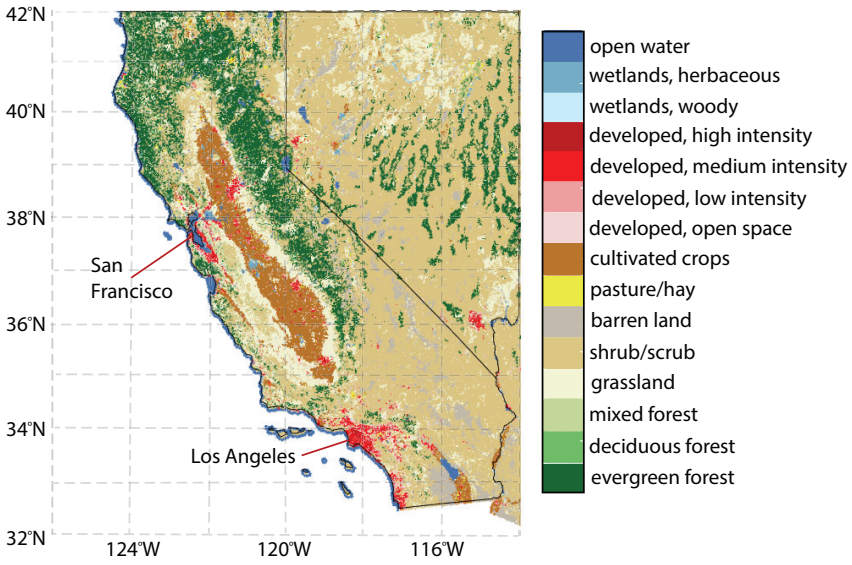

Figure 4.A1: Landcover types for California from the NLCD Land Cover (CONUS) for 2016. The locations of two major cities are indicated.

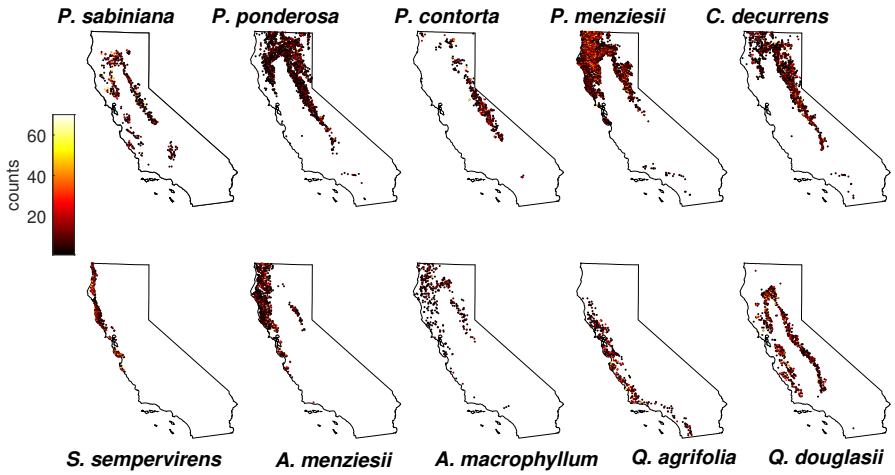

Figure 4.A2: Counts of trees examined in this study from the Forest Inventory and Analysis Database

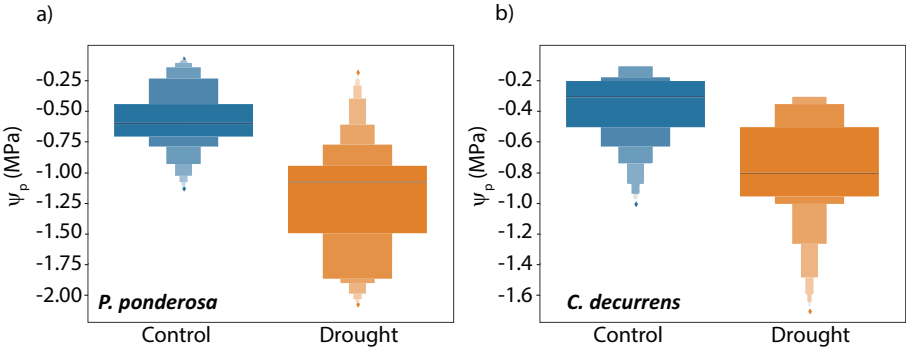

Figure 4.A3: Box and whisker plots of water potentials for the control and drought groups of (a) *P. ponderosa* and (b) *C. decurrens*

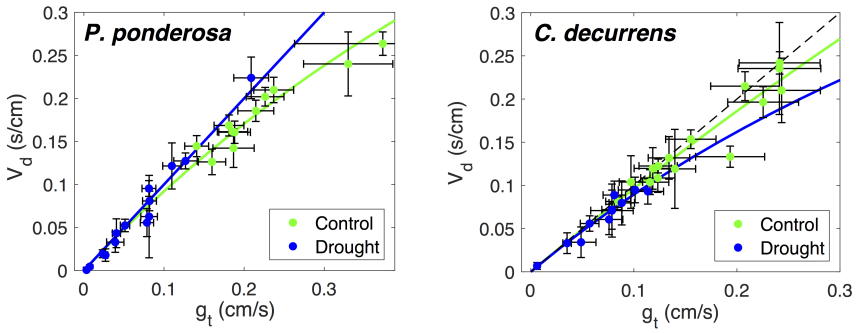

Figure 4.A4: Plot of V_d versus g_t for (left) *P. ponderosa* and (right) *C. decurrens*. Blue markers and lines are data from drought-stressed trees and fits to the resistance model, respectively. Green markers and lines are data from control group trees and fits to the resistance model, respectively.

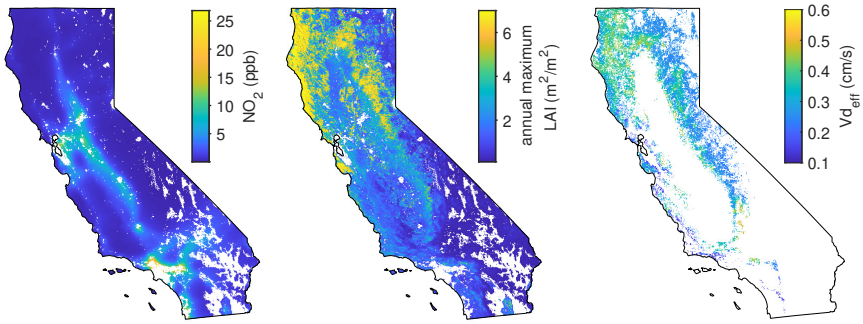

Figure 4.A5: (left) Average midday NO_2 mixing ratios in the month of June 2014.(center) Maximum LAI during the year 2019 from MODIS. (right) Effective daytime state-wide deposition velocities of NO_2 to forests.

Chapter 5

Conclusions

5.1 Summary

Deposition to vegetation has previously been identified as a significant loss process for atmospheric NO_x. However, laboratory measurements and field observations have resulted in large discrepancies in their conclusions of the scale and even direction of this atmosphere-biosphere exchange. These disagreements reflect an inadequate understanding of the rates and mechanisms controlling this important sink. In this dissertation laboratory measurements at the leaf and branch levels are combined with a modeling approach at the canopy and regional scales to examine the importance of foliar removal of NO_x, particularly NO_2, on NO_x lifetimes and budgets.

The laboratory work, which is outlined in Ch. 2 and Ch. 4, adds to the body of work on leaf-level chamber experiments investigating the factors driving NO_x stomatal deposition. The maximum laboratory-measured deposition velocities reported here for stomatal NO_2 uptake range from 0.15—0.5 cm s^{-1}. Deposition velocities of NO_2 are essentially equivalent, from an atmospheric perspective, to the rate of diffusion through open stomata for all tree species discussed in this dissertation. This provides an indication that diffusion, under all environmental conditions, is the rate-limiting step to uptake. Deposition of NO by contrast is much slower by an order of magnitude than the stomatal diffusion rate, indicating reactions within the mesophyll of the leaf are rate-limiting in this case. For no tree species measured, is there any evidence for an NO_2 compensation point. NO compensation points may be as high as 3 ppb, but the extremely slow bi-directional exchange results in only net uptake of NO_x as a chemical family at all non-zero NO_x mixing ratios–considering NO only reaches $\sim$50% of the total NO_x budget during the day. There is a large degree of inter-species variability in stomatal NO_2 uptake rates during the daytime, as well as a significant degree of stomatal deposition occuring at night. Neither phenomenon is currently represented in atmospheric models.

The modelling work, which is described in Ch. 3, and also discussed in Ch. 2 and Ch. 4, characterizes the implications of laboratory measurements on NO_x budgets, NO_x lifetimes

and O_3 production in both remote and near-urban forests. Laboratory-measured deposition velocities result in modeled canopy reductions of soil-emitted NO_x of ∼20—60%. This result explains the range of canopy reduction factors observed in a variety of forests (Jacob and Wofsy 1990; Yienger and Levy, 1995) and provides a physical understanding of the in-canopy processes that cause this reduction. The stomatal control over NO_2 deposition implies that appropriate representations of stomatal conductance are required for accurate depictions of NO_x chemistry in atmospheric models. Changes in stomatal conductance can have a substantial effect on NO_x lifetimes, which is discussed in Ch. 3. Two such parameters that are particularly important for consideration for use in atmospheric models are vapor pressure deficit and soil water content. Inclusion of these parameters can change the maximum rate of deposition by as much as 60% on days with equivalent temperatures and solar radiation.

Finally, the conjunction of the modelling and laboratory work presented suggests important implications for NO_x near cities. In remote forests, despite substantial loss of NO_2 to foliar deposition, soil emission of NO generally results in a net NO_x emission flux from the forest system. By contrast, large deposition losses of NO_2 result in a net deposition flux of NO_x in forests heavily influenced by anthropogenic emissions of NO_x. This has important consequences for near-urban and urban air-quality. The rates of deposition measured for the variety of native California tree species imply substantial NO_2 deposition fluxes throughout the state, particularly in forests near the San Francisco Bay Area and in the Sierra foothills. These fluxes reflect a daytime and nighttime lifetime of NO_x to deposition on the order of the lifetime to chemical loss. This substantial physical loss impacts the regional production of ozone in the state.

5.2 Future work

This dissertation is part of on-going laboratory work on the exchange of reactive nitrogen between the atmosphere and biosphere. Recognized here are a few questions for future consideration.

1. How fast is the foliar deposition of acylperoxy nitrates (APNs) and alkyl nitrates (ANs)? Two of the important chemical reservoirs for NO_x are APNs and ANs, most notably peroxyacetyl nitrate (PAN). PAN formed in urban regions can thermally decompose down-wind, effectively transporting urban-emitted NO_x to rural and remote regions (Stockwell et al., 2011). The degree to which PAN, APNs, and ANs serve as a chemical sink (through their formation and subsequent deposition) or as a reservoir (by reacting or decomposing to re-release NO_x) will have consequences for NO_x lifetimes. Laboratory measurements of the stomatal deposition of a variety of APN and AN species are needed.

2. How fast is foliar deposition to California crops? The Central Valley of California contains elevated levels of NO_x (Fig. 4.A5). However, uptake of reactive atmospheric nitrogen to the crop species making up the Central Valley has never been measured.

Substantial leaf areas and high mixing ratios of NO_x in this region indicates the potential for large deposition fluxes.

3. Do trees from other regions in North America behave similarly to trees in California with respect to reactive nitrogen deposition? The studies presented here are the first laboratory measurements of NO_x deposition that have been carried out on North American trees. There is a need for additional experiments on species from outside California, particularly deciduous broadleaf trees from the northeastern and mid-western states of the United States. Trees in California are particularly drought-adapted, and their stomatal responses may differ from trees in other regions. There are ample field measurement sites in these regions, most notably the University of Michigan Field Station and Harvard Forest, with which to compare field observations and laboratory measurements.

4. Finally, the findings presented in this dissertation should be implemented in global chemical transport models (CTMs), including WRF-CHEM and GEOS-CHEM.